THE GEOLOGICAL SOCIETY OF AMERICA®

Tectonic inversion of an intracontinental rift basin: An example from the opening and closure of the Paleo-Tethys Ocean, northern Tibetan Plateau

Jie Li[1,2], Chen Wu[1,†], Xiaogang Li[2], Andrew V. Zuza[3], Peter J. Haproff[4], Yonghui Zhao[1,5], Wentao Zhao[6], Yahui Yue[1], and Lin Ding[1,5]

[1]*State Key Laboratory of Tibetan Plateau Earth System, Environment and Resources (TPESER), Institute of Tibetan Plateau Research, Chinese Academy of Sciences, Beijing 100101, China*

[2]*Chongqing Key Laboratory of Complex Oil and Gas Field Exploration and Development, Chongqing University of Science and Technology, Chongqing 401331, China*

[3]*Nevada Bureau of Mines and Geology, Nevada Geosciences, University of Nevada, Reno, Nevada 89557, USA*

[4]*Department of Earth and Ocean Sciences, University of North Carolina, Wilmington, North Carolina 28403, USA*

[5]*University of Chinese Academy of Sciences, Beijing 100049, China*

[6]*Geological Engineering Department, Qinghai University, Xining 810016, China*

ABSTRACT

Suture zones located across the Tibetan region clearly demarcate the rift-and-drift and continental accretion history of the region. However, the intraplate responses to these marginal plate-tectonic events are rarely quantified. Our understanding of the Paleo-Tethyan orogenic system, which involved ocean opening and closing events to grow the central Asian continent, depends on the tectonic architecture and histories of major late Paleozoic–early Mesozoic orogenic belts. These opening and collision events were associated with coupled intracontinental deformation, which has been difficult to resolve due to subsequent overprinting deformation. The late Paleozoic–early Mesozoic Zongwulong Shan–Qinghai Nanshan belt in northern Tibet separates the Qilian and North Qaidam regions and is composed of Carboniferous–Triassic sedimentary materials and mantle-derived magmatic rocks. The tectonic setting and evolutional history of this belt provide important insight into the paleogeographic and tectonic relationships of the Paleo-Tethyan orogenic system located ~200 km to the south. In this study, we integrated new and previous geological observations, detailed structural mapping, and zircon U-Pb geochronology data from the Zongwulong Shan–Qinghai Nanshan to document a complete tectonic inversion cycle from intraplate rifting to intracontinental shortening associated with the opening and closing of the Paleo-Tethyan Ocean. Carboniferous–Permian strata in the Zongwulong Shan were deposited in an intracontinental rift basin and sourced from both the north and the south. At the end of the Early–Middle Triassic, foreland molasse strata were deposited in the southern part of the Zongwulong Shan during tectonic inversion in the western part of the tectonic belt following the onset of regional contraction deformation. The Zongwulong Shan–Qinghai Nanshan system has experienced polyphase deformation since the late Paleozoic, including: (1) early Carboniferous intracontinental extension and (2) Early–Middle Triassic tectonic inversion involving reactivation of older normal faults as thrusts and folding of pre- and synrift strata. We interpret that the Zongwulong Shan–Qinghai Nanshan initiated as a Carboniferous–Early Triassic intracontinental rift basin related to the opening of the Paleo-Tethyan Ocean to the south, and it was then inverted during the Early–Middle Triassic closing of the Paleo-Tethyan Ocean. This work emphasizes that pre-Cenozoic intraplate structures related to the opening and closing of ocean basins in the Tethyan realm may be underappreciated across Tibet.

1. INTRODUCTION

Plate-margin processes such as rifting, subduction, and continental accretion/collision are well explained by plate-tectonic theory, but the intraplate responses to these plate-margin events remain rarely quantified, especially in the ancient geologic record (e.g., Isacks et al., 1968; Le Pichon, 1968; Dewey and Bird, 1970; Molnar, 1988; Fraser et al., 2007; Brombin et al., 2019; Soret et al., 2021; Xu et al., 2021). Tibet and the Tethyan realm in central Asia involved repeated ocean opening and closing events to grow the central Asia continent, which were associated with coupled phases of intracontinental extension and contraction (Yin and Harrison, 2000; Royden et al., 2008; Yin, 2010; Xu et al., 2013; Zuza et al., 2018; Kapp and DeCelles, 2019; Wu et al., 2022, 2023a). Although the rift-and-drift and continental accretion history is clearly evidenced by the suture zones located across Tibet, the intraplate responses to these tectonic events are poorly known and rarely quantified. The Kunlun-Qaidam-Qilian continent, located along the northeastern margin of the Tibetan Plateau, recorded multiple phases of deformation associated with the tectonic evolution of the larger pre-Cenozoic Proto- and Paleo-Tethyan orogenic system (Fig. 1A; Şengör, 1984; Yin and Harrison, 2000; Mattinson et al., 2006; Shi et al., 2006; Song et al., 2006, 2007, 2012; Chen et al., 2008; Wu et al., 2016, 2019a, 2022; Zuza et al., 2018). The most recent phase of Cenozoic deformation associated with the growth of the Tibetan Plateau (Fig. 1B; e.g., Yin et al., 2007, 2008; Yin, 2010; Zuza et al., 2016, 2018; Zuza and Yin, 2016; Cheng et al., 2019) partly obscures the pre-Cenozoic tectonic history across the region, hindering our ability to resolve the intraplate tectonic response(s) to the plate-margin events associated with the Proto- and Paleo-Tethyan Oceans to the south.

Chen Wu https://orcid.org/0000-0003-0647-3530

[†]wuchen@itpcas.ac.cn

GSA Bulletin;
published online 24 May 2024

https://doi.org/10.1130/B37605.1.

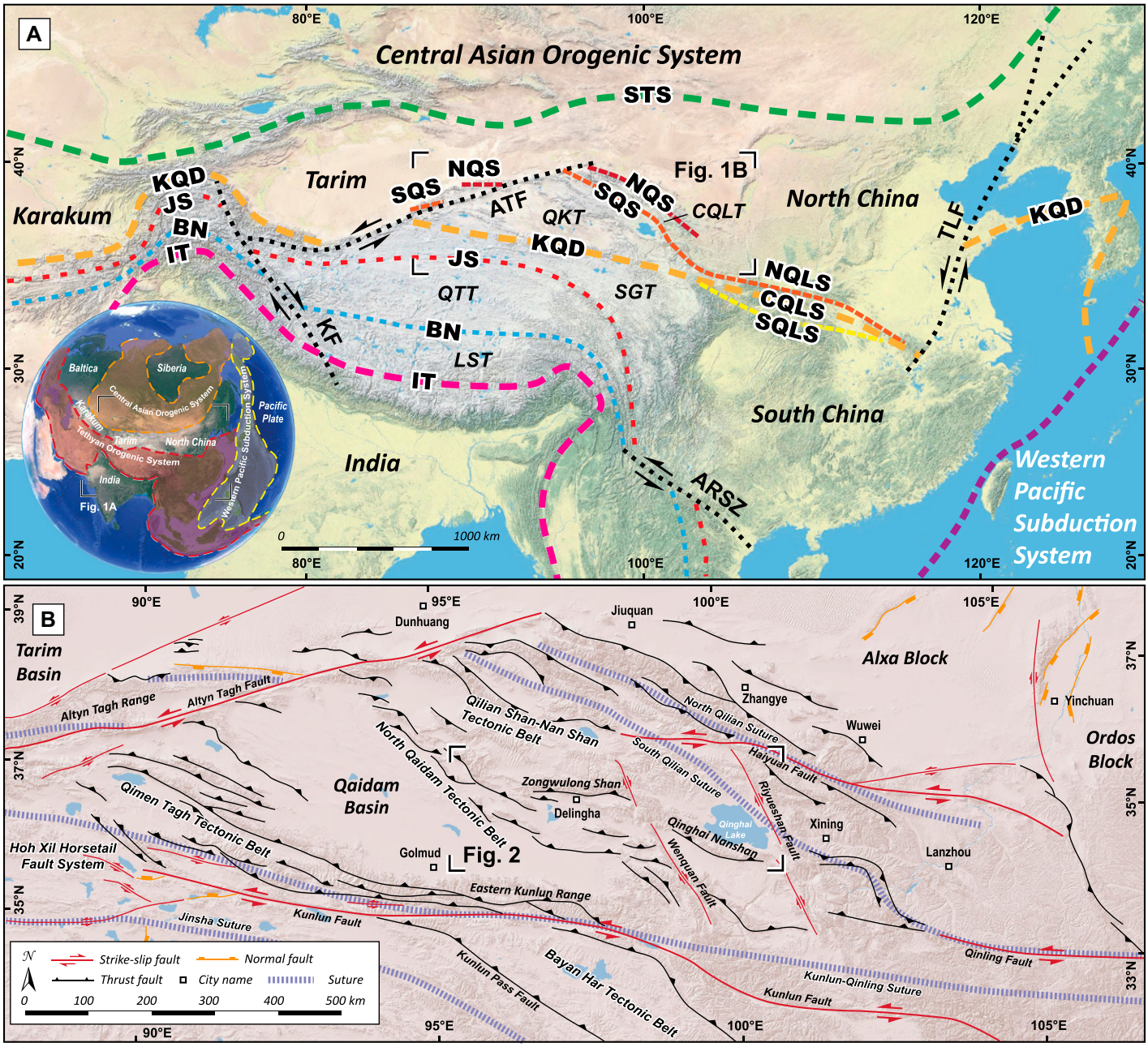

Figure 1. (A) Tectonic division of the Tethyan orogenic system across the Tibetan Plateau, modified from Yin and Nie (1996), Yin and Harrison (2000), and Wu et al. (2019a). Bottom left inset shows the location of Figure 1A in the context of the Asian continent. Also shown is the location of Figure 1B. (B) Tectonic map of northern Tibet showing major fault systems and suture zones (Yin and Harrison, 2000; Yin, 2010; Wu et al., 2021a). Also shown is the location of Figure 2. Abbreviations: STS—South Tianshan–Solonker suture, NQS—North Qilian suture, SQS—South Qilian suture, KQD—Kunlun-Qinling-Dabie suture, NQLS—North Qinling suture, CQLS—Central Qinling suture, SQLS—South Qinling suture, JS—Jinsha suture, BN—Bangong-Nujiang suture, IT—Indus-Tsangpo suture, ATF—Altyn Tagh fault, KF—Karakorum fault, TLF—Tanlu fault, ARSZ—Ailao Shan–Red River shear zone, CQLT—Central Qilian terrane, QKT—Qaidam-Kunlun terrane, SGT—Songpan-Ganzi terrane, QTT—Qiangtang terrane, LST—Lhasa terrane.

The Zongwulong Shan–Qinghai Nanshan region, located between North Qaidam in the south and the South Qilian Shan in the north within the Kunlun-Qaidam-Qilian continent, is composed of late Paleozoic–early Mesozoic rocks (Figs. 1 and 2; Guo et al., 2009; Sun et al., 2015, 2022; Peng et al., 2016a, 2018; Fu et al., 2021). During the late Paleozoic–early Mesozoic, this belt was located in the interior of the Kunlun-Qaidam-Qilian continent apart from the Paleo-Tethyan Ocean (i.e., Neo-Kunlun Ocean; Wu et al., 2019a) within an intraplate setting. Previous studies suggest that this intracontinental belt experienced late Paleozoic crustal extension (Li and Nie, 1985; Zhao et al., 2020, 2022) and early Mesozoic intracontinental contraction (Guo et al., 2009; Gao et al., 2021), which were associated with the opening and closing of the

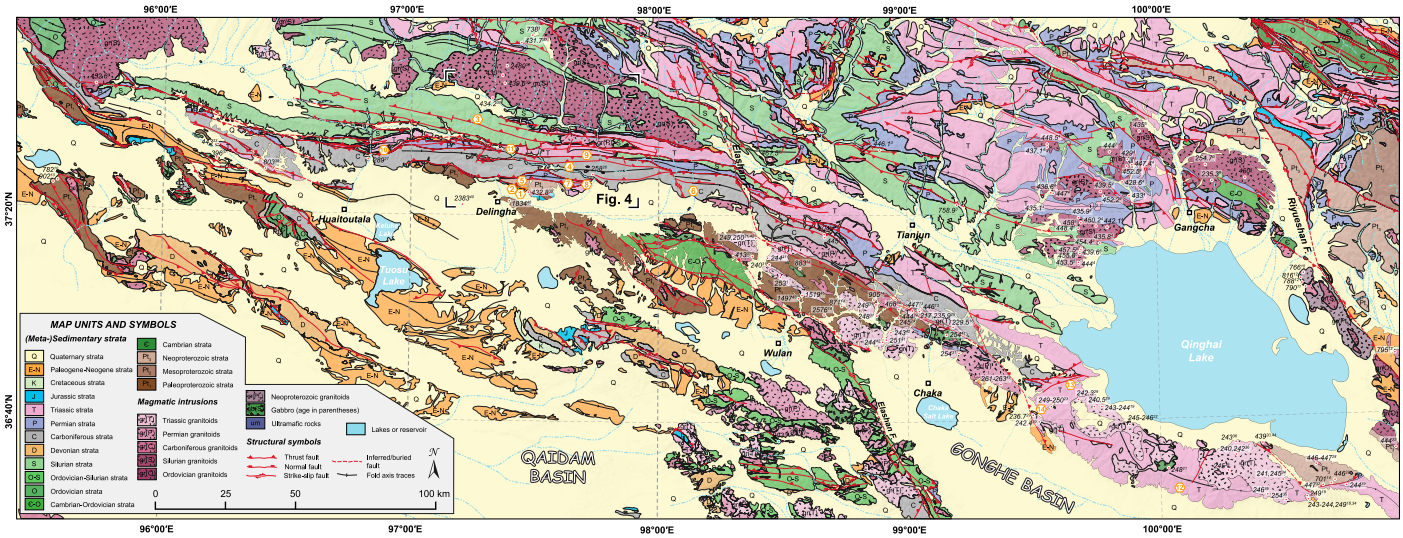

Figure 2. Geological map of the Zongwulong Shan–Qinghai Nanshan and the adjacent region of northern Tibet showing regional geochronologic results from magmatic rocks. The map is compiled from Pan et al. (2004) and this study. The location of Figure 4 is shown. Orange numbered hexagons represent the locations of the collected samples. Zircon U-Pb geochronological data are compiled from: 1—Li et al. (2021a); 2—Liao et al. (2014b); 3—Qin (2018); 4—Zhang et al. (2016); 5—Chang (2017); 6—Shi et al. (2015); 7—Shi et al. (2017); 8—Huang et al. (2015); 9—Xie et al. (2014); 10—Peng et al. (2019); 11—Tung et al. (2007); 12—Tung et al. (2013); 13—Li et al. (2022c); 14—Li et al. (2022b); 15—Wu et al. (2021c); 16—Li et al. (2021b); 17—Fu et al. (2021); 18—Zhang et al. (2017c); 19—Zhang et al. (2017a); 20—Zhang et al. (2019b); 21—Zhang et al. (2019c); 22—Wang et al. (2019b); 23—Huang et al. (2014); 24—Ding et al. (2022b); 25—Wang et al. (2020a); 26—Chen et al. (2020a); 27—Chen (2020); 28—Zhang et al. (2019a); 29—Wang (2019); 30—Yu et al. (2019b); 31—Wu et al. (2019b); 32—Tian et al. (2018a); 33—Sun et al. (2018); 34—Li et al. (2018a); 35—Hao et al. (2018); 36—Zhang (2017); 37—Yang et al. (2017); 38—Yan et al. (2017); 39—Li et al. (2017); 40—Yu et al. (2017b); 41—Wang and Zhou (2016); 42—Peng et al. (2016a); 43—Huo (2016); 44—Guo et al. (2016); 45—Wang et al. (2016); 46—Liao et al. (2014a).

Paleo-Tethyan Ocean in the south (Wu et al., 2016, 2019a). However, the structural framework and tectonic evolution of the Zongwulong Shan–Qinghai Nanshan are still unclear and controversial, which limits our knowledge of the regional tectonic processes in the Paleo-Tethyan orogenic system.

The late Paleozoic–early Mesozoic development of the Zongwulong Shan–Qinghai Nanshan region can be explained by one of two end-member models. The first suggests that Late Devonian–Carboniferous crustal extension developed an ocean basin that was closed by Permian southward subduction and Triassic collisional and postcollisional orogeny (i.e., the "ocean basin" model; Wang et al., 2001; Guo et al., 2009; Peng et al., 2016a; Sun et al., 2016a, 2016b, 2022; Li, 2017; Zhang et al., 2017a, 2017b, 2017c, 2019b; Hao et al., 2018; Li et al., 2018a; Tian et al., 2018b; Wang, 2019; Wang et al., 2019b; Wu et al., 2019b; Xu et al., 2019; Zhuang et al., 2020; Gao et al., 2021; Yang et al., 2022). In contrast, the second model suggests that the region developed as an intracontinental rift basin without generating new oceanic crust (i.e., the "intracontinental rift basin" model; Chen et al., 2020a; Zhao et al., 2022). These two models make specific predictions regarding the occurrence of prerifting basement rocks, rock assemblages and sedimentary characteristics, and deformation styles within the Zongwulong Shan–Qinghai Nanshan region (e.g., Zappettini et al., 2017; Corti et al., 2018; Leprêtre et al., 2018; Boone et al., 2019; Morley, 2020; Chenin et al., 2022; Manatschal et al., 2022; Wang et al., 2021a). For example, the ocean basin model predicts subduction-related magmatism and deformation and the absence of pre-extensional basement rocks, whereas the intracontinental rift basin model requires the occurrence of pre-extensional basement rocks comparable to those of the North Qaidam and South Qilian regions. At present, the late Paleozoic–early Mesozoic tectonic processes of the Zongwulong Shan–Qinghai Nanshan region during the evolution of the Paleo-Tethyan realm are inadequately understood. A major challenge in unraveling the geological history of the Zongwulong Shan–Qinghai Nanshan tectonic belt is significant overprinting by Mesozoic–Cenozoic deformation (Yin et al., 2007; Cheng et al., 2019; Dong et al., 2019; Lin et al., 2021).

To provide new insights into this issue, we performed detailed geological mapping and zircon U-Pb geochronology and compiled the results with previous geological data. These data allowed us to better constrain the tectonic setting and history of the tectonic belt and its relationships to the larger Paleo-Tethyan orogenic system.

2. GEOLOGICAL FRAMEWORK

The Kunlun-Qaidam-Qilian continent is the main part of the northern margin of the present-day Tibetan Plateau, and it experienced Neoproterozoic–Mesozoic subduction, arc magmatism, and orogeny (e.g., Gehrels et al., 2003a, 2003b; Song et al., 2013, 2014; Wu et al., 2016, 2019a, 2022, 2023a; Zuza et al., 2018; Yu et al., 2021; Yan et al., 2022; Wu et al., 2023c), as evidenced by the widespread exposures of ophiolitic mélanges (Fu et al., 2020; Fu et al., 2021; Zhang et al., 2021), (ultra)high-pressure rocks (Song et al., 2004; Yin et al., 2007; Bi et al., 2022; Hernández-Uribe et al., 2023; Wu et al., 2023b), and plutons (Zhu et al., 2022) (Figs. 1 and 2). During the Cenozoic, structures in northern Tibet were reactivated as a result of the India-Asia collision (Wu et al., 2021a; Wang et al., 2022; Li et al., 2023; Xie et al., 2023). The Zongwulong Shan–Qinghai Nanshan region is located between the North Qaidam region in the south and the South Qilian region in the north,

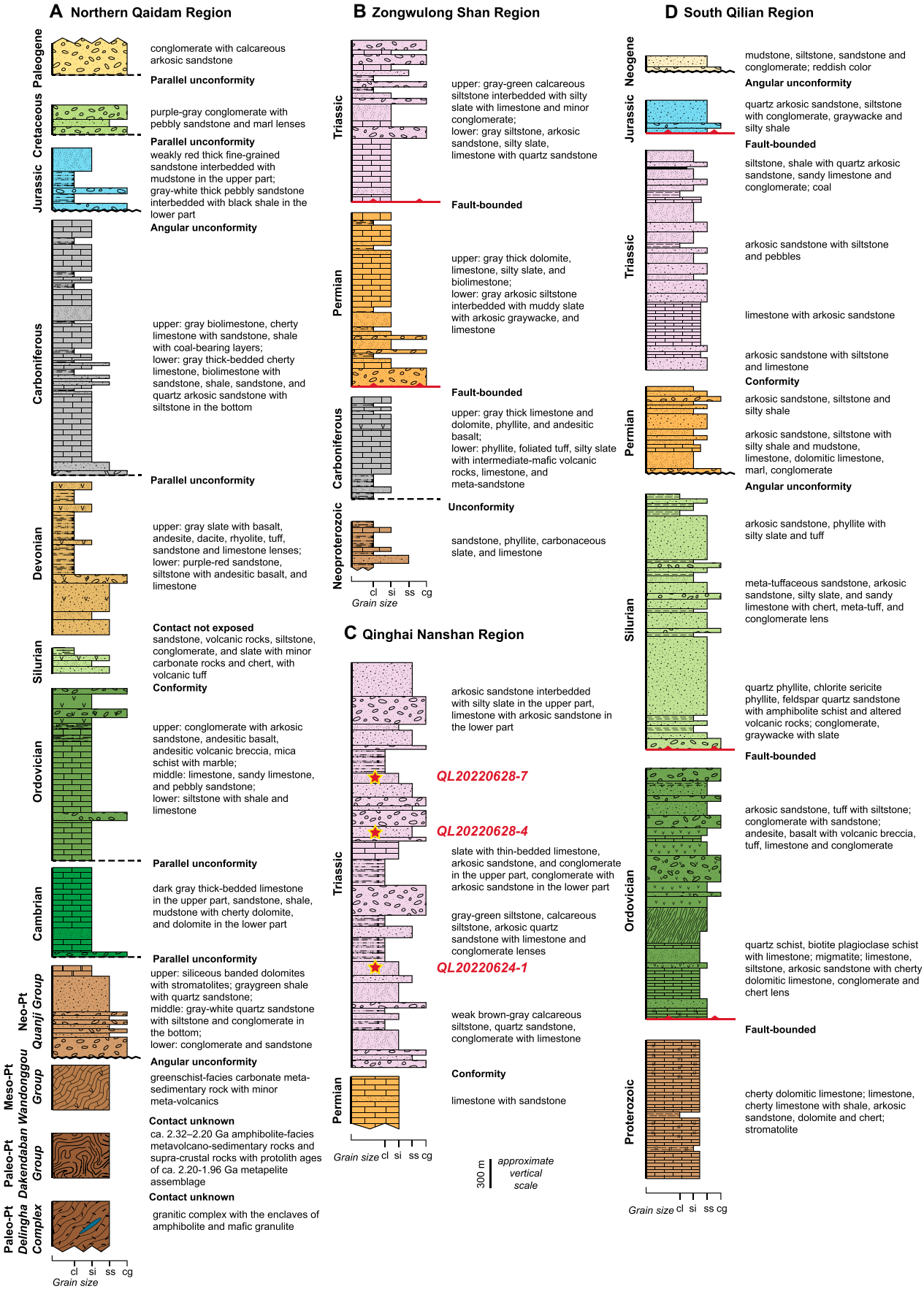

Figure 3. Lithostratigraphy of the North Qaidam region, Zongwulong Shan region, Qinghai Nanshan region, and South Qilian Shan region of northern Tibet compiled from Qinghai BGMR (1991), Pan et al. (2004), Wang et al. (2013), and this study. The approximate locations of the sampled rocks in the Qinghai Nanshan region are also shown in the lithostratigraphic sections. Pt—Proterozoic; cl—clay; si—silt; ss—sand; cg—conglomerate.

separated by the southern Zongwulong Shan fault and Qinghai Nanshan fault, respectively (Figs. 1 and 2; Guo et al., 2009). To provide a regional context, we describe the geology of the North Qaidam region, Zongwulong Shan–Qinghai Nanshan region, and South Qilian region in the following sections (Fig. 2).

2.1. North Qaidam Region

The northwest-trending, ~100-km-wide and ~500-km-long North Qaidam continent is located along the northern margin of the Qaidam Basin, and it is bounded to the south by the northwest- to west-striking Cenozoic North Qaidam thrust belt (Fig. 2; Yin et al., 2008). The heterogeneous basement of the North Qaidam continent consists of Paleoproterozoic crystalline rocks and Mesoproterozoic passive-margin strata (Qinghai BGMR, 1991; Xia, 1996; Xin et al., 2002; Pan et al., 2004; Mattinson et al., 2006; Yu et al., 2017b). The Quanji massif in the North Qaidam region consists of medium- to high-grade metamorphic rocks of the Delingha, Dakendaban, and Wandonggou Groups, which are unconformably overlain by Neoproterozoic strata (Fig. 3; Qinghai BGMR, 1991; Chen et al., 2009, 2013a; Wang et al., 2009; Gong et al., 2012). The Delingha granitic gneiss yields Paleoproterozoic zircon ages of ca. 2390–2360 Ma (Gong et al., 2012; Yu et al., 2017b; Yu et al., 2017a). Based on their geochemistry results, the granite protoliths are interpreted to have formed in an extensional setting, possibly related to the breakup of a Neoarchean continent (Gong et al., 2012). The Dakendaban metasedimentary rocks were deposited after ca. 2470 Ma and before ca. 2430 Ma based on detrital zircon analyses (Wang et al., 2008; Gong et al., 2012; Zhang et al., 2014). The Wandonggou metasedimentary rocks were deposited ca. 2240–1950 Ma (Huang et al., 2011; Zhang et al., 2014). The Quanji massif experienced ca. 1960–1900 Ma amphibolite-facies metamorphism (Wang et al., 2008, 2009; Zhang et al., 2011; Chen et al., 2013a; Lu et al., 2017; Yu et al., 2017a) and was subsequently intruded by ca. 1830 Ma mafic dikes (Liao et al., 2014a) and ca. 1800 Ma rapakivi granite (Chen et al., 2013b). The tectonic setting of the Mesoproterozoic metasedimentary strata is poorly constrained, as they are overlain by Neoproterozoic–early Paleozoic strata including tillite-bearing glacial strata and Neoproterozoic–Ordovician siliciclastic and carbonate rocks (Ma et al., 2019). The North Qaidam continent was intruded by ca. 970–900 Ma and ca. 850–800 Ma plutons, which are similar in age to plutons in the Kunlun and Qilian regions, suggesting that these regions were contiguous by the Neoproterozoic (Fig. 2; Mattinson et al., 2006; Tung et al., 2013; Fu et al., 2015; Yan et al., 2015; He et al., 2016, 2018; Zuza and Yin, 2017; Peng et al., 2019; Wu et al., 2021b; Zhu et al., 2022). Recently, ca. 1500 Ma trondhjemite, ca. 1100–1000 Ma magmatic arc and metamorphic rocks, and ca. 480–450 Ma amphibolite- to granulite-facies rocks were identified in the North Qaidam region (Li et al., 2015; Wang et al., 2016, 2019a; Yu et al., 2019a). The North Qaidam ultrahigh-pressure metamorphic belt consists of ca. 460–410 Ma eclogite, garnet peridotite, and mafic granulite, surrounded by ca. 1120–900 Ma granitic and psammitic/pelitic gneisses that experienced regional amphibolite-facies metamorphism (Menold et al., 2009; Chen et al., 2018, 2019; Li et al., 2020; Wang et al., 2020b; Ren et al., 2021; Wang et al., 2021b; Hernández-Uribe et al., 2023). The North Qaidam continent was covered by a thick sequence of Mesozoic–Cenozoic sedimentary strata formed in an intracontinental basin. All pre-Cenozoic rocks in the North Qaidam region are bounded by north-dipping Cenozoic thrust faults, and their basin-and-range–style exposures were strongly controlled by Cenozoic deformation (Yin et al., 2007, 2008).

2.2. Zongwulong Shan–Qinghai Nanshan Region

The Zongwulong Shan–Qinghai Nanshan is an ~10- to 30-km-wide and ~600-km-long tectonic strip that trends west in the west and northwest in the east (Fig. 2). The western part of this belt is composed of the Middle Carboniferous–Lower Permian Zongwulong Group intruded by minor Permian plutons and the Lower–Middle Triassic Longwuhe Formation (Figs. 2 and 3; Li and Nie, 1985; Guo et al., 2009; Chen et al., 2020a; Zhao et al. 2020, 2022). The Zongwulong Group, with a thickness of ~6000 m, is composed of meta-sandstone and schist, dolomitic limestone, mylonitic limestone, meta-basalt, andesitic basalt, and pillow basalt, which have been interpreted to have been deposited within a rift basin (Li and Nie, 1985; Xu et al., 2019; Zhao et al., 2020). These Carboniferous–Permian rocks subsequently experienced ductile shear deformation in the Early–Middle Triassic, based on muscovite and biotite $^{40}Ar/^{39}Ar$ analyses, which is interpreted to have been related to oblique collision between the South Qilian and North Qaidam continents (Gao et al., 2021). The Triassic Longwuhe Formation is composed of coarse-grained clastic rock and limestone interlayers in the lower part, sandstone, slate, and limestone in the middle part, and slate, sandstone, conglomerate, and minor limestone in the upper part, which were deposited in a shallow-marine environment (Li and Nie, 1985; Qinghai BGMR, 1991). To the east, the Qinghai Nanshan region is mainly composed of Permian metasedimentary rocks and the Triassic Longwuhe Formation flysch clastic deposits intruded by Early Triassic mafic-felsic magmatic plutons (Figs. 2 and 3; Peng et al., 2016b; Li, 2017; Zhang et al., 2017a, 2017c, 2019c; Li et al., 2018b; Wang et al., 2019b; Yang et al., 2022; Zou et al., 2022).

2.3. South Qilian Region

The western part of the South Qilian region is dominated by the thick Balonggonggaer Formation and Paleozoic granitic intrusions (Ji et al., 2018; Li et al., 2019; Li et al., 2022a). The eastern part of the South Qilian region is primarily composed of the Neoproterozoic Hualong Complex, which contains ca. 940–850 Ma granitic gneiss and metasedimentary rocks intruded by ca. 470–410 Ma mafic and granitic plutons (Fig. 2; Yan et al., 2015, 2020). The Balonggonggaer Formation consists of meta-siltstone and quartzofeldspathic sandstone, gray slates, meta-tuffaceous sandstone, phyllite, schist, and minor metavolcanic rocks and limestone, which are interpreted to be a thick turbidite sequence (Fig. 3; Qinghai BGMR, 1991). In the Zongwulong Shan, the Balonggonggaer Formation mainly consists of phyllite and mica schist, transitioning to tuffaceous sandstone to the north. The Balonggonggaer Formation is unconformably overlain by Permian–Triassic marginal marine sedimentary strata (Figs. 2 and 3). The Balonggonggaer Formation in the South Qilian region was previously assumed to be early Silurian based on regional geological maps and limited graptolite biostratigraphy from meta-sandstones (Qinghai BGMR, 1978, 1991). However, recent zircon ages suggest that this formation can be divided into a Neoproterozoic (younger than or ca. 720 Ma) passive-margin sequence and an early Paleozoic (younger than 560 Ma) sequence related to a Gondwana superfan system (Ji et al., 2018, 2021; Li et al., 2019).

3. GEOLOGICAL MAPPING OF THE ZONGWULONG SHAN–QINGHAI NANSHAN REGION

Detailed field observations for this study were focused on the middle part of the Zongwulong Shan between the South Qilian and North Qaidam regions, near the city of Delingha (Fig. 4). The Zongwulong Shan–Qinghai Nanshan is bounded by the Cenozoic North Zongwulong thrust fault to the north and South Zongwulong thrust fault to the south (Fig. 4). Our investigation was conducted along major river valleys in the Zongwulong Shan, including the Bayinguole river valley. Major river valleys, located at ~3500 m elevation, cut through east-trending ranges with moderate relief (~500 m) and ~5000 m peak elevations. Key geological observations and detrital zircon geochronologic samples are shown in a regional-scale geological map, cross sections, and a simplified tectonostratigraphic column in Figures 4–6.

Stratigraphic age assignments for the major lithologic units of the Zongwulong Shan are primarily from Pan et al. (2004). Detailed constraints on geological relationships are from Qinghai BGMR (1978) and new field observations and detrital zircon ages. Lithologic units range in age from Paleoproterozoic to Quaternary and are described in the following sections.

3.1. Metamorphic Basement and Sedimentary Rocks

Metamorphic basement rocks of the Dakendaban Group are distributed in the southern part of the Zongwulong Shan and divided into lower (labeled Pt_1^a) and upper (labeled Pt_1^b) sequences (Qinghai BGMR, 1978) (Fig. 4). The lower sequence is characterized by mica schist, quartzofeldspathic gneiss, migmatite, marble, quartzite, and plagioclase amphibolite with Paleoproterozoic zircon U-Pb ages, interpreted to be part of the Tarim craton (Yu et al., 2017b; Yu et al., 2017a). The upper sequence is composed of Paleoproterozoic marble and amphibolite (Pan et al., 2004).

The Neoproterozoic metasedimentary strata (labeled Pt_3) are widespread in the Zongwulong Shan but feature different metamorphic grades and rock assemblages based on their location. Neoproterozoic metasedimentary rocks are distributed in three regions of the Zongwulong Shan based on their juxtaposition by the South Zongwulong and North Zongwulong faults (Fig. 4). Neoproterozoic rocks on the southern side of the South Zongwulong fault consist of mica ± garnet quartz schist, marble, quartzofeldspathic gneiss, migmatite, and plagioclase amphibolite. These rocks were intruded by early Paleozoic plutons and subsequently experienced early Paleozoic amphibolite-facies metamorphism (Figs. 5A and 6). The stratigraphic thickness of the Neoproterozoic rocks probably exceeds 2–4 km, although the section features internal deformation, and the basal contact with Paleoproterozoic metamorphic rocks is not observed. Foliated granitic intrusions crosscut both the gneiss and schist. All metamorphic rocks contain parallel foliation across lithologic contacts and are variously mylonitized. These metamorphic rocks were inferred to have Paleoproterozoic ages based on previous geological mapping (Pan et al., 2004; Yu et al., 2017b). However, geochronological results indicate that at least some of the rocks formed in the Neoproterozoic (see below). Neoproterozoic metasedimentary rocks exposed in the core of the Zongwulong Shan region between the South Zongwulong and North Zongwulong faults consist of meta-sandstone, phyllite, carbonaceous slate, and thin-bedded limestone (Figs. 5B and 6). Previous studies attributed a Carboniferous age to these rocks based on geological mapping (Qinghai BGMR, 1978); however, detrital zircon ages from this study suggest a Neoproterozoic age (discussed below). Neoproterozoic metasedimentary rocks on the northern side of the North Zongwulong fault consist of meta-sandstone, carbonaceous slate, and phyllite (Figs. 5C and 6). Previous studies considered these rocks to be Silurian based on geological mapping (Qinghai BGMR, 1978); however, detrital zircon ages reported here and by Li et al. (2019) suggest a Neoproterozoic age (discussed below).

Cambrian–Devonian strata are absent in the study area but are exposed in the North Qaidam and South Qilian regions (e.g., Zhang et al., 2015; Fu et al., 2018; Qin et al., 2018; Yan et al., 2019, 2020). Carboniferous strata in the Zongwulong Shan are only distributed between the South Zongwulong and North Zongwulong faults and can be divided into lower and upper sequences (labeled C_a and C_b, respectively; Fig. 4). The lower sequence consists of phyllite, foliated tuff, silty slate, limestone, and meta-sandstone. The upper sequence is dominated by thick-bedded limestone and dolomite with minor phyllite. Permian strata (labeled P) in the Zongwulong Shan consist of limestone, which is underlain by basal gray-green arkosic sandstone and conglomerate atop Precambrian rocks (Figs. 4 and 5D). Triassic strata (labeled T) on the southern side of the South Zongwulong thrust fault overlie Precambrian rocks along a regional disconformity and consist of conglomerate, sandstone, siltstone, and limestone (Figs. 4, 5E, and 5F). Triassic strata on the northern side of the North Zongwulong thrust fault conformably overlie Permian strata and consist of arkosic sandstone, siltstone, and limestone (Figs. 4 and 6). Jurassic strata (labeled J) overlie Precambrian rocks along a regional angular conformity and are divided into lower and upper sequences (Figs. 4 and 6). The lower sequence consists of gray-green and gray-purple arkosic sandstone, quartz siltstone, sandy conglomerate, and carbonaceous siltstone with coal layers. The upper sequence consists of purple conglomerate, arkosic sandstone, and quartz sandstone. Cretaceous rocks (labeled K) consist of polymictic conglomerate and red coarse sandstone. Cenozoic rocks consist of Eocene (labeled E) conglomerate and sandy arkosic sandstone deposited in fluvial and lacustrine environments (Fig. 4). Quaternary strata consist of alluvial and fluvial strata.

Figure 4. Geological map and cross sections of the Zongwulong Shan, north of Delingha city. The map is compiled from the 1:200,000 geological map of the Delingha sheet (Qinghai BGMR, 1978), satellite-image analysis (e.g., Google Earth), and our structural observations and interpretations. Locations of geochronologic samples collected for this study are shown with orange numbered hexagons. The locations of field photographs in Figures 5, 7, 8, and 9 are also shown on the map. NZF—North Zongwulongshan fault; SZF—South Zongwulongshan fault.

3.2. Magmatic Intrusions

Early Paleozoic felsic granitoid and mafic plutons (e.g., Yu et al., 2019b; Ding et al., 2022b; Li et al., 2022c; Wu et al., 2022) are widespread in the South Qilian region and scattered in the North Qaidam region (Fig. 4). One large (~2000 km^2) and several minor early Paleozoic plutonic bodies (~1–10 km^2) occur in the study area (Fig. 4). These magmatic bodies have ca. 440–425 Ma ages (Yu et al., 2019b; Li et al., 2022a) and compositions including amphibolite gabbro, quartz diorite, granodiorite, and granite. The magmatic bodies intrude Precambrian gneiss and schist and are unconformably overlain by Permian and younger strata. These relationships suggest that plutonism was initiated after the Precambrian and ceased by the Permian. Numerous latest Paleozoic–early Mesozoic granitoid plutons are also exposed in the North Qaidam and Qinghai Nashan regions (e.g., Peng et al., 2016a; Chen et al., 2020a; Chen et al., 2020b; Yang et al., 2022; Zou et al., 2022; Wang et al., 2023) (Fig. 2). One large (~80 km^2) and several small (~0.5–1 km^2) Permian granodioritic to granitic plutons are exposed in the study area (Fig. 4). Minor Permian leucogranite dikes occur

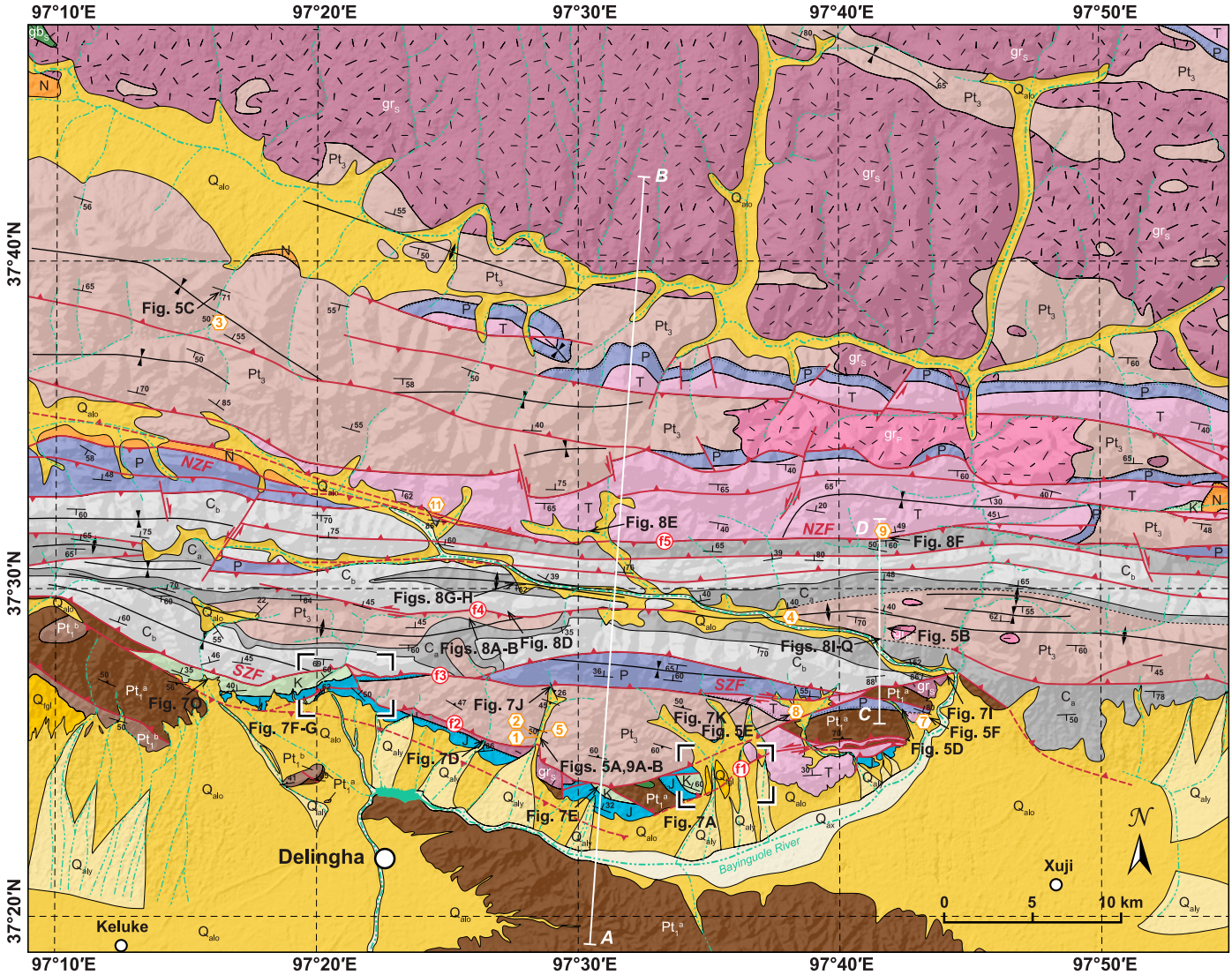

MAP UNITS AND SYMBOLS

(Meta-)Sedimentary strata

- Q_{ax} Quaternary active axial river deposits
- Q_{aly} Quaternary active alluvial deposits
- Q_{alo} Quaternary inactive alluvial deposits
- Q_{tgl} Pleistocene alluvial deposits
- N Neogene red fluvial and lacustrine clastic deposits
- K Cretaceous red fluvial and alluvial clastic deposits
- J Jurassic red alluvial and lacustrine clastic deposits with coal layers
- T Triassic sandstone, slate, and limestone
- P Permian sandstone, shale, conglomerate, and limestone
- C_b Carboniferous massive limestone, dolomite, and minor metapelite
- C_a Carboniferous phyllite, slate, sandstone and minor limestone
- Pt_3 Neoproterozoic slate, sandstone, and limestone
- Pt_1^b Paleoproterozoic upper *Dakendaban Group*, including dolomite marble with minor mica amphibole schist
- Pt_1^a Paleoproterozoic lower *Dakendaban Group*, including mica schist, gneiss, marble, migmatite, plagioclase amphiolite

Magmatic intrusions

- gr_P Permian granitoids
- gr_S Silurian granitoids
- gb_S Silurian gabbro intrusion

Lakes or reservoir

Structural symbols

- Unconformity contact
- Thrust fault
- Strike-slip fault
- Inferred/buried fault
- Syncline axial traces
- Anticline axial traces
- 40 Bedding attitude
- 40 Foliation attitude

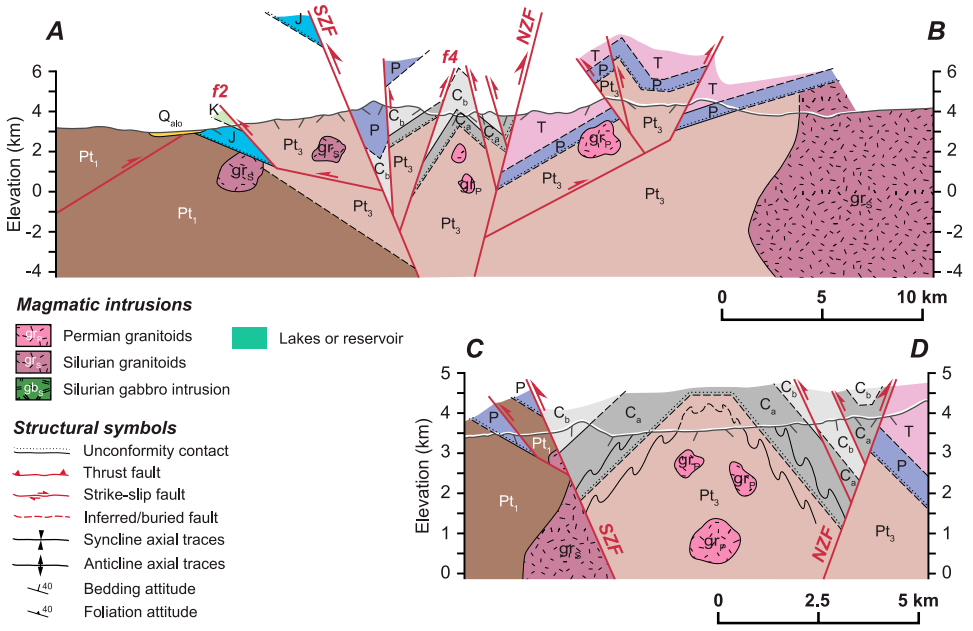

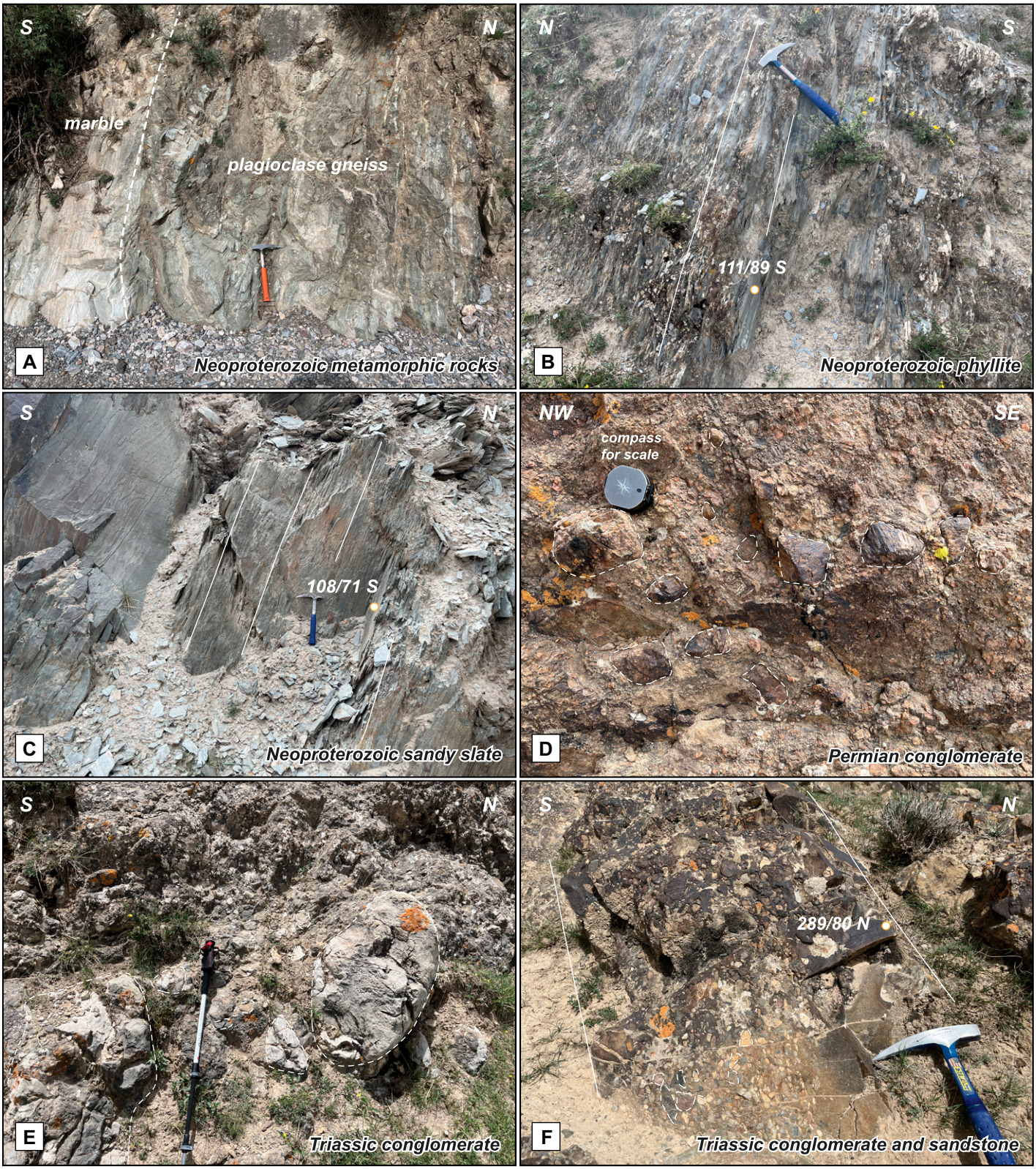

Figure 5. Representative field photographs showing the metamorphic and sedimentary characteristics of strata. Neoproterozoic strata include (A) marble and plagioclase gneiss in the southern side of the South Zongwulong thrust fault, (B) gray-green phyllite in the core of the Zongwulong Shan, and (C) gray-green, sandy slate in the northern side of the North Zongwulongshan fault. (D) Permian conglomerate with pebbles dominantly composed of early Paleozoic gneissic granite of the North Qaidam region. (E, F) Triassic molasse deposits mainly contain Carboniferous and Permian limestone gravels of varying sizes and shapes derived from the Zongwulong Shan.

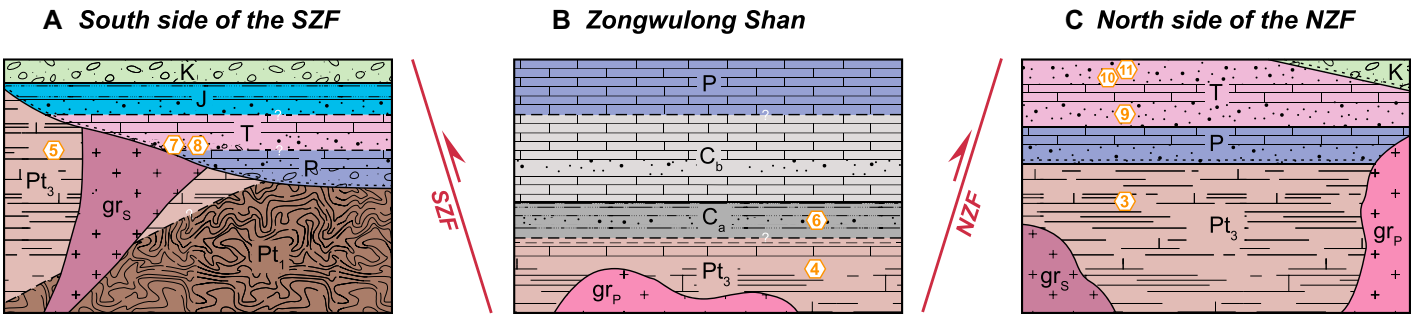

Figure 6. Tectonostratigraphy of the Zongwulong Shan, highlighting the compositions and structure between the southern side of the South Zongwulong thrust fault (SZF), the Zongwulong Shan, and the northern side of the North Zongwulong thrust fault (NZF), compiled from Qinghai BGMR (1978) and our observations. Orange numbered hexagons show the locations of U-Pb detrital zircon samples. Qinghai BGMR (1978) and our observations in Figures 4 and 5. Orange numbered hexagons show the locations of U-Pb detrital zircon samples. Pt_1—Paleoproterozoic; Pt_3—Neoproterozoic; gr_S—Silurian granitoid; gr_P—Permian granitoid; C_a—lower Carboniferous; C_b—upper Carboniferous; P—Permian; T—Triassic; J—Jurassic; K—Cretaceous.

within Neoproterozoic gneiss and schist units in the study area.

3.3. Regional Unconformities

Several Phanerozoic unconformities are recognized in the study area (Figs. 4 and 6), herein named for the lithologic unit that they overlie. These unconformities are significant as they formed during periods of rock uplift and erosion and can be used to determine the pre-unconformity geometries of older lithologic units. For example, Permian, Triassic, and Jurassic unconformities on the southern side of the South Zongwulong thrust fault overlie Precambrian rocks (Figs. 4 and 6). This requires the Precambrian rocks to have been located at or near the surface in the Permian–Jurassic. Therefore, the Precambrian strata reached the surface before Cenozoic deformation. The oldest unconformity, which is also the most widespread in the study area, divides Permian strata above Neoproterozoic metasedimentary rocks (i.e., Balonggonggaer Formation in the South Qilian region) to the north of the North Zongwulong thrust fault and Paleoproterozoic/Neoproterozoic basement rocks (i.e., Dakendaban Group) to the south of the South Zongwulong thrust fault (Figs. 4 and 6). However, Carboniferous strata unconformably overlie Neoproterozoic rocks between the South Zongwulong thrust fault and the North Zongwulong thrust fault (Figs. 4 and 6). This is one of the most important observations for crustal extension, which requires a pronounced and abrupt topographic low in the Carboniferous here compared to the north and south. Along the southern flank of the Zongwulong Shan, Triassic–Jurassic strata unconformably overlie Precambrian rocks. The last two unconformities at the bases of Cretaceous and Cenozoic strata, respectively, are only exposed in the northeastern portions of the study area (Fig. 4). These unconformities indicate that pre-Cenozoic rocks were close to the surface before Cenozoic deformation.

3.4. Structural Geology

Structures in the Zongwulong Shan dominantly trend east, including the strikes of sedimentary bedding and metamorphic foliation, trends of mountain ranges, and fault traces. Deformation can be divided into four distinct episodes: (1) Cenozoic contraction (i.e., folds and thrusts), (2) early Mesozoic tectonic inversion, evidenced by folds, thrusts, lithologic unit juxtapositions, and ductile shear fabrics on folds, (3) late Paleozoic extension, and (4) early Paleozoic ductile shearing and metamorphism.

We interpret the deformation of Paleoproterozoic and younger rocks to be Cenozoic based on the following observations: (1) most of the observed faults and folds of pre-Cenozoic rocks merge with present-day, active range-bounding thrusts, and (2) these thrusts truncate Cenozoic terrestrial deposits and Quaternary alluvial strata (Liu and Yuan, 2004; Dong et al., 2019). The Mesozoic deformational history can be constrained by examining unconformities between Cenozoic and Mesozoic strata. Scattered angular unconformities between Cenozoic and underlying Triassic–Cretaceous strata and between Jurassic–Cretaceous and underlying Precambrian–Triassic strata are the most prominent in the study area. One unconformity occurs along the northern edge of the North Zongwulong thrust fault, where Triassic strata dip ~30°–50° steeper than the overlying Cenozoic strata. Despite the difference in dip angles, the two sequences have similar strikes (Fig. 4). The unconformity between Cenozoic and underlying Cretaceous strata is less obvious, and the dips of the two sequences above and below the unconformity are similar. In the Zongwulong Shan, we did not observe direct evidence of major late Paleozoic deformation. However, the presence of Carboniferous strata and abnormal thickness variations of Permian strata in the study area possibly indicate a deformation event associated with Carboniferous–Permian sedimentation (Fig. 6). Strong ductile shear deformation and amphibolite-facies metamorphism are only preserved in Precambrian rocks along the southern flank of the Zongwulong Shan. New and previous geochronologic results indicate that the deformation and amphibolite-facies metamorphism occurred in the early Paleozoic (see below).

In the following sections, we describe our structural observations, including lithologic unit juxtapositions, map-view relationships, and kinematics from south to north in the Zongwulong Shan. Key thrust faults are labeled f1 through f5 from south to north (Fig. 4) and are discussed in this order below.

3.4.1. Fault f1

Thrust fault f1 strikes northeast and dips 85°NW. Fault striations on the main fault surface steeply plunge (70°) to the northeast, indicating dominant reverse-slip kinematics and a minor strike-slip component (Figs. 7A and 7B). The f1 fault zone is defined by an ~100-m-wide cataclastic zone (Figs. 7B and 7C). Uplifted hanging-wall rocks include Proterozoic rocks unconformably overlain by Triassic–Cretaceous strata. Although the f1 fault trace is covered by Pleistocene strata, the fault is expressed by topographic lineaments and a few fault exposures along river channels (Fig. 7A). The age of f1 may be late Cenozoic, prior to the Quaternary, based on the above observations. The fault is possibly a splay of thrust fault f3 (see below), which has

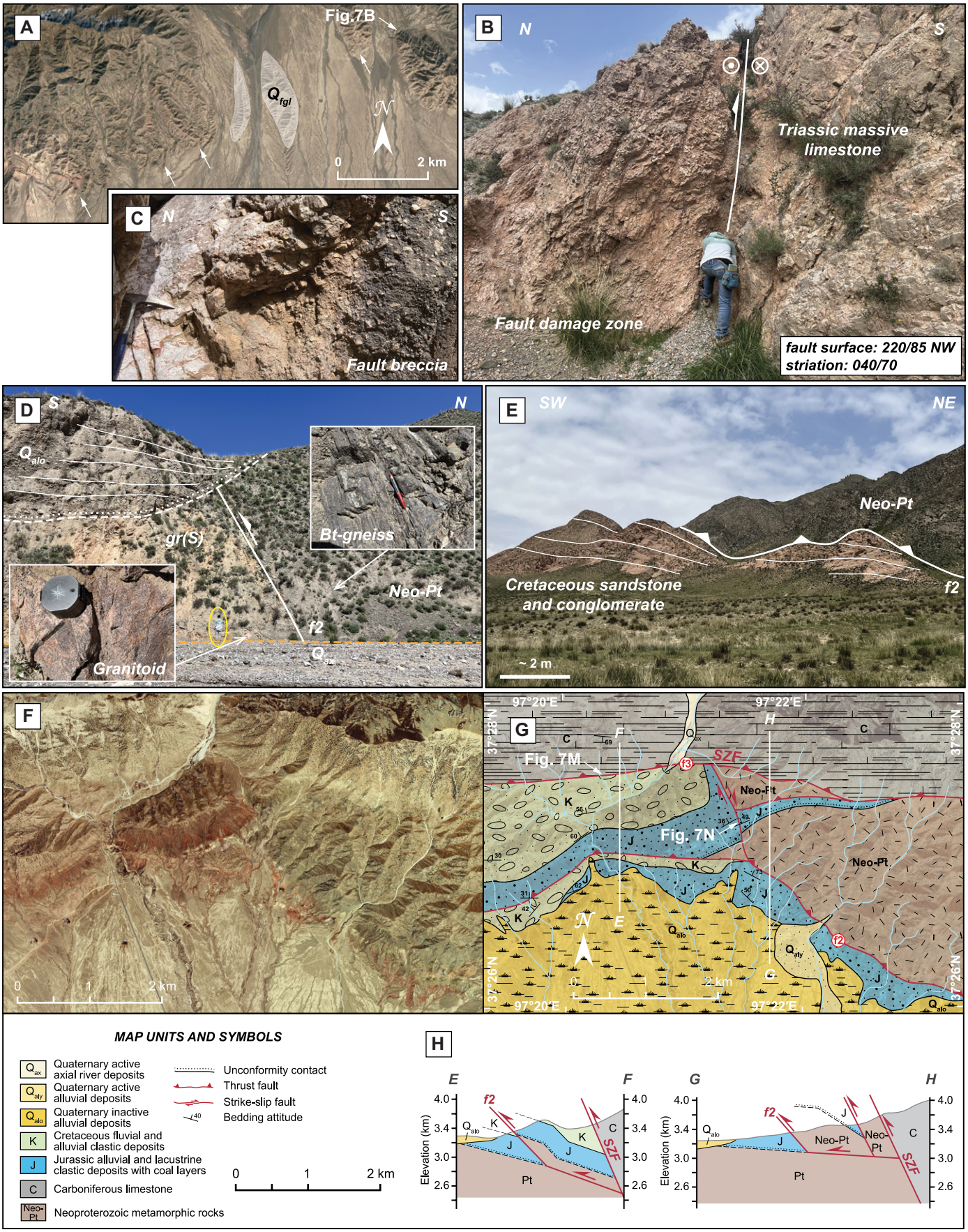

Figure 7. Representative satellite images, detailed geological maps, and field photographs showing structures associated with faults f1–f3 and related deformation. (A) Google Earth satellite image showing the linear topography formed by fault f1 and the fault trace overlain by Pleistocene alluvial deposits (Q_{fgl}). (B, C) River-cut exposure of the left-slip reverse f1 fault zone that occurs within Triassic massive limestone. The exposure consists of the fault core including fault gouge and principal slip plane. The fault damage zone is pervasively fractured to the extent that the original bedding is obliterated. (D) The river flowing south has incised the f1 fault zone exposure. Gray to dark-gray Neoproterozoic biotite (Bt) gneiss in the hanging wall of the f2 fault zone is thrust over yellowish to reddish brown Silurian granitoid. The fault zone and its hanging wall and footwall are unconformably overlain by Quaternary conglomerates. (E) Fault f2 places Neoproterozoic metamorphic rocks over Cretaceous sandstone and conglomerate. (F–H) Uninterpreted satellite image and interpreted structural map and cross sections showing the relationship between faults f2 and f3. SZF—South Zongwulongshan fault. (I) Road-cut exposure showing the f3 fault zone that places Carboniferous limestone over early Paleozoic altered granitoid. (J) Northward view of the range front of the Zongwulong Shan, showing stacked thrust sheets. Note that the foothill is underlain by Neoproterozoic metamorphic rocks at the bottom, where the hanging-wall rocks of fault f3 are Carboniferous and Permian. (K, L) Permian thick-bedded limestone is faulted and thin-bedded limestone is folded due to different rock competencies in response to the f3 faulting. Kinematic data indicate right-slip thrust kinematics. The red rectangle and black circle dots in the inset stereonet plot represent the attitudes of fault striation and fold hinge, respectively. Red and black lines represent the attitudes of fault and bedding, respectively. (M) Fault f3 places Carboniferous massive limestone over Cretaceous sandstone and conglomerate. (N) A thrust fault places Neoproterozoic gneiss over Jurassic coal-bearing clastic rocks that overlie the Neoproterozoic rocks. (O) Fault f3 places Carboniferous limestone over Cretaceous clastic rocks and another thrust juxtaposing the Paleoproterozoic Dakendaban Group rocks over Cretaceous clastic rocks. Note that the formats of planar and linear structure attitudes are strike/dip and dip quadrant and trend/plunge, respectively. (*Continued*)

a larger displacement associated with the southward growth of the Zongwulong Shan (Fig. 4).

3.4.2. Fault f2

Thrust fault f2 fault strikes northwest in the west and northeast in the east and exhibits a southward convex trace, suggesting a north dip (Fig. 4). The fault places Neoproterozoic rocks and overlying Triassic deposits atop Neoproterozoic basement rocks intruded by Paleozoic magmatic intrusions and overlying Mesozoic strata. The fault trace is buried by Quaternary alluvial strata, suggesting the fault was active prior to that time (Figs. 7D and 7E). The fault trace in the east and west merges with the South Zongwulong thrust fault in map view. We assume that the fault also merges with the South Zongwulong thrust fault at depth as a southern branch of the South Zongwulong Shan thrust system (Figs. 4 and 7F–7H). The western segment of f2 has displacement >1 km based on the geological mapping relationships (Figs. 4 and 7H).

3.4.3. South Zongwulong Shan Fault (Fault f3)

The east-striking South Zongwulong Shan thrust fault (labeled f3) dips north and juxtaposes Carboniferous–Permian strata atop Precambrian rocks and overlying Permian–Cretaceous strata (Figs. 4 and 7I–7O). Fault striations on splay fault surfaces and asymmetrically folded Permian strata adjacent to the f3 fault zone indicate right-slip, south-directed kinematics (Figs. 7K and 7L). Along its strike, f3 has both older-over-younger and younger-over-older relationships, indicating the fault experienced multiple slip episodes (Fig. 4).

3.4.4. Fault f4

Thrust fault f4 strikes east, dips south, and juxtaposes Carboniferous and Neoproterozoic rocks atop Carboniferous massive limestone (C_b). The fault is laterally continuous for ~20 km in the study area (Fig. 4). The hanging wall consists of Carboniferous limestone, phyllite, and sandstone (C_a and C_b) unconformably overlying Neoproterozoic rocks (Fig. 8A). Fault striations in the hanging wall (Neoproterozoic meta-sandstone) and footwall (C_b mylonitic limestone) located adjacent to the fault zone and asymmetric fault-bounded blocks within the fault zone indicate north-directed left-slip kinematics (Figs. 8B–8D). The fault is inferred to be a back thrust of the South Zongwulong thrust fault and to merge at depth with this structure (Fig. 4). Folded Neoproterozoic and Cambrian strata in the hanging wall have wavelengths of ~4–6 km. Whether the fault is Cenozoic in age or older remains unknown.

3.4.5. North Zongwulong Shan Fault (Fault f5)

The North Zongwulong Shan thrust fault (labeled f5) strikes east, dips south, and juxtaposes the Carboniferous–Permian strata atop Precambrian rocks and overlying Permian–Triassic and Neogene strata (Figs. 4, 8E, and 8F). Although no direct kinematic measurements were made for this fault, fold axes parallel to the fault suggest dip-slip kinematics. Along its strike, the fault has both older-over-younger and younger-over-older relationships, indicating the fault experienced multiple slip episodes (Fig. 4). In the west, Permian strata are thrust over Neogene strata, indicating that f5 was active in the Neogene (Fig. 4).

3.4.6. Fold and Fault Relationships

Kilometer-scale folds involving Carboniferous–Permian strata and underlying Neoproterozoic rocks occur between the South Zongwulong thrust fault in the south and the North Zongwulong thrust fault in the north (Fig. 4). The core of the Zongwulong Shan contains a broad, east-trending anticline of Carboniferous and Neoproterozoic rocks (Fig. 4). In the west, the anticline is divided into two ~4–6-km-wavelength anticlines by f4 (Figs. 4, 8A, 8G, and 8H). In the east, a broad, ~8- to 10-km-wavelength anticline in the Zongwulong Shan features different deformation within its outer and inner layers. The outer layers and limbs are formed by competent Carboniferous massive limestone (C_b). The outer layer limestone is locally mylonitized likely due to flexural slip during folding. The inner layers are formed by incompetent Carboniferous (C_a) and Neoproterozoic rocks, including phyllite, thin-bedded limestone, and minor sandstone. Thin-bedded limestone forms parasitic folds of the larger-scale anticline (Figs. 8I–8N). The orientations of the parasitic folds indicate north-south contraction (Fig. 8J). The inner layer of phyllite is ductilely deformed and features multiscale folds, thickened and thinned sublayers, and pull-apart folds (Figs. 8O–8Q). The formation of the broad, kilometer-scale anticline may have been associated with the tectonic inversion of the South Zongwulong and North Zongwulong thrust faults.

4. ANALYTICAL METHODS

In total, 14 samples were collected in the Zongwulong Shan–Qinghai Nanshan for zircon U-Pb geochronology. Detailed geochronologic methods are described below.

4.1. Zircon U-Pb Geochronology of Igneous Rocks

Zircon grains from two sampled leucogranite dikes (Table 1) that intrude Neoproterozoic

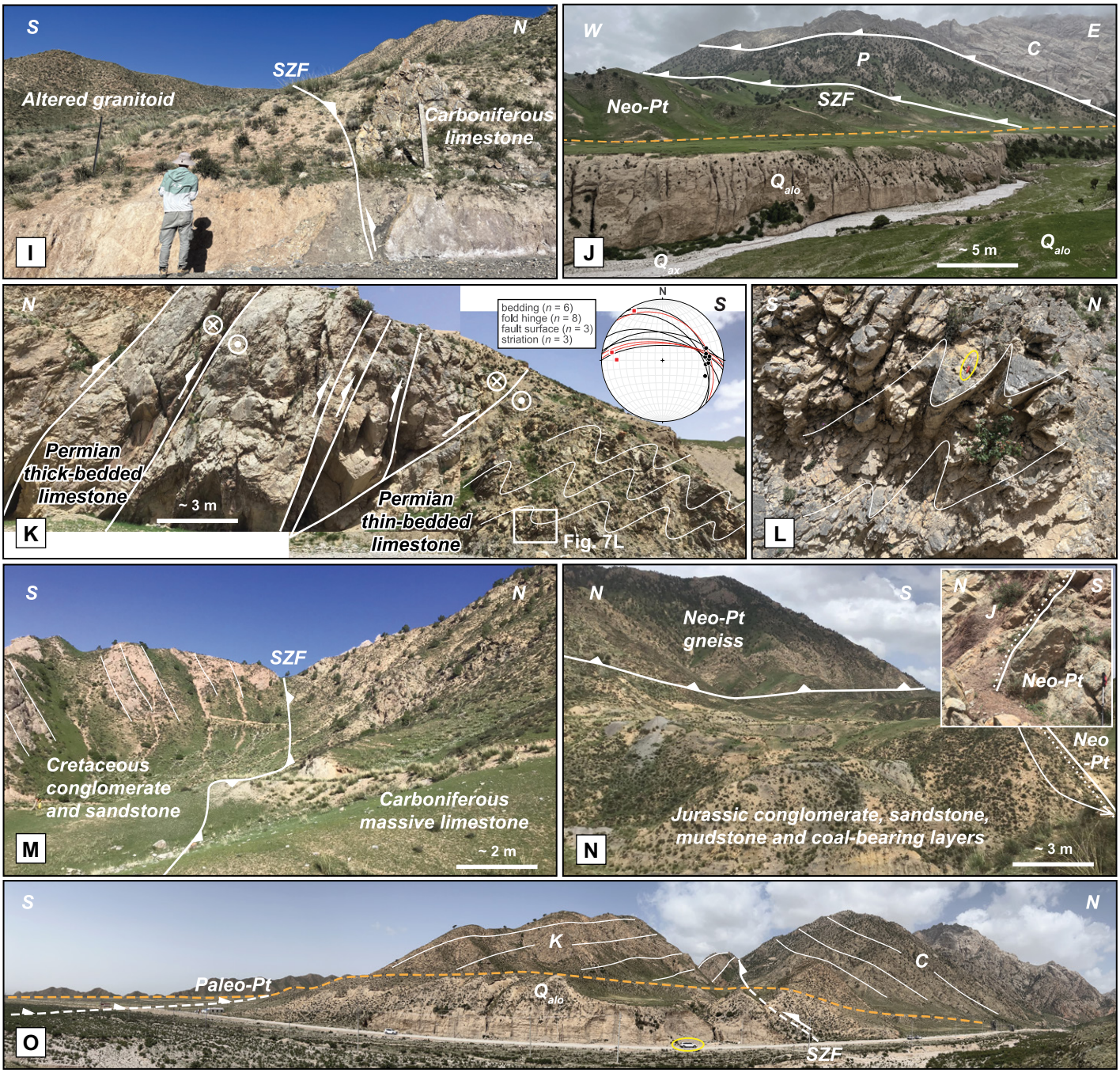

Figure 7. (*Continued*)

Figure 8. Representative field photographs and sketches showing structures associated with faults f4 and f5 and related deformation. (A) Annotated photograph of the north-directed f4 thrust and a well-developed hanging-wall anticline. Hanging-wall rocks consist of Carboniferous limestone and clastic rocks and Neoproterozoic (Neo-Pt) rocks. (B–D) Kinematic indicators indicate left-slip thrust kinematics. (E, F) Fault f5 thrust places Carboniferous limestone, marble, and phyllite over Triassic sandstone and limestone. NZF—North Zongwulongshan fault. (G, H) A west-plunging anticline in the western part of the study area is composed of Carboniferous massive limestone (C_b), marble, and phyllite (C_a). (I–N) Small-scale folds in Neoproterozoic thin-bedded argillaceous banded limestone in the core of the fold. Axial planes of folds are vertical, and hinge lines plunge to the west. Note the rounded and sharp hinges of folds. (O–Q) Ductilely folded and sheared meta-sandstone (brown) and phyllite (dark gray). The folds show that more rigid sandstone layers were disrupted by layer-parallel extension and thickened by folding and small-scale shear zones. Metapelite appears to have filled gaps in the sandstone layer by ductile flow, and meta-quartz fluids occur in the metapelite as irregular boudins. The pronounced difference in the style of deformation reflects the different rheological properties of the two sedimentary packages. Note that the format of planar structure attitudes is strike/dip and dip quadrant. (*Continued*)

metamorphic rocks were analyzed for U-Pb crystallization ages using an Agilent 7500a laser ablation–inductively coupled plasma–mass spectrometer (LA-ICP-MS) at the Key Laboratory of Continental Collision and Plateau Uplift, Institute of Tibetan Plateau Research, Chinese Academy of Sciences, Beijing, China. Prior to analysis, zircon grains were separated from whole-rock samples using standard pro-

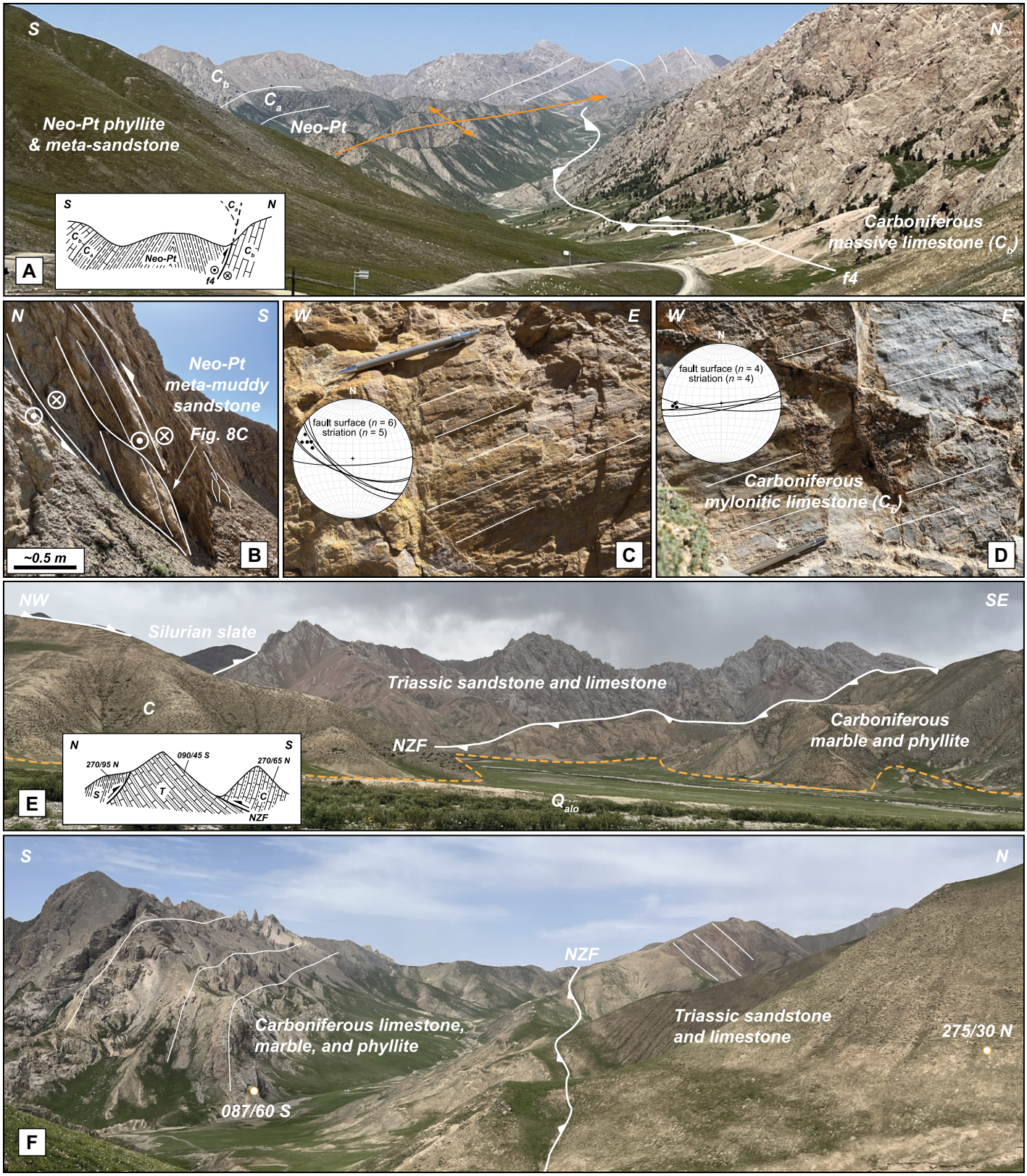

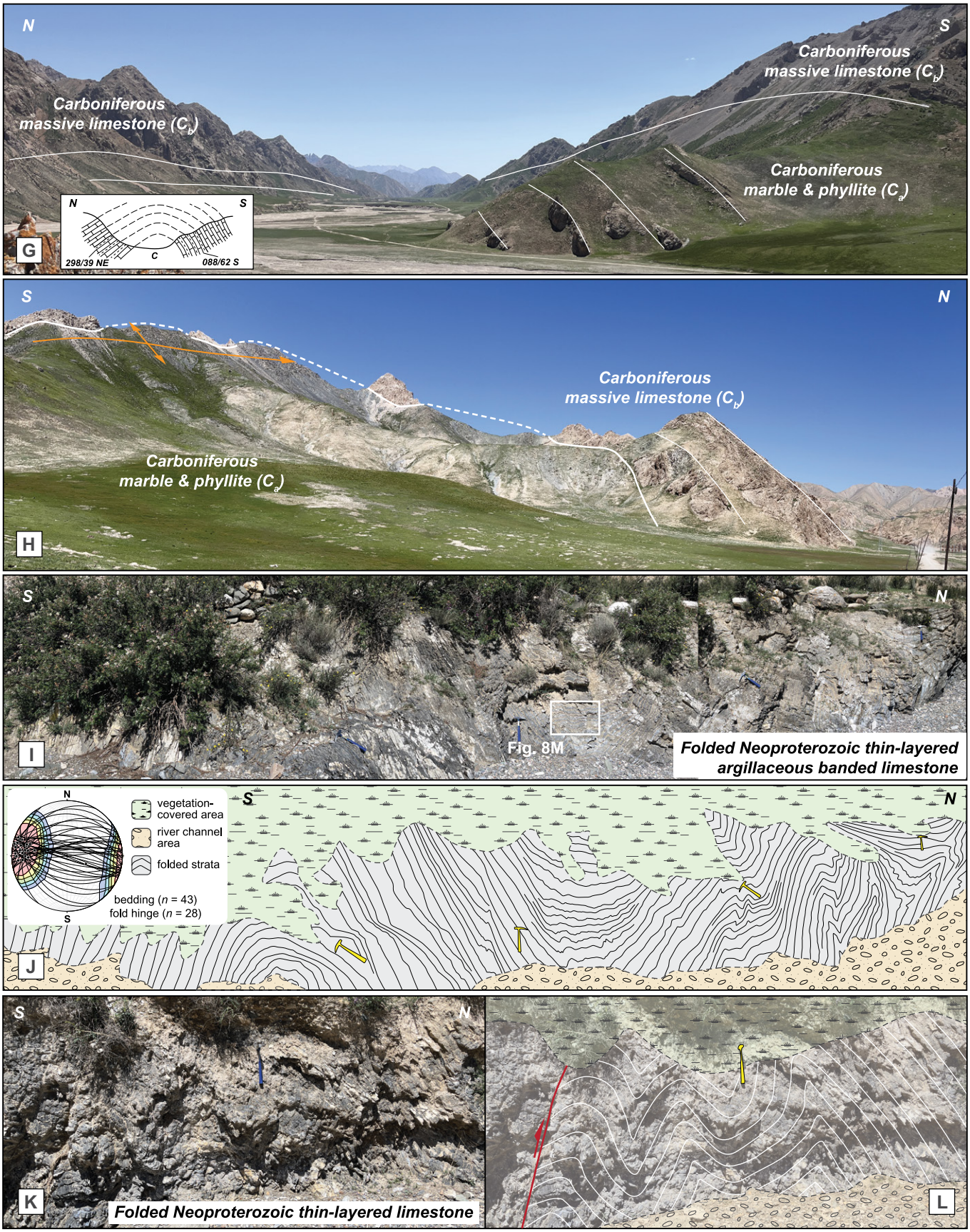

Figure 8. (*Continued*)

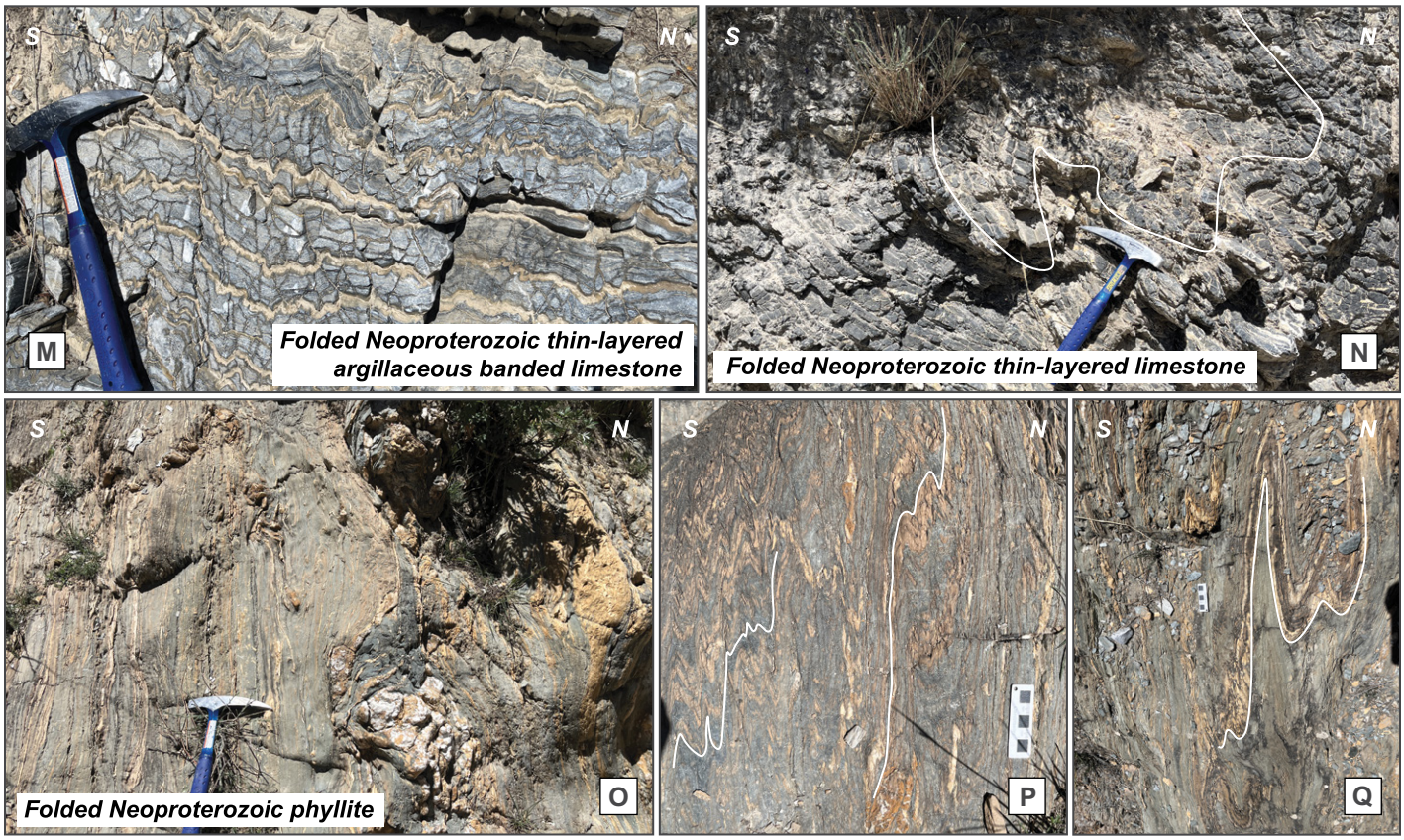

Figure 8. (*Continued*)

cedures, including handpicking from heavy-mineral yields under a binocular microscope, and mounted in epoxy resin with standard zircon grains at the Institute of the Hebei Regional Geology and Mineral Survey, Langfang, China. Cathodoluminescence (CL) images were collected using a scanning electron microscope (SEM) at Beijing Geoanalysis Co., Ltd., Beijing, China, to observe any internal texture. Considering zircon grain sizes and signal stability, we used ~30-μm-diameter ablation spots for all selected grains. U-Pb isotopic ratios ($^{206}Pb/^{238}U$, $^{207}Pb/^{235}U$, and $^{207}Pb/^{206}Pb$) and fractionation corrections were calculated using the GLITTER 4.0 program (Macquarie University, Sydney, Australia; http://gemoc.mq.edu.au/glitter/home.html) and corrected for common lead (Andersen, 2002). The $^{206}Pb/^{238}U$ ages are reported for zircon grains younger than 1000 Ma, and $^{207}Pb/^{206}Pb$ ages are reported for grains older than 1000 Ma (Ludwig, 2003). Weighted mean ages, concordia diagrams, and relative probability plots were generated using Isoplot/Ex (Ludwig, 2003). Isotopic data for all zircon analyses are shown in Table S1 in the Supplemental Material[1]. Analyses were excluded based on low radiogenic lead concentrations, large analytical errors, inherited zircon grains that were signifi-

[1]Supplemental Material. Table S1: LA-ICP-MS results of zircon U-Pb geochronology from this study. Table S2: LA-ICP-MS results of zircon U-Pb geochronology from previous studies. Please visit https://doi.org/10.1130/GSAB.S.25814542 to access the supplemental material; contact editing@geosociety.org with any questions.

TABLE 1. SUMMARY OF SAMPLE LOCATIONS IN THE ZONGWULONG SHAN–QINGHAI NANSHAN REGION, NORTHERN TIBETAN PLATEAU

Sample number	Rock type	Age	Latitude (°N)	Longitude (°E)	Elevation (m)	Numbers in figures
QL20220624-1	Sandstone	Triassic	36°26′47.55″	100°4′23.12″	3370	12
QL20220628-4	Sandstone	Triassic	36°46′17.10″	99°38′51.25″	3471	13
QL20220628-7	Sandstone	Triassic	36°42′12.24″	99°31′30.63″	3513	14
QL20220701-2	Sandstone	Carboniferous	37°24′37.83″	98°08′19.19″	3675	6
QL20220702-3	Sandstone	Triassic	37°32′14.36″	96°53′07.94″	3675	10
QL20220705-5	Sandstone	Neoproterozoic	37°38′15.00″	97°16′00.24″	4142	3
QL20220707-2	Sandstone	Triassic	37°31′38.89″	97°42′15.20″	4015	9
QL20220707-3	Sandy slate	Neoproterozoic	37°29′15.73″	97°38′01.15″	3610	4
QL20220708-2	Sandstone	Triassic	37°25′58.86″	97°43′20.86″	3273	7
QL20220709-2	Sandstone	Triassic	37°25′59.36″	97°38′30.35″	3544	8
QL20220712-2A	Sandstone	Triassic	37°32′23.73″	97°24′22.52″	3983	11
QL20220713-10	Leucogranite vein	Permian	37°25′14.86″	97°28′15.27″	3402	1
QL20220713-11	Leucogranite vein	Permian	37°25′15.60″	97°28′15.63″	3413	2
QL20220713-15-1	Garnet-bearing mica quartz schist	Neoproterozoic	37°25′18.90″	97°28′16.83″	3414	5

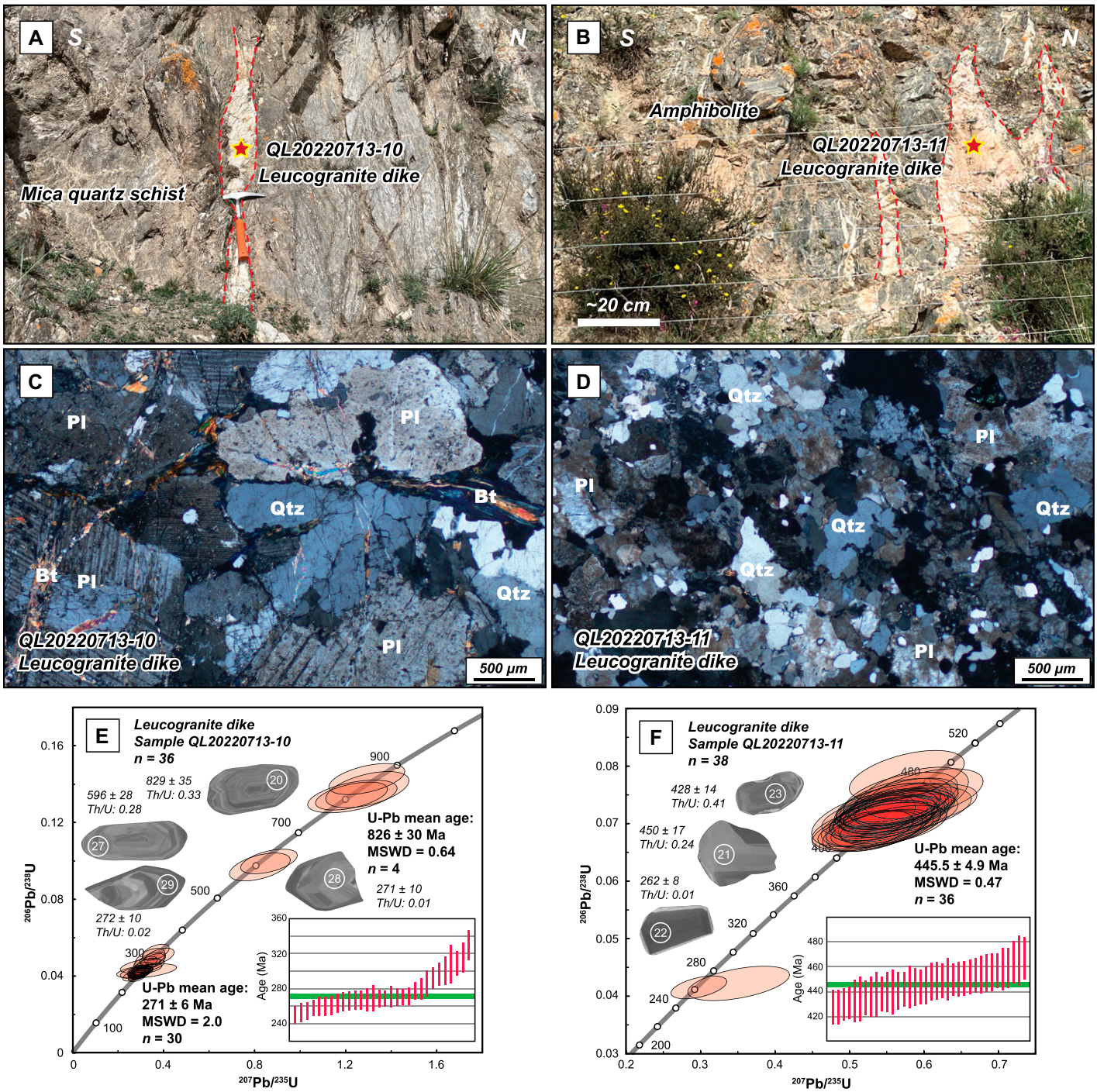

Figure 9. (A) An ~20-cm-wide gray to white leucogranite dike (sample QL20220713-10) intruding Neoproterozoic gray to dark-gray mica quartz schist. (B) Gray leucogranite dikes (QL20220713-11) intrude early Paleozoic amphibolite-facies metamorphic rocks. (C, D) Photomicrographs of two leucogranite samples. Bt—biotite; Pl—plagioclase; Qtz—quartz. (E, F) U-Pb concordia diagrams, weighted mean ages, and representative zircon cathodoluminescence images for two leucogranite samples. Error ellipses are 2σ. Circles represent ~30 μm analyzed spots for U-Pb dating. The numbers in the circles represent the experimental sampling numbers. MSWD—mean square of weighted deviates.

cantly older than the dominant zircon-age population, and discordant ages. We calculated the weighted mean age of the youngest population of concordant analyses to estimate the crystallization age of the magmatic samples.

4.2. U-Pb Detrital Zircon U-Pb Dating

We performed detrital zircon U-Pb geochronology on 12 samples from Carboniferous–Triassic strata to determine the detrital provenance, distinguish lithologic units, and test correlations between rocks in the North Qaidam region to the south and the South Qilian region to the north (Table 1). Isotopic data for all detrital zircon analyses are shown

in Table S1. Prior to analysis, zircon grains were separated from whole-rock samples at the Institute of the Hebei Regional Geology and Mineral Survey, Langfang, China, using standard procedures, including mounting on epoxy rounds with 91500 zircon standards (ca. 1065 Ma age; Wiedenbeck et al., 1995) and polishing with carbide paper. Zircon grains were analyzed via LA-ICP-MS at the Key Laboratory of Continental Collision and Plateau Uplift, Institute of Tibetan Plateau Research, Chinese Academy of Sciences, Beijing (for detailed analytical methods, see Xie et al., 2008). Spot sizes of ~30 μm were shot with a laser at a 10 Hz pulse rate.

5. LITHOLOGIC DESCRIPTIONS AND RESULTS OF ZIRCON U-Pb GEOCHRONOLOGY

5.1. Igneous Rocks

Two samples of undeformed, gray leucogranite dikes (QL20220713-10 and QL20220713-11; sites 1 and 2 in Figs. 2 and 4, respectively) that intrude Neoproterozoic metamorphic rocks were analyzed (Figs. 9A and 9B; Table 1). The main mineral assemblages included quartz, plagioclase, and minor biotite. Plagioclase grains were characterized by polysynthetic and gridiron twinning and light clay development and chloritization (Figs. 9C and 9D). CL images of representative zircon grains are shown in Figures 9E and 9F. Zircon grains were typically ~100–150 μm long, transparent in color, and prismatic in shape. Edges of some zircon grains were straight and broken, and minor grains were subrounded. Most zircon grains showed typical oscillatory zoning in CL images, whereas some grains exhibited the characteristics of metamorphism such as accretive and vague zoning.

Zircon U-Pb ages of the leucogranite dikes were found to be clustered at ca. 330–250 Ma, ca. 486–428 Ma, ca. 613–596 Ma, and ca. 860–809 Ma (Figs. 9E and 9F; Table S1). The youngest age cluster yielded a weighted mean age of 271 ± 6 Ma (mean square of weighted deviates [MSWD = 2.0]; $n = 30$), which we interpret as representing the crystallization age of the leucogranite. Several older age populations are interpreted to be inherited due to their similarity with the ages of surrounding wall rocks.

5.2. Metasedimentary Samples

Twelve Neoproterozoic–Triassic detrital zircon samples were collected from the Zongwulong Shan–Qinghai Nanshan and analyzed by LA-ICP-MS dating (Figs. 10 and 11).

5.2.1. Neoproterozoic Strata of the Zongwulong Shan

We collected three samples of Neoproterozoic strata from the Zongwulong Shan, including sandstone sample QL20220705-5 (site 3 in Figs. 2, 4, and 10A) from the northern side of the North Zongwulong thrust fault, sandy slate sample QL20220707-3 (site 4 in Figs. 2, 4, and 10B) from the core of the Zongwulong Shan, and garnet mica quartz schist sample QL20220713-15-1 (site 5 in Figs. 2, 4, and 10C) from the southern side of the South Zongwulong thrust fault. Zircon grains from these three samples were colorless and had subangular to rounded morphologies (Figs. 11A–11C). Grains were ~50–200 μm long and had aspect ratios of 1:1–5:1. Most grains displayed oscillatory or banded zoning. Grain Th/U ratios were found to be 0.1–3.4 (Figs. 11A–11C and 11A′–11C′; Table S1).

Sample QL20220705-5 yielded three dominant age clusters at ca. 867–793 Ma (~37%), ca. 1883–1824 Ma (~10%), and ca. 2724–2314 Ma (~33%), with age peaks at ca. 816 Ma, ca. 1865 Ma, and ca. 2622 Ma, respectively (Fig. 11A′). The two youngest detrital zircons ages were found to be ca. 766 Ma and ca. 772 Ma, which correspond to a weighted mean age of 770 ± 37 Ma (MSWD = 0.021; Fig. 11A). Sample QL20220707-3 yielded a dominant age cluster at ca. 951–825 Ma (~66%), with an age peak at ca. 864 Ma. Minor age clusters occurred at ca. 1756 Ma and ca. 2454 Ma. The three youngest detrital zircon ages were found to be ca. 590 Ma, ca. 602 Ma, and ca. 617 Ma, which correspond to a weighted mean age of 603 ± 39 Ma (MSWD = 0.14; Figs. 11B and 11B′).

Sample QL20220713-15-1 yielded a dominant age cluster at ca. 879–634 Ma (~66%), with an age peak at ca. 816 Ma. The remaining zircon ages were ca. 488–416 Ma (~6%) and ca. 2767–2533 Ma (~14%), with age peaks at ca. 454 Ma and ca. 2588 Ma, respectively. Early Paleozoic zircon grains from this sample showed characteristics of metamorphic origin, such as low Th/U values (<0.1) and unclear CL zoning (Figs. 11C and 11C′).

5.2.2. Carboniferous Strata of the Zongwulong Shan

We collected Carboniferous sandstone sample QL20220701-2 from the central-eastern portion of the Zongwulong Shan (site 6 in Figs. 2, 4, and 10D). Most zircon grains were colorless and subrounded and exhibited magmatic oscillatory or banded zoning (Fig. 11D). Grains had long-axis lengths of ~50–100 μm and aspect ratios of 1:1–3:1. Grain Th/U ratios were found to be 0.04–1.6, suggesting some metamorphic origins (Figs. 11D and 11D′; Table S1). The sample yielded a dominant age cluster at ca. 511–427 Ma (~69%), with an age peak at ca. 442 Ma. A broad age cluster occurred at ca. 2628–661 Ma, with peaks at ca. 883 Ma, ca. 1812 Ma, and ca. 2489 Ma (Figs. 11D and 11D′). The four youngest zircon ages yielded a weighted mean age of 421.2 ± 9.7 Ma (MSWD = 0.7).

5.2.3. Triassic Strata around the Zongwulong Shan

We collected two samples of Triassic sandstone (samples QL20220708-2 and QL20220709-2; sites 7 and 8 in Figs. 2, 4, 10E, and 10F) from the southern side of the South Zongwulong thrust fault. Zircon grains from both samples were subrounded and had long-axis lengths of ~50–150 μm and aspect ratios of 1:1–3:1. Most grains exhibited oscillatory zoning, although few grains showed metamorphic characteristics in CL images. Grain Th/U values were found to be 0.005–2.55 (Figs. 11E, 11F, 11E′, and 11F′; Table S1).

Sample QL20220708-2 yielded dominant age clusters at ca. 462–419 Ma (~24%) and ca. 988–899 Ma (~27%), with age peaks at ca. 433 Ma and ca. 939 Ma. Approximately 33% of grains had ca. 2514–1294 Ma ages, with age peaks at ca. 1470 Ma and ca. 2464 Ma (Fig. 11E′).

Sample QL20220709-2 yielded dominant age clusters at ca. 503–374 Ma (~34%) and ca. 991–872 Ma (~27%), with age peaks at ca. 442 Ma and ca. 945 Ma. Approximately 20% of the grains had ca. 2628–1525 Ma ages, with age peaks at ca. 1558 Ma and ca. 2484 Ma (Figs. 11F and 11F′). The three youngest detrital zircon ages were ca. 279 Ma, ca. 280 Ma, and ca. 294 Ma, which correspond to a weighted mean age of 283.6 ± 9.4 Ma (MSWD = 0.93). Early Paleozoic zircon grains showed characteristics of metamorphic origin, such as low Th/U values (<0.1) and unclear zoning in CL images.

We collected three Triassic sandstone samples (QL20220707-2, QL20220702-3, and QL20220712-2A; sites 9, 10, and 11 in Figs. 2 and 10G–10I, respectively) from the South Qilian region, adjacent to the northern margin of the Zongwulong Shan. Most zircon grains were subrounded and displayed magmatic oscillatory and weak banded zoning. Grains had long-axis lengths of~30–300 μm and aspect ratios of 1:1–5:1 (Figs. 11G–11I and 11G′–11I′).

Sample QL20220707-2 yielded a dominant age cluster at ca. 406–509 Ma (~21%), with an age peak at ca. 442 Ma. Approximately 8% of the analyses from sample QL20220707-2 were younger than 300 Ma. A minor age peak occurred at ca. 934 Ma (~5%). Nearly 60% of the ages were found to be ca. 2538–1537 Ma, with two age peaks at ca. 1880 Ma

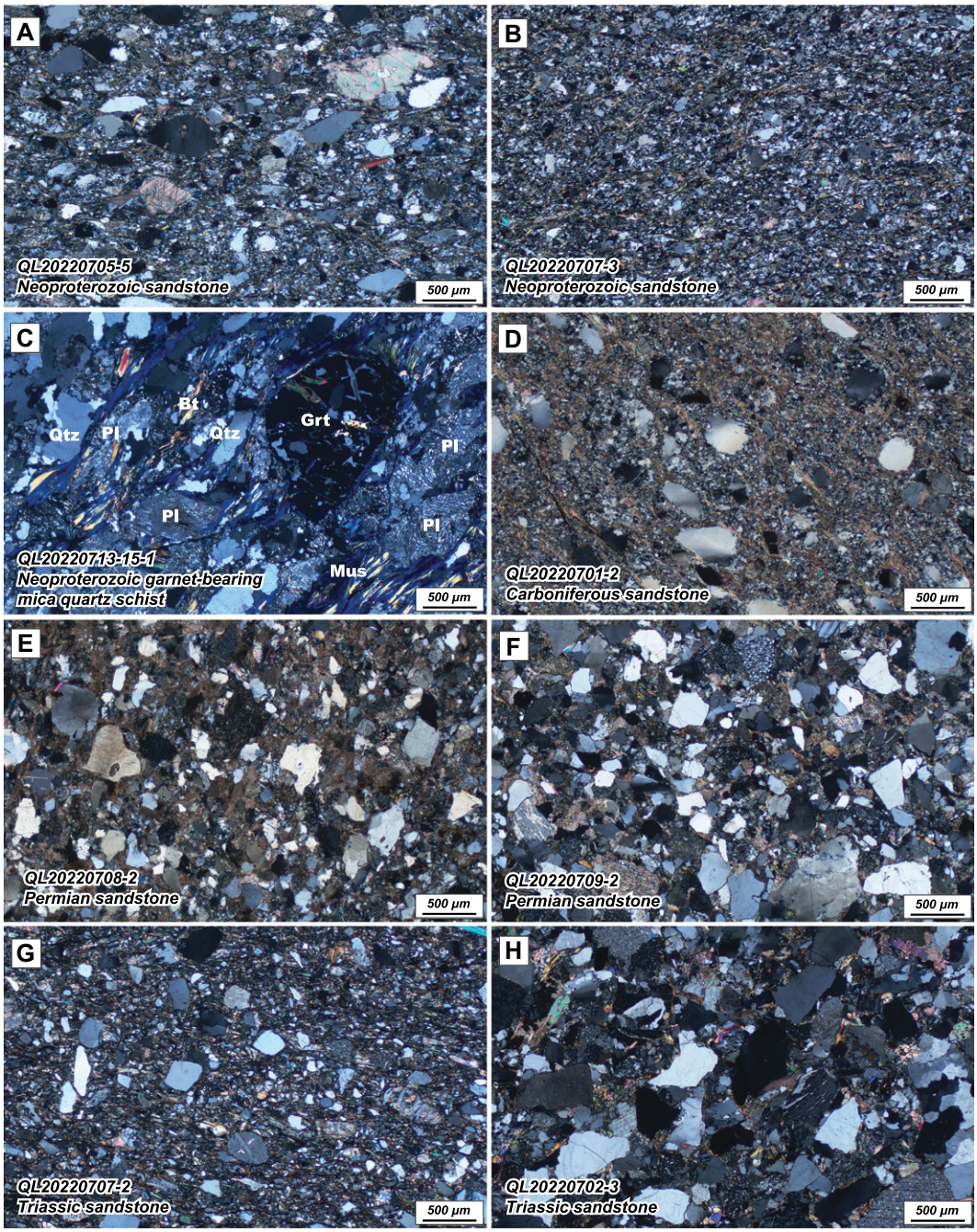

Figure 10. Photomicrographs in cross-polarized light of collected (meta-)sedimentary rocks showing the main mineral and detrital assemblages and petrological textures. Bt—biotite; Grt—garnet; Mus—muscovite; Pl—plagioclase; Qtz—quartz. (*Continued*)

and ca. 2360 Ma. Few ages were clustered at ca. 3520 Ma. The four youngest ages were ca. 271 Ma, ca. 274 Ma, ca. 275 Ma, and ca. 279 Ma, which correspond to a weighted mean age of 275 ± 14 Ma (MSWD = 0.05; Figs. 11G and 11G′).

Sample QL20220702-3 yielded a dominant age cluster at ca. 286–236 Ma (53%). The remaining ages displayed a discontinuous distribution from ca. 2518 Ma to 340 Ma, with several age peaks at ca. 448 Ma, ca. 861 Ma, ca. 1996 Ma, and ca. 2402 Ma. The five youngest ages were ca. 236 Ma, ca. 237 Ma, ca. 242 Ma, ca. 243 Ma, and ca. 244 Ma, which correspond to a weighted mean age of 240.5 ± 5 Ma (MSWD = 0.39; Figs. 11H and 11H′). Ages younger than 500 Ma accounted for ~26% of total dated grains and had two age peaks at ca. 270 Ma and ca. 416 Ma. Several grains of ca. 911 Ma ages were also recorded. The remaining age clusters were ca. 2077–783 Ma (~60%) and ca. 2652–2315 Ma (~14%), with age peaks at ca. 1793 Ma and ca. 2396 Ma, respectively (Figs. 11I and 11I′).

5.2.4. Triassic Strata of the Qinghai Nanshan

We collected three Triassic sandstone samples (QL20220624-1, QL20220628-4, and QL20220628-7; sites 12, 13, and 14 in Figs. 2 and 10J–10L, respectively) from the Qinghai Nanshan. Most zircon grains were subrounded and displayed magmatic oscillatory zoning and dim internal structure. Grains had long-axis lengths of ~50–200 μm and aspect ratios of 1:1–5:1 (Figs. 11J–11L and 11J′–11L′).

Approximately 44% of zircon ages from sample QL20220624-1 were found to be

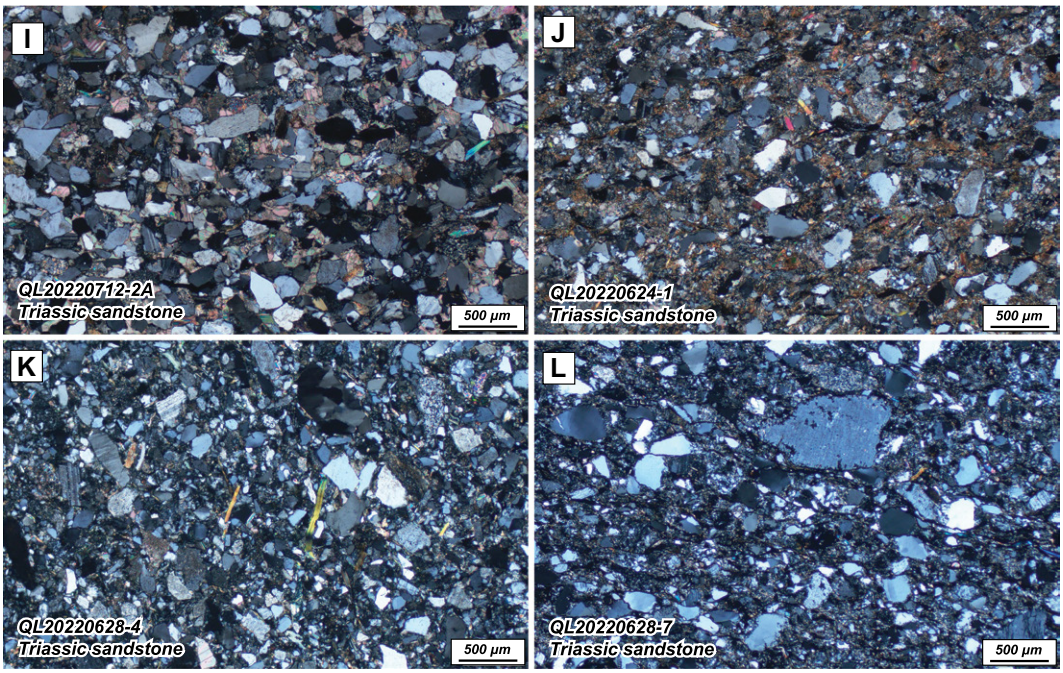

Figure 10. (*Continued*)

younger than 450 Ma, with an age peak of ca. 390 Ma. The ca. 1064–706 Ma grains (~16%) had age peaks of ca. 830 Ma and ca. 1009 Ma. The remaining ages (~40%) were ca. 2543–1635 Ma, with an age gap at ca. 2335–1981 Ma and peaks of ca. 1723 Ma, ca. 1943 Ma, and ca. 2429 Ma. The two youngest detrital zircon ages were ca. 255 Ma and ca. 256 Ma, which corresponds to a weighted mean age of 256 ± 21 Ma (MSWD = 0.002; Figs. 11J and 11J′).

Approximately 24% of zircon ages from sample QL20220628-4 were younger than 450 Ma, with age peaks of ca. 270 Ma and ca. 422 Ma. Several grains with ages ca. 878 Ma were also recorded. Ages were mainly distributed between ca. 1939 Ma and ca. 1551 Ma (~54%), with an age peak at ca. 1792 Ma. The remaining ages (~11%) were ca. 2728–2320 Ma, with age peaks of ca. 2379 Ma and ca. 2720 Ma. The two youngest zircon ages were ca. 246 Ma and ca. 248 Ma, which correspond to a weighted mean age of 247 ± 9 Ma (MSWD = 0.047; Figs. 11K and 11K′).

Approximately 65% of zircon ages from sample QL20220628-7 were younger than 500 Ma, with two age peaks of ca. 248 Ma and ca. 420 Ma. Approximately 16% of ages were ca. 1093–707 Ma, with a peak at ca. 892 Ma. The remaining ages (~17%) were ca. 2555–1712 Ma, with weakly defined age peaks at ca. 1940 Ma and ca. 2363 Ma. The three youngest zircon ages were ca. 227 Ma, ca. 235 Ma, and ca. 240 Ma, which correspond to a weighted mean age of 234 ± 11 Ma (MSWD = 0.47; Figs. 11L and 11L′).

6. DISCUSSION

6.1. Detrital Provenance and Stratigraphic Analysis

The Neoproterozoic strata sample QL20220705-5 contains zircon ages between ca. 3000 Ma and 700 Ma, with a dominant ca. 870–760 Ma age cluster and two minor clusters at ca. 1900–1600 Ma and ca. 2800–2300 Ma (Figs. 11A′ and 12A). The Balonggonggaer Group of the South Qilian region shares similar detrital zircon ages with Neoproterozoic strata, indicating that the former rocks located adjacent to the Zongwulong Shan were deposited in the Neoproterozoic (Fig. 12A; Li et al., 2019). Sample QL20220713-15-1 and previously collected samples from the North Qaidam region on the southern side of the South Zongwulong thrust fault are characterized by a ca. 900–660 Ma age cluster and minor clusters at ca. 490–410 Ma, ca. 2000–1700 Ga, and ca. 2700–2400 Ma (Figs. 11C′ and 12A; Yu et al., 2017b). All early Paleozoic zircon grains show evidence of metamorphism, such as low Th/U values, core-mantle structures, and unclear zoning in CL images (Figs. 11C and 11C′), suggesting that Neoproterozoic strata in the North Qaidam region experienced early Paleozoic high-grade metamorphism. Metasedimentary samples collected from the core of the Zongwulong Shan (sample QL20220707-3; Peng et al., 2018) that were previously assigned Carboniferous–Permian ages show a dominant age cluster at ca. 950–600 Ma and two older age peaks at ca. 1750 Ma and ca. 2450 Ma (Figs. 11B′ and 12A). These ages from Neoproterozoic rocks suggest that the Zongwulong Shan has a Precambrian rock component, which allows for correlation with similar-aged rocks in the North Qaidam and South Qilian regions (Fig. 12A).

Detrital zircons from Carboniferous–Permian strata in the Zongwulong Shan have a dominant ca. 445 Ma age and minor age clusters at ca. 280 Ma, ca. 880 Ma, ca. 1800 Ma, and 2450 Ma (Figs. 11D′ and 12B). The shared ages and similar lithologies among the Carboniferous–Permian strata suggest that they are correlative (Peng et al., 2018; Zhao, 2023). The abundant early Paleozoic and minor late Paleozoic zircon grains in the Carboniferous strata show characteristics of a magmatic origin and a proximal source that may have been the South Qilian and North Qaidam regions (Fig. 11D; Zhang et al., 2016; Chang, 2017; Yu et al., 2017b; Qin, 2018; Li et al., 2022a). Carboniferous–Permian strata also yield minor early Paleozoic metamorphic zircons potentially sourced from the northern Qaidam metamorphic belt, suggesting that the belt may have been uplifted and eroded during the Carboniferous (Fig. 11D).

The basal Triassic strata on the southern side of the South Zongwulong thrust fault are characterized by weak sorting and size-independent conglomerate, and gravel-sized clasts are dominantly composed of limestone and slate derived from Carboniferous–Permian rocks in the Zongwulong Shan (Figs. 5E and 5F). These observations suggest that the Triassic strata were deposited in a molasse

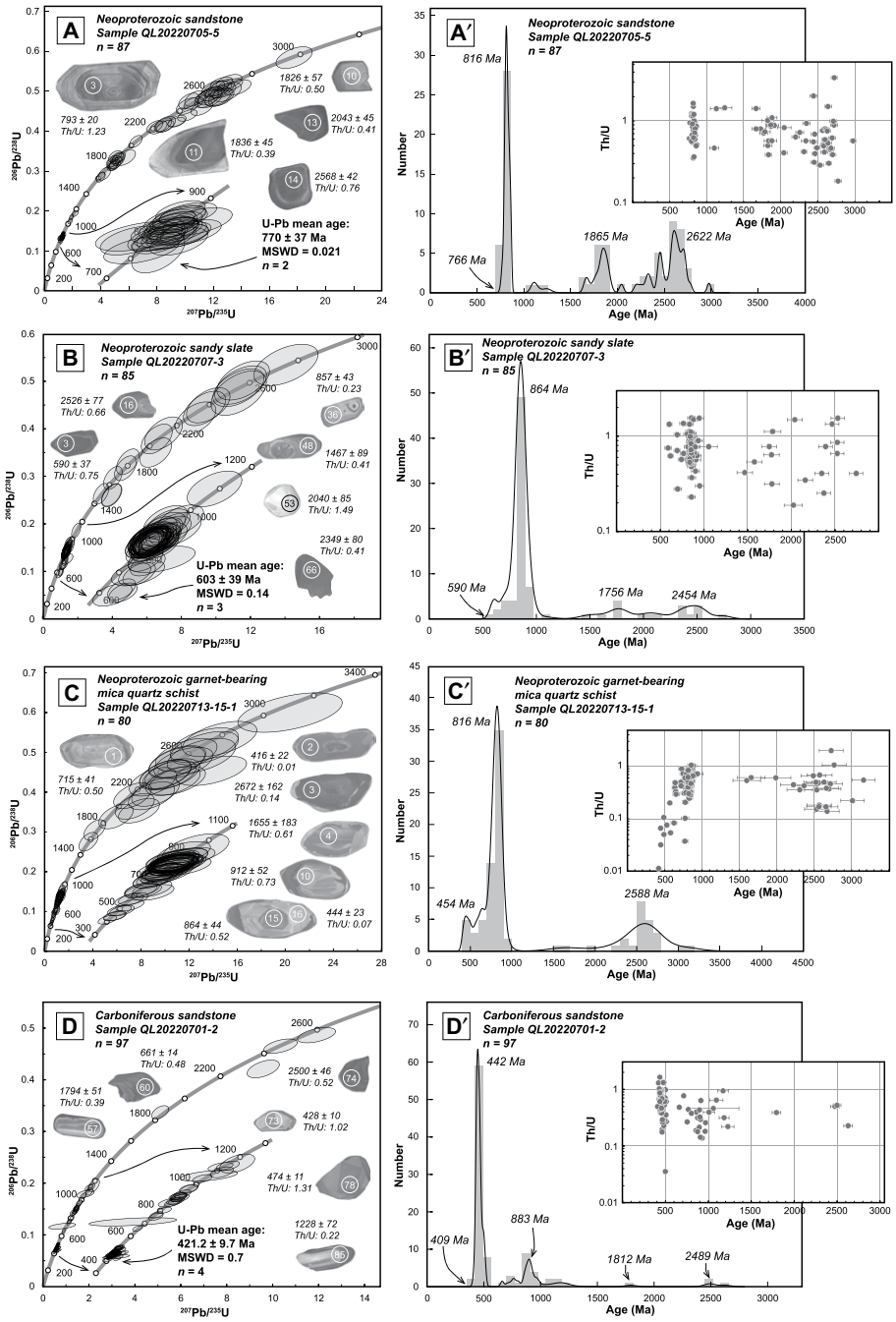

Figure 11. (A–L) U-Pb concordia diagrams showing results of single-shot zircon analyses, and representative cathodoluminescence (CL) images of detrital zircon grains for each sample showing ages in Ma and Th/U ratios. Error ellipses are 2σ. Circles represent ~30 μm analyzed spots for U-Pb dating. The numbers in the circles represent the analytical sampling numbers. (A′–L′) Relative probability plots of U-Pb detrital zircon ages for sedimentary rocks and insets showing detrital zircon age distributions and relationships between ages and Th/U values. MSWD—mean square of weighted deviates. (*Continued*)

basin. Detrital zircon ages of strata on the southern side of the South Zongwulong thrust fault are nearly identical with those of Carboniferous–Permian rocks in the Zongwulong Shan, including enrichment in Neoproterozoic grains (Fig. 12C). This implies that detrital materials may have been derived from the Zongwulong Shan and North Qaidam regions and were deposited after ca. 250 Ma in a foreland basin (Figs. 11E, 11F, and 12C; Tables S1 and S2). The detrital zircon age populations of Triassic strata from the South Qilian and Qinghai Nanshan are similar and involve abundant late Permian–Early Triassic magmatic records, indicating a common source in the south. In addition, the Zongwulong Shan–Qinghai Nanshan likely was not the significant detrital source during the Late Triassic, which provided sediment that was transported to the north (Figs. 11G–11L and 12C).

6.2. Nature of the Zongwulong Shan–Qinghai Nanshan

In several of the tectonic reconstructions of the Zongwulong Shan–Qinghai Nanshan, the exposures of ophiolite and mélange complexes, arc plutons, and flysch deposits have been used as evidence to suggest that this belt resulted from the southward subduction and closure of a limited ocean in the late Paleozoic–early Mesozoic (Wang et al., 2001; Guo et al., 2009; Li, 2017; Wu et al., 2019b; Chen et al., 2020b; Zhuang et al., 2020). However, recent geologic observations require modification of this previous interpretation. First, updated geochronology has confirmed the ophiolitic mélange exposed in this belt is actually early Paleozoic in age (Wang et al., 2001; Fu et al., 2021), not late Paleozoic. Second, the exposure of late Paleozoic–early Mesozoic arc-related plutons (Peng et al., 2016a; Chen et al., 2020a; Chen et al., 2020b; Yang et al., 2022; Zou et al., 2022; Wang et al., 2023) has been more recently interpreted as the products of subduction of the north-dipping Neo-Kunlun (Paleo-Tethys) oceanic slab along a margin located to the south (Fig. 2; Wu et al., 2016, 2022), not a local arc-subduction system. Finally, Mesozoic and Cenozoic intracontinental deformation has partly modified the original geological configuration (Yin et al., 2007; Cheng et al., 2019; Lin et al., 2021).

Any viable model for the Zongwulong Shan–Qinghai Nanshan must explain the following key observations: (1) the Carboniferous strata are thicker here and lie unconformably on the Neoproterozoic basement, whereas to the north and south, the Permian strata overlie Precambrian bedrock (Figs. 5 and 6); (2) the rift-related rock assemblage of alkaline middle-mafic volcanic rock, shallow-marine flysch clastic deposits, and carbonate rocks outcrops in this belt (Figs. 7 and 8; Li and Nie, 1985; Li, 2017; Xu et al., 2019); (3) the thrust faults exhibit some out-of-sequence structural relationships, like younger-on-older strata, which are atypical for a classic thrust fault (Figs. 4, 7, and 8); and (4) the Triassic molasse-like deposits external to

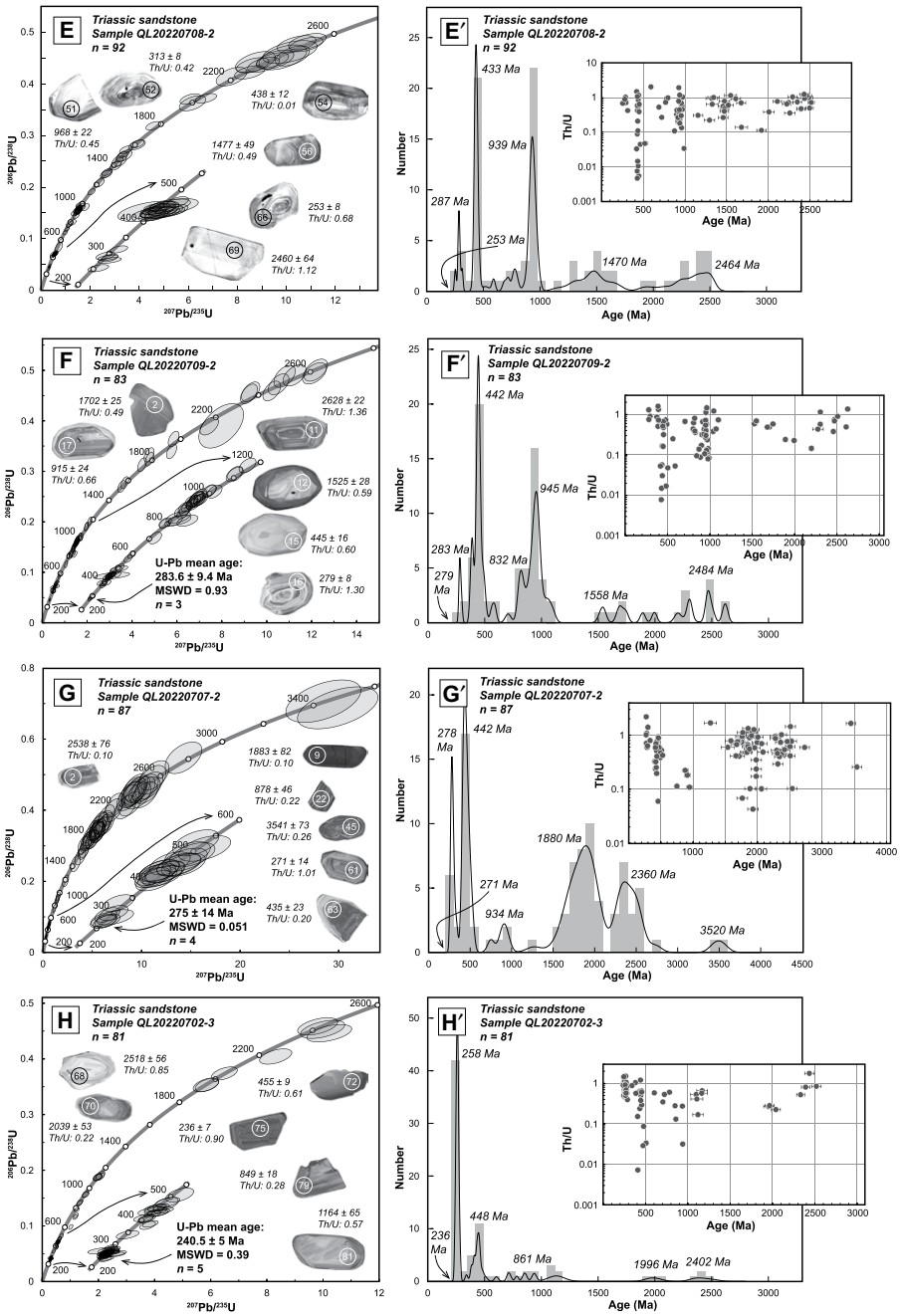

Figure 11. (*Continued*)

the interpreted rift basin can be used to imply uplift and therefore thrust-fault activity during contractional reactivation of this basin (Figs. 4 and 5; Zhao et al., 2022). These relationships do not support the scenario where the Zongwulong Shan–Qinghai Nanshan region experienced the opening and closing of an oceanic basin in the late Paleozoic, but rather they suggest a relatively narrow region of crustal extension and thinning in the late Paleozoic. This late Paleozoic extensional sedimentary basin contains shallow-marine-related deposits and mantle-derived volcanic records and was inverted and uplifted in the Early Triassic, which is supported by the molasse-like rock records.

In light of these considerations, we interpret that a late Paleozoic intracontinental rift basin operated along the southern edge of the South Qilian continent (Li and Nie, 1985). This explains the lack of late Paleozoic oceanic materials and minor volumes of synchronous mantle-derived magmatism. Across the Qinghai Nanshan and the Eastern Kunlun Range, the wide belt of Permian–Triassic arc plutons that generally are younger to the south can be explained by a southward rollback of the Neo-Kunlun (Paleo-Tethys) oceanic slab (Wu et al., 2016, 2022). This also explains why Triassic arc plutons intrude contemporaneous flysch sediments in the Qinghai Nanshan (Fig. 2). Based on the similar lithological assemblages and geologic histories, it has been argued that the rift basin gradually disappears in the Da Qaidam area to the west and may extend to the Jianzha-Tongren area to the east or farther east (Fig. 2; Guo et al., 2009; Wang et al., 2010). Previous studies suggested that the eastern rift basin may have undergone greater crustal extension, leading to the formation of new oceanic crust (Wang et al., 2010).

6.3. Deformation Stages of the Zongwulong Shan–Qinghai Nanshan

Based on geological mapping, we constrained the stratigraphic and structural relationships among the North Qaidam region, Zongwulong Shan region, and South Qilian region (Fig. 4). Our field observations also allowed us to elucidate the complex deformation history of the Zongwulong Shan–Qinghai Nanshan, including the slip histories of the South Zongwulong thrust fault and North Zongwulong thrust fault, which had protracted lifespans and may have been inverted and reactivated. Our interpretations regarding the deformation styles and timing of activity in the Zongwulong Shan–Qinghai Nanshan are based on the following key observations: (1) the South Zongwulong thrust fault and North Zongwulong thrust fault are the main rift-bounding faults that controlled the distribution and sedimentary records of Carboniferous–Triassic strata within the region; (2) out-of-sequence thrusting along the South Zongwulong thrust fault and North Zongwulong thrust fault placed younger Carboniferous–Permian strata over older Neoproterozoic rocks; (3) the tectonic belt contains a broad, east-trending anticlinorium composed of Neoproterozoic and Carboniferous strata, and the timing of ductile shearing in the fold core is Early–Middle Triassic (Gao et al., 2021); and (4) the South Zongwulong thrust fault and North Zongwulong thrust fault juxtapose rift-related strata over Cretaceous and younger strata.

From these observations, we present a brief deformation history of the Zongwulong Shan–Qinghai Nanshan. In the early Carboniferous, intracontinental rifting led to the formation of the South Zongwulong thrust fault and North Zongwulong thrust fault as major rift-bounding normal faults, which created space in their hanging walls for infill deposits (Figs. 13A and 13B). By the end of the Early–Middle Triassic,

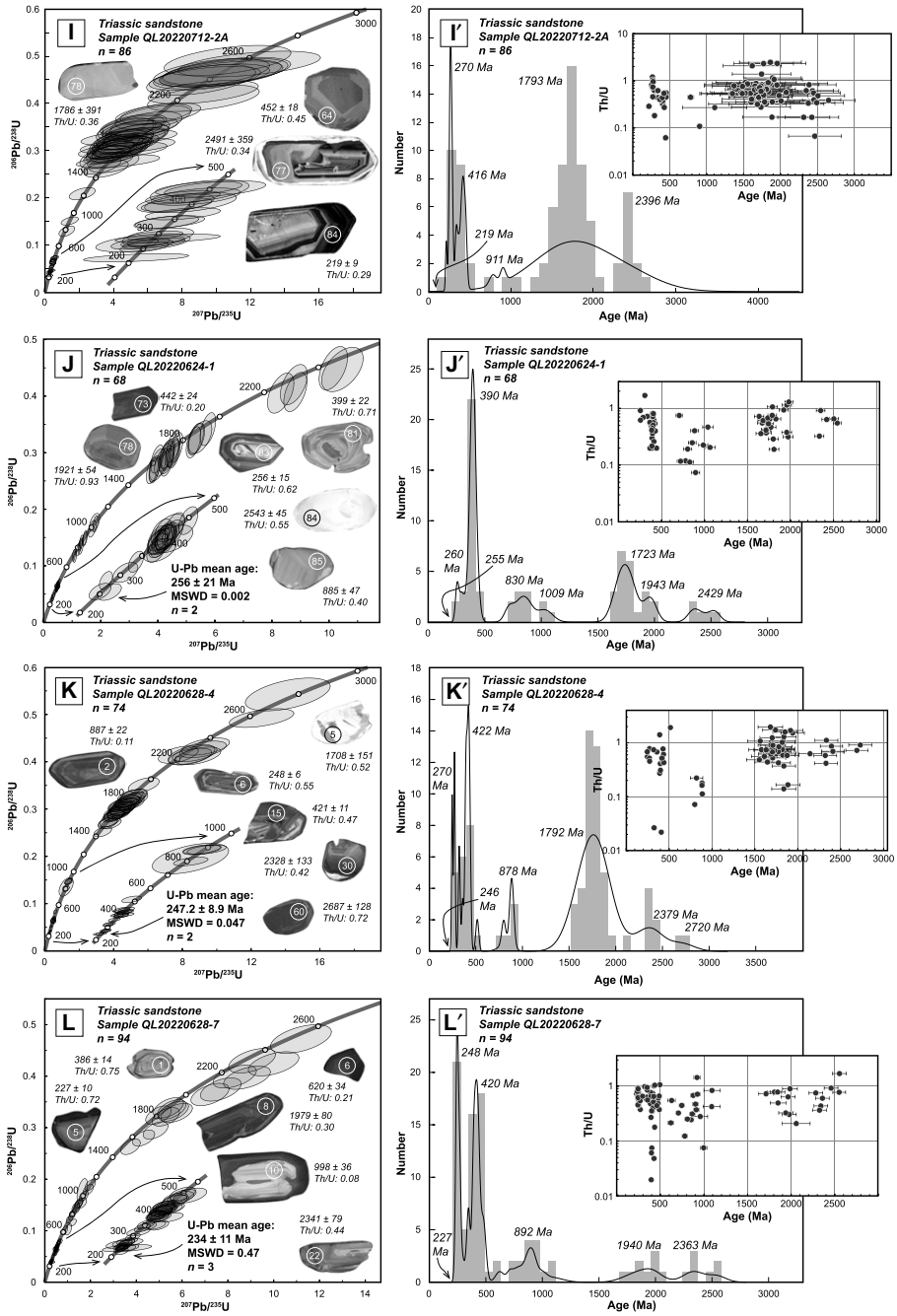

Figure 11. (*Continued*)

the Zongwulong rift basin experienced tectonic inversion due to rift-perpendicular compression, which uplifted and folded syn- and prerift strata in the Zongwulong Shan (Fig. 13C; Gao et al., 2021). The South Zongwulong thrust fault reactivated as a south-directed thrust, and foreland molasse strata were deposited south of the South Zongwulong thrust fault (Zhao et al., 2022). The continuity of Early–Late Triassic sedimentation north of the North Zongwulong thrust fault in the South Qilian may indicate that the North Zongwulong thrust fault was inactive. Later, in response to the Cenozoic India-Asia collision, preexisting structural weaknesses, including the South Zongwulong thrust fault and North Zongwulong thrust fault, were reactivated and accommodated the uplift of the Zongwulong Shan–Qinghai Nanshan. The present-day geomorphology of the Zongwulong Shan–Qinghai Nanshan reflects the morphology of the early rift basin to some extent.

6.4. Late Paleozoic–Early Mesozoic Intraplate Deformation in the Zongwulong Shan–Qinghai Nanshan

The Zongwulong Shan–Qinghai Nanshan rift basin was coeval with the late Paleozoic opening of the Paleo-Tethyan Ocean along the southern edge of the Kunlun-Qaidam continent (Fig. 13D; Wu et al., 2016, 2022; Yu et al., 2020; Metcalfe, 2021). We interpret that opening of the Paleo-Tethyan Ocean led to distributed extension across the Qaidam-Qilian continent to the north, including opening of the Zongwulong Shan–Qinghai Nanshan rift basin (Wu et al., 2016, 2019a; Dong et al., 2018). Hyperextension of the crust during the Carboniferous–Permian caused Carboniferous mantle-derived, bimodal volcanic rocks along the Zongwulong basin axis and Permian anatectic leucogranite diking (Fig. 13E; Xu et al., 2019). This rift basin was a relatively narrow and immature rift basin, such that it did not involve the generation of new oceanic crust (Wang et al., 2001; Fu et al., 2021; Zhao et al., 2022). Deposition of marine strata, including siliciclastic and carbonate turbidite sequences, within the rift basin began in the Carboniferous and continued to the Early Triassic (Guo et al., 2009; Li, 2017; Zhao et al., 2022; Zhao, 2023). Terrigenous and hemipelagic strata, mainly shales and sandstone, were deposited before the Late Triassic.

Subsequent Triassic north-south contractional deformation, evidenced by east-trending folds and thrusts and ductile kinematics in the core of the belt (Figs. 7 and 8), inverted and closed the Zongwulong Shan–Qinghai Nanshan rift basin (Figs. 5E and 5F; Gao et al., 2021; Zhao et al., 2022). This intracontinental contraction is interpreted to have resulted from the Triassic collision between the Qaidam and Songpan-Ganzi (and joined South China) continents to the south, which is well expressed in the Eastern Kunlun orogen (Wu et al., 2016, 2019a, 2022; Jian et al., 2020; Yu et al., 2020). The onset of tectonic inversion was coeval with regional deposition of molasse strata in a foreland basin adjacent to the Zongwulong Shan (Zhao et al., 2022; Zhao, 2023).

The Tibetan lithosphere and the Tethyan oceanic realm involved several suture zones that represent repeated ocean opening and closing events to grow the central Asian continent (Yin and Harrison, 2000; Gehrels et al., 2011; Wu et al., 2016, 2019a, 2022, 2023a; Zuza et al., 2018; Kapp and DeCelles, 2019). For each of these opening and closing events, the tectonic processes recorded along the continental plate margins were likely associated with an intraplate tectonic response within the continental interior. The archetypal example is how the Cenozoic

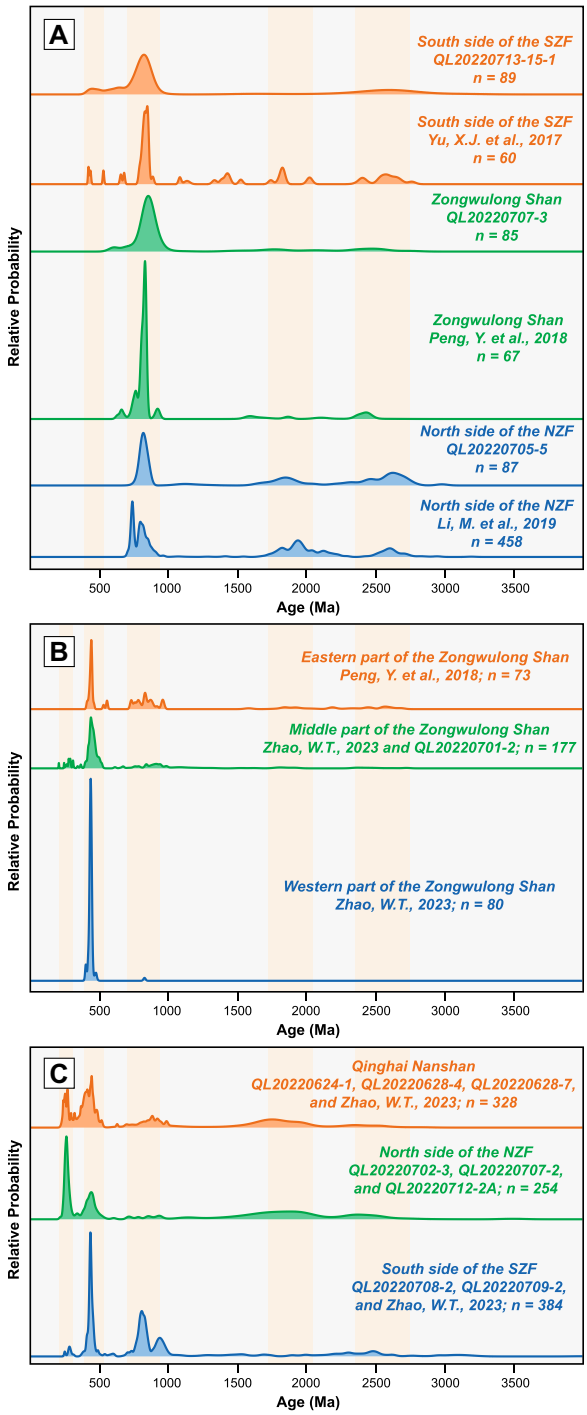

Figure 12. Relative probability plots of U-Pb detrital zircon ages for (meta-)sedimentary rocks from this study and previous results. (A) Neoproterozoic rocks distributed on the northern side of the North Zongwulong fault (NZF), the Zongwulong Shan, and the southern side of the South Zongwulong fault (SZF). (B) Carboniferous–Permian rocks distributed in the western, middle, and eastern parts of the Zongwulong Shan. (C) Triassic rocks distributed on the southern side of the South Zongwulong fault, the northern side of the North Zongwulong fault, and the Qinghai Nanshan. Previous detrital zircon U-Pb isotopic data are listed in Table S2 (see text footnote 1).

India-Asia collision greatly deformed the Asian continent, leading to uplift of a >1000-km-wide orogenic plateau, the development of north-south–oriented intracontinental rifts, the formation of large strike-slip faults that stretch for thousands of kilometers, and the uplift and reactivation of the intracontinental ancient orogenic belt (Yin and Harrison, 2000; Yin, 2010; Yin and Taylor, 2011; Xu et al., 2016; Zuza and Yin, 2017; Zuza et al., 2020; Campbell et al., 2019; Ding et al., 2022a). However, for most of the suture zones across the Tibetan lithosphere, tectonic models involve the collision of rigid continents with limited intraplate deformation. Notable exceptions include documentation of Mesozoic deformation across Lhasa (Murphy et al., 1997) and Qiangtang (e.g., Kapp et al., 2003a, 2003b, 2005). Part of this issue stems from the protracted and polyphase history of tectonic overprinting and Cenozoic intracontinental modification associated with the Himalayan-Tibetan orogen (e.g., Yin et al., 2007; Zuza et al., 2018).

Here, based on detailed regional geological data, we have reported the intraplate tectonic processes associated with the opening and closing of the Paleo-Tethyan Ocean. The Neo-Kunlun Ocean (a part of the Paleo-Tethyan Ocean) opened in the Late Devonian–early Carboniferous and began to subduct northward at ca. 270 Ma, followed by slab rollback southward at ca. 225 Ma (Wu et al., 2016, 2019a, 2022). The opening of the Neo-Kunlun Ocean resulted in coupled intraplate extension across the Qaidam-Qilian continent, which led to the formation of the Zongwulong Shan–Qinghai Nanshan rift. Later, during the northward subduction of the Neo-Kunlun (Paleo-Tethyan) oceanic slab, the intracontinental rift was compressed and inverted during the convergence and collision with the Songpan-Ganzi continent to the south. Our interpretation suggests that similar complex structures associated with the opening and closing of ocean basins may be more widespread across Tibet than currently recognized. Such pre-Cenozoic structures imply initial topography and structural inheritance across the Tibetan continent prior to Cenozoic orogeny. Careful analysis and field observations are required to disentangle such structures from widespread overprinting Cenozoic deformation.

7. CONCLUSIONS

In this study, we combined new field observations and geochronologic results with previous data to reassess the tectonic architecture and setting of the Zongwulong Shan–Qinghai Nanshan in northern Tibet. The following key results are drawn from this study:

(1) Precambrian rocks of the Zongwulong Shan–Qinghai Nanshan correlate with those in the South Qilian and North Qaidam regions. Carboniferous–Permian strata in this belt were deposited in an intracontinental rift basin and sourced from the South Qilian and North Qaidam regions.

(2) By the end of the Early–Middle Triassic, foreland molasse strata were deposited in the southern Zongwulong Shan, corresponding with the initiation of tectonic inversion in the western Zongwulong Shan–Qinghai Nanshan. During this time, the South Qilian and Qinghai Nanshan (the eastern part of this belt) still received detrital materials from the North Qaidam region.

(3) The Zongwulong Shan–Qinghai Nanshan experienced multiple tectonic events after the late Paleozoic. During the opening of the Paleo-Tethyan Ocean, early Carboniferous intraconti-

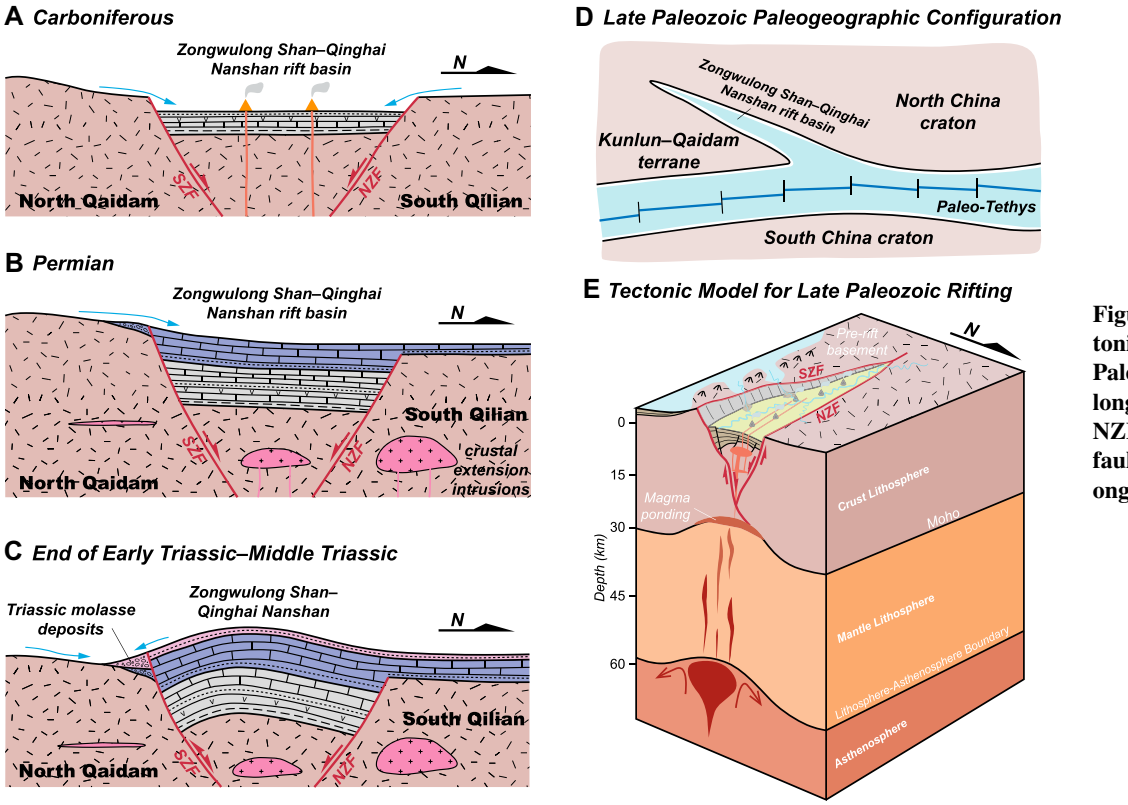

Figure 13. Model for the tectonic evolution of the late Paleozoic–Mesozoic Zongwulong Shan–Qinghai Nanshan. NZF—North Zongwulongshan fault; SZF—South Zongwulongshan fault.

nental rifting resulted in the formation of bounding normal faults (i.e., South Zongwulong and North Zongwulong thrust faults), and subsequently, tectonic inversion of the South Zongwulong thrust fault and folding of pre- and synrift strata occurred at the end of the Early–Middle Triassic along with the closing of the Paleo-Tethyan Ocean. Cenozoic intracontinental contraction resulted in the reactivation of preexisting structural weaknesses in this belt and controlled the present-day geomorphology.

ACKNOWLEDGMENTS

This research was supported by grants from the Basic Science Center for Tibetan Plateau Earth System (grant no. 41988101), the National Natural Science Foundation of China (grant no. 42372256), the Second Tibetan Plateau Scientific Expedition and Research Program (grant no. 2019QZKK0708), and the U.S. National Science Foundation (grant nos. EAR 2210074, 2210075). We are grateful to Wenyou Liu from China University of Geosciences (Beijing) for his assistance in the field. We appreciate science editor Mihai Ducea, associate editor Junpeng Wang, Xiangjiang Yu, and two anonymous reviewers for their critical, careful, and very constructive reviews that helped to improve the clarity and interpretations of the original draft.

REFERENCES CITED

Andersen, T., 2002, Correction of common lead in U-Pb analyses that do not report ^{204}Pb: Chemical Geology, v. 192, p. 59–79, https://doi.org/10.1016/S0009-2541(02)00195-X.

Bi, H.Z., Whitney, D.L., Song, S.G., and Zhou, X., 2022, HP-UHP eclogites in the East Kunlun orogen, China: *P-T* evidence for asymmetric suturing of the Proto-Tethys Ocean: Gondwana Research, v. 104, p. 199–214, https://doi.org/10.1016/j.gr.2021.04.008.

Boone, S.C., Kohn, B.P., Gleadow, A.J.W., Morley, C.K., Seiler, C., and Foster, D.A., 2019, Birth of the East African Rift system: Nucleation of magmatism and strain in the Turkana Depression: Geology, v. 47, no. 9, . 886–890, https://doi.org/10.1130/G46468.1.

Brombin, V., Bonadiman, C., Jourdan, F., Roghi, G., Coltorti, M., Webb, L.E., Callegaro, S., Bellieni, G., De Vecchi, G., Sedea, R., and Marzoli, A., 2019, Intraplate magmatism at a convergent plate boundary: The case of the Cenozoic northern Adria magmatism: Earth-Science Reviews, v. 192, p. 355–378, https://doi.org/10.1016/j.earscirev.2019.03.016.

Campbell, G.E., Walker, R.T., Abdrakhmatov, K., Carolin, S., Carr, A.S., Elliott, J.R., Jackson, J., Mackenzie, D., Rizza, M., and Rodes, A., 2019, Rapid late Quaternary slip, repeated prehistoric earthquake rupture, and widespread landsliding associated with the Karakudzhur thrust, central Kyrgyz Tien Shan: Tectonics, v. 38, no. 11, p. 3740–3764, https://doi.org/10.1029/2018TC005433.

Chang, P.Y., 2017, Analysis of Jiermeng Granite Pluton Zircon U-Pb Age and Tectonic Environments, South Qilian [Master's thesis]: Beijing, China, China University of Geosciences (Beijing), 69 p.

Chen, M., 2020, Geological Environment and Controlling Elements of the Metallogeny in Zongwulong Tectonic Belt, Northern Margin of Qaidam Basin [Ph.D. thesis]: Beijing, China, China University of Geosciences (Beijing), 149 p.

Chen, M., Xue, C.J., Xue, W.W., and Zhao, W.T., 2020a, Discovery and geological significance of Xuji diorite in Zongwulong tectonic belt on the northern margin of Qaidam Basin: Acta Petrologica et Mineralogica, v. 39, no. 5, p. 552–568 [in Chinese with English abstract].

Chen, N.S., Sun, M., Wang, Q.Y., Zhang, K.X., Wan, Y.S., and Chen, H.H., 2008, U-Pb dating of zircon from the Central Zone of the East Kunlun orogen and its implications for tectonic evolution: Science in China–Earth Sciences, v. 51, no. 7, p. 929–938, https://doi.org/10.1007/s11430-008-0072-x.

Chen, N.S., Gong, S.L., Sun, M., Li, X.Y., Xia, X.P., Wang, Q.Y., Wu, F.Y., and Xu, P., 2009, Precambrian evolution of the Quanji block, northeastern margin of Tibet: Insights from zircon U-Pb and Lu-Hf isotope compositions: Journal of Asian Earth Sciences, v. 35, no. 3–4, p. 367–376, https://doi.org/10.1016/j.jseaes.2008.10.004.

Chen, N.S., Liao, F.X., Wang, L., Santosh, M., Sun, M., Wang, Q.Y., and Mustafa, H.A., 2013a, Late Paleoproterozoic multiple metamorphic events in the Quanji Massif: Links with Tarim and North China cratons and implications for assembly of the Columbia supercontinent: Precambrian Research, v. 228, p. 102–116, https://doi.org/10.1016/j.precamres.2013.01.013.

Chen, N.S., Gong, S.L., Xia, X.P., Geng, H.Y., Wang, L., Sun, M., and Kusky, T.M., 2013b, Zircon Hf isotope of Yingfeng rapakivi granites from the Quanji Massif and ~2.7 Ga crustal growth: Journal of Earth Science, v. 24, no. 1, p. 29–41, https://doi.org/10.1007/s12583-013-0309-2.

Chen, X., Xu, R.K., Schertl, H.P., and Zheng, Y.Y., 2018, Eclogite-facies metamorphism in impure marble from North Qaidam orogenic belt: Geodynamic implications for early Paleozoic continental-arc collision: Lithos, v. 310–311, p. 201–224, https://doi.org/10.1016/j.lithos.2018.04.005.

Chen, X., Schertl, H.P., Cambeses, A., Gu, P.Y., Xu, R.K., Zheng, Y.Y., Jiang, X.J., and Cai, P.J., 2019, From magmatic generation to UHP metamorphic overprint and subsequent exhumation: A rapid cycle of plate movement recorded by the supra-subduction zone ophiolite from the North Qaidam orogen: Lithos, v. 350–351, https://doi.org/10.1016/j.lithos.2019.105238.

Chen, X.J., Yun, X.R., Lei, M., Cai, Z.H., Zhang, S.S., Liu, R.H., Li, Y.B., and He, B.Z., 2020b, Petrogenesis of Middle Triassic granite association in the Gonghe basin, Qinghai: Constraints from geochemistry, U-Pb ages and Hf isotopes: Acta Petrologica Sinica (Yanshi Xuebao), v. 36, no. 10, p. 3152–3170, https://doi.org/10

.18654/1000-0569/2020.10.13 [in Chinese with English abstract].

Cheng, F., Jolivet, M., Guo, Z.J., Lu, H.Y., Zhang, B., Li, X.Z., Zhang, D.W., Zhang, C.H., Zhang, H.Z., Wang, L., Wang, Z.Q., and Zhang, Q.Q., 2019, Jurassic–early Cenozoic tectonic inversion in the Qilian Shan and Qaidam Basin, north Tibet: New insight from seismic reflection, isopach mapping, and drill core data: Journal of Geophysical Research: Solid Earth, v. 124, p. 12,077–12,098, https://doi.org/10.1029/2019JB018086.

Chenin, P., Manatschal, G., Ghienne, J.F., and Chao, P., 2022, The syn-rift tectono-stratigraphic record of rifted margins (Part II): A new model to break through the proximal/distal interpretation frontier: Basin Research, v. 34, no. 2, p. 489–532, https://doi.org/10.1111/bre.12628.

Corti, G., Molin, P., Sembroni, A., Bastow, I.D., and Keir, D., 2018, Control of pre-rift lithospheric structure on the architecture and evolution of continental rifts: Insights from the main Ethiopian Rift, East Africa: Tectonics, v. 37, p. 477–496, https://doi.org/10.1002/2017TC004799.

Dewey, J.F., and Bird, J.M., 1970, Mountain belts and the new global tectonics: Journal of Geophysical Research, v. 75, no. 14, p. 2625–2647, https://doi.org/10.1029/JB075i014p02625.

Ding, L., Kapp, P., Cai, F.L., Garzione, C.N., Xiong, Z.Y., Wang, H.Q., and Wang, C., 2022a, Timing and mechanisms of Tibetan Plateau uplift: Nature Reviews–Earth & Environment, v. 3, p. 652–667, https://doi.org/10.1038/s43017-022-00318-4.

Ding, Q.F., Pan, T., Zhou, X., Cheng, L., Li, S.P., Han, J., Qian, Y., Gao, Y., and Shang, M.Y., 2022b, Geochronology, petrogenesis, and tectonic significance of the granites in the Chaqiabeishan area of the Quanji Massif, northwestern China: Geological Journal, v. 57, no. 3, p. 1241–1261, https://doi.org/10.1002/gj.4338.

Dong, J.Y., Li, C.Y., Zheng, W.J., Li, T., Li, X.N., Zhang, P.Z., Ren, G.X., Dong, S.P., and Liu, J.R., 2019, Geomorphic features and late Quaternary slip rate of the southern Zongwulong Shan fault: Seismology and Geology (Dizhen Dizhi), v. 41, no. 2, p. 341–362 [in Chinese with English abstract].

Dong, Y.P., He, D.F., Sun, S.S., Liu, X.M., Zhou, X.H., Zhang, F.F., Yang, Z., Cheng, B., Zhao, G.C., and Li, J.H., 2018, Subduction and accretionary tectonics of the East Kunlun orogen, western segment of the Central China orogenic system: Earth-Science Reviews, v. 186, p. 231–261, https://doi.org/10.1016/j.earscirev.2017.12.006.

Fraser, S.I., Fraser, A.J., Lentini, M.R., and Gawthorpe, R.L., 2007, Return to rifts—The next wave: Fresh insights into the petroleum geology of global rift basins: Petroleum Geoscience, v. 13, p. 99–104, https://doi.org/10.1144/1354-079307-749.

Fu, C.L., Yan, Z., Wang, Z.Q., Buckman, S., Aitchison, J.C., Niu, M.L., Cao, B., Guo, X.Q., Li, X.C., Li, Y.S., and Li, J.L., 2018, Lajishankou ophiolite complex: Implications for Paleozoic multiple accretionary and collisional event in the South Qilian belt: Tectonics, v. 37, p. 1321–1346, https://doi.org/10.1029/2017TC004740.

Fu, C.L., Yan, Z., Xiao, W.J., Wang, B.Z., Niu, M.L., Li, X.C., and Yu, L.J., 2021, Identification and geological significance of the early Paleozoic Tianjunnanshan remnant ocean basin in the Zongwulong belt, NE Tibetan Plateau: Acta Petrologica Sinica (Yanshi Xuebao), v. 37, no. 8, p. 2401–2418, https://doi.org/10.18654/1000-0569/2021.08.09 [in Chinese with English abstract].

Fu, D., Kusky, T.M., Wilde, S.A., Windley, B.F., Polat, A., Huang, B., and Zhou, Z., 2020, Structural anatomy of the early Paleozoic Laohushan ophiolite and subduction complex: Implications for accretionary tectonics of the Proto-Tethyan North Qilian orogenic belt, northeastern Tibet: Geological Society of America Bulletin, v. 132, p. 2175–2201, https://doi.org/10.1130/B35442.1.

Fu, J.G., Liang, X.Q., Zhou, Y., Wang, C., Jiang, Y., and Zhong, Y.S., 2015, Geochemistry, zircon U-Pb geochronology and Hf isotopes of granitic rocks in the Xitieshan area, North Qaidam, Northwest China: Implications for Neoproterozoic geodynamic evolution of North Qaidam: Precambrian Research, v. 264, p. 11–29, https://doi.org/10.1016/j.precamres.2015.04.006.

Gao, W.L., Wang, Z.X., Li, L.L., Qian, T., and Cui, M.M., 2021, $^{40}Ar/^{39}Ar$ laser dating of the Zongwulong ductile shear zone in northeastern Tibetan Plateau: Constraints on the time of Indosinian orogeny: Geology in China, v. 48, no. 1, p. 149–160 [in Chinese with English abstract].

Gehrels, G., Kapp, P., DeCelles, P., Pullen, A., Blakey, R., Weislogel, A., Ding, L., Guynn, J., Martin, A., McQuarrie, N., and Yin, A., 2011, Detrital zircon geochronology of pre-Tertiary strata in the Tibetan-Himalayan orogen: Tectonics, v. 30, no. 5, TC5016, https://doi.org/10.1029/2011TC002868.

Gehrels, G.E., Yin, A., and Wang, X.F., 2003a, Magmatic history of the northeastern Tibetan Plateau: Journal of Geophysical Research: Solid Earth, v. 108, no. B9, 2423, https://doi.org/10.1029/2002JB001876.

Gehrels, G.E., Yin, A., and Wang, X.F., 2003b, Detrital-zircon geochronology of the northeastern Tibetan Plateau: Geological Society of America Bulletin, v. 115, p. 881–896, https://doi.org/10.1130/0016-7606(2003)115<0881:DGOTNT>2.0.CO;2.

Gong, S.L., Chen, N.S., Wang, Q.Y., Kusky, T.M., Wang, L., Zhang, L., Ba, J., and Liao, F.X., 2012, Early Paleoproterozoic magmatism in the Quanji Massif, northeastern margin of the Qinghai–Tibet Plateau, and its tectonic significance: LA-ICPMS U-Pb zircon geochronology and geochemistry: Gondwana Research, v. 21, no. 1, p. 152–166, https://doi.org/10.1016/j.gr.2011.07.011.

Guo, A.L., Zhang, G.W., Qiang, J., Sun, Y.G., Li, G., and Yao, A.P., 2009, Indosinian Zongwulong orogenic belt on the northeastern margin of the Qinghai-Tibet plateau: Acta Petrologica Sinica (Yanshi Xuebao), v. 25, no. 1, p. 1–12 [in Chinese with English abstract].

Guo, X.Q., Yan, Z., Fu, C.L., and Wang, Z.Q., 2016, Formation age and tectonic attribute of Jinshuikou Group complex in the Nanshan area, Qinghai: Acta Geologica Sinica, v. 90, no. 3, p. 589–606 [in Chinese with English abstract].

Hao, Y.Q., Yang, Q.A., Shi, Y.L., and Li, S.H., 2018, The intrusive rocks in the Wukou region, Qinghainanshan area, Qinghai: Zircon U-Pb chronology, geochemistry and geological implications: Sedimentary Geology and Tethyan Geology (Chenji Yu Tetisi Dizhi), v. 38, no. 4, p. 13–23 [in Chinese with English abstract].

He, D.F., Dong, Y.P., Zhang, F.F., Yang, Z., Sun, S.S., Cheng, B., Zhou, B., and Liu, X.M., 2016, The 1.0 Ga S-type granite in the East Kunlun orogen, northern Tibetan Plateau: Implications for the Meso- to Neoproterozoic tectonic evolution: Journal of Asian Earth Sciences, v. 130, p. 46–59, https://doi.org/10.1016/j.jseaes.2016.07.019.

He, D.F., Dong, Y.P., Liu, X.M., Zhou, X.H., Zhang, F.F., and Sun, S.S., 2018, Zircon U-Pb geochronology and Hf isotope of granitoids in East Kunlun: Implications for the Neoproterozoic magmatism of Qaidam block, northern Tibetan Plateau: Precambrian Research, v. 314, p. 377–393, https://doi.org/10.1016/j.precamres.2018.06.017.

Hernández-Uribe, D., Mattinson, C.G., Regel, M.E., Zhang, J., Stubbs, K.A., and Kylander-Clark, A.R.C., 2023, Protracted eclogite-facies metamorphism of the Dulan area, North Qaidam ultrahigh-pressure terrane: Insights on zircon growth during continental subduction and collision: Journal of Metamorphic Geology, v. 41, no. 4, p. 557–581, https://doi.org/10.1111/jmg.12708.

Huang, H., Niu, Y.L., Nowell, G., Zhao, Z.D., Yu, X.H., Zhu, D.C., Mo, X.X., and Ding, S., 2014, Geochemical constraints on the petrogenesis of granitoids in the East Kunlun orogenic belt, northern Tibetan Plateau: Implications for continental crust growth through syn-collisional felsic magmatism: Chemical Geology, v. 370, p. 1–18, https://doi.org/10.1016/j.chemgeo.2014.01.010.

Huang, H., Niu, Y.L., Nowell, G., Zhao, Z.D., Yu, X.H., and Mo, X.X., 2015, The nature and history of the Qilian block in the context of the development of the Greater Tibetan Plateau: Gondwana Research, v. 28, no. 1, p. 209–224, https://doi.org/10.1016/j.gr.2014.02.010.

Huang, W., Zhang, L., Ba, J., Liao, F.X., and Chen, N.S., 2011, Detrital zircon LA-ICP-MS U-Pb dating for K-feldspar leptite of Quanji massif in the north margin of Qaidam block: Constraint on the age of Dakendaban Group: Geological Bulletin of China (Dizhi Tongbao), v. 30, no. 9, p. 1353–1359 [in Chinese with English abstract].

Huo, Y.A., 2016, Geochemistry Characteristics and Geological Significance of Gaweiji Rocks in Gonghe County of Qinghai Province [Master's thesis]: Shijiazhuang, China, Heibei GEO University, 69 p.

Isacks, B., Oliver, J., and Sykes, L.R., 1968, Seismology and the new global tectonics: Journal of Geophysical Research, v. 73, no. 18, p. 5855–5899, https://doi.org/10.1029/JB073i018p05855.

Ji, B., Yu, J.Y., Li, X.M., Huang, B.T., and Wang, L., 2018, The disintegration of Balonggongge'er Formation and the definition of lithostratigraphic units in Danghenanshan area of South Qilian Mountain: Evidence from petrology and chronology: Geological Bulletin of China (Dizhi Tongbao), v. 37, no. 4, p. 621–633 [in Chinese with English abstract].

Ji, B., Li, X.M., Huang, B.T., Wang, L., and Wang, G.Q., 2021, Geochronology of detrital zircons from the Guaizhangshan Group from the southern Danghe Mountains in South Qilian and its geological implications: Acta Geologica Sinica, v. 95, no. 3, p. 765–778 [in Chinese with English abstract].

Jian, X., Weislogel, A., Pullen, A., and Shang, F., 2020, Formation and evolution of the Eastern Kunlun Range, northern Tibet: Evidence from detrital zircon U-Pb geochronology and Hf isotopes: Gondwana Research, v. 83, p. 63–79, https://doi.org/10.1016/j.gr.2020.01.015.

Kapp, P., and DeCelles, P.G., 2019, Mesozoic–Cenozoic geological evolution of the Himalayan-Tibetan orogen and working tectonic hypotheses: American Journal of Science, v. 319, p. 159–254, https://doi.org/10.2475/03.2019.01.

Kapp, P., Murphy, M.A., Yin, A., Harrison, T.M., Ding, L., and Guo, J., 2003a, Mesozoic and Cenozoic tectonic evolution of the Shiquanhe area of western Tibet: Tectonics, v. 22, no. 4, 1029, https://doi.org/10.1029/2001TC001332.

Kapp, P., Yin, A., Manning, C.E., Harrison, T.M., Taylor, M.H., and Ding, L., 2003b, Tectonic evolution of the early Mesozoic blueschist-bearing Qiangtang metamorphic belt, central Tibet: Tectonics, v. 22, no. 4, 1043, https://doi.org/10.1029/2002TC001383.

Kapp, P., Yin, A., Harrison, T.M., and Ding, L., 2005, Cretaceous–Tertiary shortening, basin development, and volcanism in central Tibet: Geological Society of America Bulletin, v. 117, p. 865–878, https://doi.org/10.1130/B25595.1.

Le Pichon, X., 1968, Sea-floor spreading and continental drift: Journal of Geophysical Research, v. 73, no. 12, p. 3661–3697, https://doi.org/10.1029/JB073i012p03661.

Leprêtre, R., Missenard, Y., Barbarand, J., Gautheron, C., Jouvie, I., and Saddiqi, O., 2018, Polyphased inversions of an intracontinental rift: Case study of the Marrakech High Atlas, Morocco: Tectonics, v. 37, no. 3, p. 818–841, https://doi.org/10.1002/2017TC004693.

Li, B., Zuza, A.V., Chen, X.H., Wang, Z.Z., Shao, Z.G., Levy, D.A., Wu, C., Xu, S.L., and Sun, Y.J., 2021a, Pre-Cenozoic evolution of the northern Qilian orogen from zircon geochronology: Framework for early growth of the northern Tibetan Plateau: Palaeogeography, Palaeoclimatology, Palaeoecology, v. 562, https://doi.org/10.1016/j.palaeo.2020.110091.

Li, B., Chen, X.H., Wang, Z.Z., Hu, D.G., and Sun, Y.J., 2022a, The early Paleozoic intrusive magmatism and tectonic thermal evolution in the Hala Lake area, southern Qilian, NW China: Acta Petrologica Sinica (Yanshi Xuebao), v. 38, no. 3, p. 793–812 [in Chinese with English abstract], https://doi.org/10.18654/1000-0569/2022.03.12.

Li, B., Qi, B.S., Chen, X.H., Zuza, A.V., Hu, D.G., Sun, Y.J., Wang, Z.Z., and Zhang, Y.P., 2023, Two-phase kinematic evolution of the Qilian Shan, northern Tibetan Plateau: Initial Eocene–Oligocene deformation that accelerated in the mid-Miocene: Geological Society of America Bulletin, v. 136, p. 2389–2406, https://doi.org/10.1130/B37159.1.

Li, C., Niu, M.L., Li, X.C., Yan, Z., Wu, Q., Sun, Y., and Yuan, X.Y., 2022b, Origin and Precambrian paleogeography of the North Wulan terrane, northwestern China: A coherent model of the Tarim-Qilian-Quanji continent during the Columbia-Rodinia supercontinent cycle:

Gondwana Research, v. 101, p. 132–155, https://doi.org/10.1016/j.gr.2021.08.003.

Li, L.T., 2017, Sedimentary facies analysis of the Carboniferous and Triassic strata in the Xiangpishan area of Qinghai Province and its response to the Zongwulong tectonic belt evolution: Geology and Mineral Resources of South China, v. 33, no. 1, p. 13–24 [in Chinese with English abstract].

Li, M., Wang, C., Li, R.S., Meert, J.G., Peng, Y., and Zhang, J.H., 2019, Identifying late Neoproterozoic–early Paleozoic sediments in the South Qilian belt, China: A peri-Gondwana connection in the northern Tibetan Plateau: Gondwana Research, v. 76, p. 173–184, https://doi.org/10.1016/j.gr.2019.06.010.

Li, P.A., and Nie, S.R., 1985, Structural characteristics of Zongwulong aulacogen: Geology of Qinghai, v. 2, p. 65–76 [in Chinese].

Li, S.H., Shi, Y.L., Tian, T., Tian, Q., and Wang, Z.Y., 2017, Geochemical characteristics, LA-ICP-MS dating and geological significance of Early Triassic quartz diorite in Qinghai Nanshan: Journal of Qinghai University, v. 35, no. 3, p. 25–32 [in Chinese with English abstract].

Li, S.H., Qiang, X.N., Tian, T., Zhao, L.Z., Xu, S.L., and Ma, Q., 2018a, LA-ICP-MS zircon U-Pb dating of the granites in the eastern section of Nanshan, Qinghai Province, and its geological significance: Geological Bulletin of China (Dizhi Tongbao), v. 37, no. 7, p. 1236–1245 [in Chinese with English abstract].

Li, S.P., Pan, T., Wang, B.Z., Yan, X.P., Ren, H., Yu, F.C., Qiu, W., Wang, J.J., Tang, J., Wang, J.S., and Jin, T.T., 2021b, Characteristics and tectonic significance of beryl-bearing pegmatites in Qiemoge Mountain, northern margin of Qaidam Basin: Geotectonica et Metallogenia (Dadi Gouzao Yu Chengkuangxue), v. 45, no. 3, p. 608–619 [in Chinese with English abstract].

Li, W.F., Pan, T., Wang, B.Z., Zhang, X.Y., Zheng, Y., Wang, C.T., Li, S.P., and Han, J., 2022c, Ordovician magmatic arc in the Nanshan area, Qinghai Province: Evidence from zircon U-Pb chronology, element geochemistry and Hf isotope compositions of the diorites in the Chakaibeishan area: Geotectonica et Metallogenia (Dadi Gouzao Yu Chengkuangxue), v. 46, no. 4, p. 788–802 [in Chinese with English abstract].

Li, X.C., Niu, M.L., Yan, Z., Da, L.C., Han, Y., and Wang, Y.S., 2015, LP/HT metamorphic rocks in Wulan County, Qinghai Province: An early Paleozoic paired metamorphic belt on the northern Qaidam Basin?: Chinese Science Bulletin, v. 60, no. 35, p. 3501–3513, https://doi.org/10.1360/N972015-00558 [in Chinese with English abstract].

Li, Z.C., Pei, X.Z., Li, R.B., Pei, L., Zhang, Y.M., Wang, X.B., Liu, C.J., Chen, Y.X., and Wang, M., 2018b, Geological characteristics and geochronology of Jiaokong metamorphic rocks from the Nanshan area, Qinghai Province, and their geological implications: Geological Bulletin of China (Dizhi Tongbao), v. 37, no. 4, p. 570–588 [in Chinese with English abstract].

Li, Z.F., Peng, Y.B., Yu, S.Y., Li, Y., Yao, Y., Zhao, X.D., and Gao, X.Y., 2020, Subduction and exhumation of Luliangshan eclogite in the North Qaidam, northern Tibet: Constraints from petrology, geochemistry and phase equilibrium modelling: Geological Journal, v. 55, no. 9, p. 6580–6605, https://doi.org/10.1002/gj.3883.

Liao, F.X., Zhang, L., Chen, N.S., Sun, M., Santosh, M., Wang, Q.Y., and Mustafa, H.A., 2014a, Geochronology and geochemistry of meta-mafic dykes in the Quanji Massif, NW China: Paleoproterozoic evolution of the Tarim craton and implications for the assembly of the Columbia supercontinent: Precambrian Research, v. 249, p. 33–56, https://doi.org/10.1016/j.precamres.2014.04.015.

Liao, H., Hu, D.G., Zhang, X.J., Yu, W.L., and Guo, T., 2014b, Zircon U-Pb age for granite of the Ordovician formation and its tectonic significance in the southern Qilian: Journal of Geomechanics, v. 20, no. 3, p. 292–298 [in Chinese with English abstract].

Lin, X., Jolivet, M., Liu-Zeng, J., Cheng, F., Tian, Y.T., and Li, C.A., 2021, Mesozoic–Cenozoic cooling history of the eastern Qinghai Nan Shan (NW China): Apatite low-temperature thermochronology constraints: Palaeogeography, Palaeoclimatology, Palaeoecology, v. 572, https://doi.org/10.1016/j.palaeo.2021.110416.

Liu, X.L., and Yuan, D.Y., 2004, Study on the new active features of Bayinguole River active fault, Delingha, Qinghai Province: Northwestern Seismological Journal, v. 26, no. 4, p. 303–308 [in Chinese with English abstract].

Lu, Z.L., Zhang, J.X., Mao, X.H., Zhou, G.S., and Peng, Y.B., 2017, Paleoproterozoic mafic granulite in the eastern Oulongbuluke block of the North Qaidam Mountains: Evidence from petrology, zircon U-Pb dating and Hf isotope: Acta Petrologica Sinica (Yanshi Xuebao), v. 33, no. 12, p. 3815–3828 [in Chinese with English abstract].

Ludwig, K.R., 2003, Isoplot 3.00: Berkeley Geochronology Center Special Publication 4, 70 p.

Ma, S., Zhou, Z.H., Chen, S.Y., Jia, B.B., Sun, J.P., Wang, Z.J., and Hou, S.Y., 2019, Glacial sedimentary characteristics of late Sinian in Quanji area in the northern margin of Qaidam Basin and its geological significance: Journal of China University of Petroleum: Natural Science Edition (Zhongguo Shiyou Daxue Xuebao: Ziran Kexue Ban), v. 43, no. 3, p. 1–12 [in Chinese with English abstract].

Manatschal, G., Chenin, P., Ghienne, J.F., Ribes, C., and Masini, E., 2022, The syn-rift tectono-stratigraphic record of rifted margins (Part I): Insights from the Alpine Tethys: Basin Research, v. 34, no. 1, p. 457–488, https://doi.org/10.1111/bre.12627.

Mattinson, C.G., Wooden, J.L., Liou, J.G., Bird, D.K., and Wu, C.L., 2006, Geochronology and tectonic significance of middle Proterozoic granitic orthogneiss, North Qaidam HP/UHP terrane, western China: Mineralogy and Petrology, v. 88, no. 1–2, p. 227–241, https://doi.org/10.1007/s00710-006-0149-1.

Menold, C.A., Manning, C.E., Yin, A., Tropper, P., Chen, X.H., and Wang, X.F., 2009, Metamorphic evolution, mineral chemistry and thermobarometry of orthogneiss hosting ultrahigh-pressure eclogites in the North Qaidam metamorphic belt, western China: Journal of Asian Earth Sciences, v. 35, no. 3–4, p. 273–284, https://doi.org/10.1016/j.jseaes.2008.12.008.

Metcalfe, I., 2021, Multiple Tethyan ocean basins and orogenic belts in Asia: Gondwana Research, v. 100, p. 87–130, https://doi.org/10.1016/j.gr.2021.01.012.

Molnar, P., 1988, A review of geophysical constraints on the deep structure of the Tibetan Plateau, the Himalaya, and the Karakorum and their tectonic implications: Philosophical Transactions of the Royal Society of London, v. 326, p. 33–88, https://doi.org/10.1098/rsta.1988.0080.

Morley, C.K., 2020, Early syn-rift igneous dike patterns, northern Kenya Rift (Turkana, Kenya): Implications for local and regional stresses, tectonics, and magma-structure interactions: Geosphere, v. 16, p. 890–918, https://doi.org/10.1130/GES02107.1.

Murphy, M.A., Yin, A., Harrison, T.M., Dürr, S.B., Chen, Z., Ryerson, F.J., Kidd, W.S.F., Wang, X., and Zhou, X., 1997, Did the Indo-Asian collision alone create the Tibetan Plateau?: Geology, v. 25, p. 719–722, https://doi.org/10.1130/0091-7613(1997)025<0719:DTIACA>2.3.CO;2.

Pan, G.T., Ding, J., Yao, D., and Wang, L., 2004, Geological Map of Qinghai-Xiang (Tibet) Plateau and Adjacent Areas, Chengdu: Chengdu, China, Chengdu Institute of Geology and Mineral Resources, China Geological Survey, Chengdu Cartographic Publishing House, scale 1:1,500,000.

Peng, Y., Ma, Y.S., Liu, C.L., Li, Z.X., Sun, J.P., and Shao, P.C., 2016a, Geological characteristics and tectonic significance of the Indosinian granodiorites from the Zongwulong tectonic belt in North Qaidam: Earth Science Frontiers, v. 23, no. 2, p. 206–221 [in Chinese with English abstract].

Peng, Y., Zhang, Y.S., Sun, J.P., Xing, E.Y., and Yu, H.T., 2018, Provenance and tectonic setting of the Zhongwunongshan Group from the Zhongwunongshan structural belt and its adjacent areas in North Qaidam, China: Evidence from geochemistry and detrital zircon geochronology: Geotectonica et Metallogenia (Dadi Gouzao Yu Chengkuangxue), v. 42, no. 1, p. 126–149 [in Chinese with English abstract].

Peng, Y.B., Yu, S.Y., Li, S.Z., Zhang, J.X., Liu, Y.J., Li, Y.S., and Santosh, M., 2019, Early Neoproterozoic magmatic imprints in the Altun-Qilian-Kunlun region of the Qinghai-Tibet Plateau: Response to the assembly and breakup of Rodinia supercontinent: Earth-Science Reviews, v. 199, https://doi.org/10.1016/j.earscirev.2019.102954.

Peng, Z.J., Wu, P.D., Liu, S.B., and Zhang, P., 2016b, An analysis of sediments characteristics of Early–Middle Triassic Longwuhe Formation from Guomaying area in Guinan County, Qinghai Province: Geological Bulletin of China (Dizhi Tongbao), v. 35, no. 9, p. 1506–1511 [in Chinese with English abstract].

Qin, Y., 2018, Neoproterozoic to Early Paleozoic Tectonic Evolution in the South Qilian Orogen [Ph.D. thesis]: Xi'an, China, Northwest University, 153 p.

Qin, Y., Feng, Q., Chen, G., Chen, Y., Zou, K.Z., Liu, Q., Jiao, Q.Q., Zhou, D.W., Pan, L.H., and Gao, J.D., 2018, Devonian post-orogenic extension-related volcano-sedimentary rocks in the northern margin of the Tibetan Plateau, NW China: Implications for the Paleozoic tectonic transition in the North Qaidam orogen: Journal of Asian Earth Sciences, v. 156, p. 145–166, https://doi.org/10.1016/j.jseaes.2018.01.009.

Qinghai BGMR (Qinghai Bureau of Geology and Mineral Resources), 1978, Geological Map of Delingha Sheet, People's Republic of China: Xining, China, Qinghai BGMR, scale 1:200,000 [in Chinese].

Qinghai BGMR (Qinghai Bureau of Geology and Mineral Resources), 1991, Regional Geology of Qinghai Province: Beijing, China, Geological Publishing House, 662 p. [in Chinese].

Ren, Y.F., Chen, D.L., Wang, H.J., Zhu, X.H., and Bai, B.W., 2021, Grenvillian and early Paleozoic polyphase metamorphism recorded by eclogite and host garnet mica schist in the North Qaidam orogenic belt: Geoscience Frontiers, v. 12, no. 4, https://doi.org/10.1016/j.gsf.2021.101170.

Royden, L.H., Burchfiel, B.C., and van der Hilst, R.D., 2008, The geological evolution of the Tibetan Plateau: Science, v. 321, p. 1054–1058, https://doi.org/10.1126/science.1155371.

Şengör, A.M.C., 1984, The Cimmeride Orogenic System and the Tectonics of Eurasia: Geological Society of America Special Paper 195, 82 p., https://doi.org/10.1130/SPE195-p1.

Shi, J.P., Huo, T.F., Lai, Q., Peng, X.H., Du, S.Y., and Yang, D.B., 2015, Petrogenesis of Early Silurian Gangchadasi granites in the eastern segment of the northern South Qilian block: Constraints from LA-ICP-MS zircon U-Pb geochronology and geochemistry: Acta Geoscientica Sinica, v. 36, no. 6, p. 781–789 [in Chinese with English abstract].

Shi, J.P., Han, X.Z., Qiao, S.Y., Wang, Z.S., Huo, T.F., Yang, H.T., and Yang, D.B., 2017, The Late Ordovician tectonic evolution of the eastern section of the northern margin of the South Qilian block: Evidence from geochronology, geochemistry, and mineral chemistry of the Duozang hornblende gabbro: Earth Science Frontiers, v. 24, no. 6, p. 46–59 [in Chinese with English abstract].

Shi, R.D., Yang, J.S., Wu, C.L., Tsuyoshi, I., and Takafumi, H., 2006, Island arc volcanic rocks in the North Qaidam UHP belt, northern Tibet Plateau: Evidence for ocean-continent subduction preceding continent-continent subduction: Journal of Asian Earth Sciences, v. 28, no. 2–3, p. 151–159, https://doi.org/10.1016/j.jseaes.2005.09.019.

Song, S.G., Zhang, L.F., and Niu, Y.L., 2004, Ultra-deep origin of garnet peridotite from the North Qaidam ultrahigh-pressure belt, northern Tibetan Plateau, NW China: The American Mineralogist, v. 89, p. 1330–1336, https://doi.org/10.2138/am-2004-8-922.

Song, S.G., Zhang, L.F., Niu, Y.L., Su, L., Song, B., and Liu, D.Y., 2006, Evolution from oceanic subduction to continental collision: A case study from the northern Tibetan Plateau based on geochemical and geochronological data: Journal of Petrology, v. 47, no. 3, p. 435–455, https://doi.org/10.1093/petrology/egi080.

Song, S.G., Zhang, L.F., Niu, Y.L., Wei, C.J., Liou, J.G., and Shu, G.M., 2007, Eclogite and carpholite-bearing metasedimentary rocks in the North Qilian suture zone, NW China: Implications for early Palaeozoic cold oceanic subduction and water transport into mantle: Journal of Metamorphic Geology, v. 25, no. 5, p. 547–563, https://doi.org/10.1111/j.1525-1314.2007.00713.x.

Song, S.G., Su, L., Li, X.H., Niu, Y.L., and Zhang, L.F., 2012, Grenville-age orogenesis in the Qaidam-Qilian block: The link between South China and Tarim: Precambrian Research, v. 220–221, p. 9–22, https://doi.org/10.1016/j.precamres.2012.07.007.

Song, S.G., Niu, Y.L., Su, L., and Xia, X.H., 2013, Tectonics of the North Qilian orogen, NW China: Gondwana Research, v. 23, no. 4, p. 1378–1401, https://doi.org/10.1016/j.gr.2012.02.004.

Song, S.G., Niu, Y.L., Su, L., Zhang, C., and Zhang, L.F., 2014, Continental orogenesis from ocean subduction, continent collision/subduction, to orogen collapse, and orogen recycling: The example of the North Qaidam UHPM belt, NW China: Earth-Science Reviews, v. 129, p. 59–84, https://doi.org/10.1016/j.earscirev.2013.11.010.

Soret, M., Larson, K.P., Cottle, J., and Ali, A., 2021, How Himalayan collision stems from subduction: Geology, v. 49, p. 894–898, https://doi.org/10.1130/G48803.1.

Sun, J., Yang, Z.Z., Zhao, Z.Y., Tian, Z., Sun, D.L., Li, D.L., Yang, Q.S., and Li, X.M., 2018, LA-ICP-MS zircon U-Pb ages and geological significance of granodiorite from Zongwulong tectonic belt in Delingha, Qinghai Province: Geological Bulletin of China (Dizhi Tongbao), v. 37, no. 4, p. 604–612 [in Chinese with English abstract].

Sun, J.P., Chen, S.Y., Peng, Y., Shao, P.C., Ma, S., and Liu, J., 2015, Determination of early Cambrian zircon SHRIMP U-Pb dating in Zongwulong tectonic belt, northern margin of Qaidam Basin, and its geological significance: Geological Review (Dizhi Lunping), v. 61, no. 4, p. 743–751 [in Chinese with English abstract].

Sun, J.P., Chen, S.Y., Liu, C.L., Ma, Y.S., Yin, C.M., Peng, Y., Shao, P.C., Ma, S., and Liu, J., 2016a, Tectonic setting of northeastern Qaidam Basin and its evolution during the late Paleozoic: Evidence from geochemical characteristics of detrital rock: Earth Science Frontiers, v. 23, no. 5, p. 45–55 [in Chinese with English abstract].

Sun, J.P., Yin, C.M., Chen, S.Y., Zhuang, Y.K., Wang, F., Shao, P.C., Ma, S., and Liu, J., 2016b, An analysis of late Carboniferous sedimentary tectonic setting and provenance of North Qaidam area: Evidence from Well Shiqian 1: Geological Bulletin of China (Dizhi Tongbao), v. 35, no. 2–3, p. 302–311 [in Chinese with English abstract].

Sun, J.P., Dong, Y.P., Ma, L.C., Chen, S.Y., and Jiang, W., 2022, Devonian to Triassic tectonic evolution and basin transition in the East Kunlun–Qaidam area, northern Tibetan Plateau: Constraints from stratigraphy and detrital zircon U-Pb geochronology: Geological Society of America Bulletin, v. 134, p. 1967–1993, https://doi.org/10.1130/B36147.1.

Tian, Q., Shi, Y.L., Hao, Y.Q., Qiang, X.N., and Li, S.H., 2018a, LA-ICP-MS zircon U-Pb dating of Nanshan subduction type intrusion in Qinghai Province and its geological significance: Geological Bulletin of China (Dizhi Tongbao), v. 37, no. 7, p. 1258–1270 [in Chinese with English abstract].

Tian, Z., Sun, J., and Zhao, Z.Y., 2018b, Composition and geological significance of tectonic mélanges in Shiaiquan area of Delingha, Qinghai: Mineral Exploration, v. 9, no. 10, p. 1862–1868 [in Chinese with English abstract].

Tung, K.A., Yang, H.J., Yang, H.Y., Liu, D.Y., Zhang, J.X., Wan, Y.S., and Tseng, C.Y., 2007, SHRIMP U-Pb geochronology of the zircons from the Precambrian basement of the Qilian block and its geological significances: Chinese Science Bulletin, v. 52, no. 19, p. 2687–2701, https://doi.org/10.1007/s11434-007-0356-0.

Tung, K.A., Yang, H.Y., Liu, D.Y., Zhang, J.X., Yang, H.J., Shau, Y.H., and Tseng, C.Y., 2013, The Neoproterozoic granitoids from the Qilian block, NW China: Evidence for a link between the Qilian and South China blocks: Precambrian Research, v. 235, p. 163–189, https://doi.org/10.1016/j.precamres.2013.06.016.

Wang, B.Z., Han, J., Xie, X.L., Chen, J., Wang, T., Xue, W.W., Bai, Z.H., and Li, S.P., 2020a, Discovery of the Indosinian (beryl-bearing) spodumene pegmatitic dike swarm in the Chakaibeishan area in the northeastern margin of the Tibetan Plateau: Implications for Li-Be mineralization: Dadi Gouzao Yu Chengkuangxue, v. 44, no. 1, p. 69–79 [in Chinese with English abstract].

Wang, H.Q., Zhu, Y.H., Lin, Q.X., Li, Y.L., and Wang, K., 2010, LA-ICP-MS zircon U-Pb dating of the gabbro from Longwu Gorge ophiolite, Jianzha-Tongren area, Qinghai, China, and its geological significance: Geological Bulletin of China (Dizhi Tongbao), v. 29, no. 1, p. 86–92 [in Chinese with English abstract].

Wang, J.W., 2019, Zircon U-Pb geochronology and tectonic significance of Middle Triassic intermediate-acid intrusion in Nanshan, Qinghai Province: Geology and Mineral Resources of South China, v. 35, no. 2, p. 200–215 [in Chinese with English abstract].

Wang, J.X., Lin, M., Liu, Z.Y., Wang, L., and Zhang, G.B., 2020b, Petrological study of the meta-ophiolite from the North Qaidam UHP metamorphic belt and its geological implications: Northwest Geology, v. 53, no. 4, p. 1–10 [in Chinese with English abstract].

Wang, L., Wang, H., He, C., Chen, N.S., Santosh, M., Sun, M., Wang, Q.Y., Jin, L.L., and Liao, F.X., 2016, Mesoproterozoic continental breakup in NW China: Evidence from gray gneisses from the North Wulan terrane: Precambrian Research, v. 281, p. 521–536, https://doi.org/10.1016/j.precamres.2016.06.016.

Wang, L., Johnston, S.T., and Chen, N.S., 2019a, New insights into the Precambrian tectonic evolution and continental affinity of the Qilian block: Evidence from geochronology and geochemistry of metasupracrustal rocks in the North Wulan terrane: Geological Society of America Bulletin, v. 131, p. 1723–1743, https://doi.org/10.1130/B35059.1.

Wang, L.Q., Pan, G.T., Ding, J., and Yao, D.S., 2013, Geological Map of the Tibetan Plateau at a Scale of 1:1.5 M with Explanations: Beijing, China, Geological Publishing House, 288 p.

Wang, M., Pei, X.Z., Liu, C.J., Zhang, Y.M., Li, Z.C., Li, R.B., Pei, L., Chen, Y.X., and Chen, G.C., 2019b, Magma mixing of the Heimahe pluton in the Qinghai Nanshan tectonic zone: Evidence from petrology, geochemistry and geochronology, and its tectonic implications: Earth Science, v. 44, no. 7, p. 2490–2504 [in Chinese with English abstract].

Wang, P.C., Li, S.Z., Suo, Y.H., Guo, L.L., Santosh, M., Li, X.Y., Wang, G.Z., Jiang, Z.X., Liu, B., Zhou, J., Jiang, S.H., Cao, X.Z., and Liu, Z., 2021a, Structural and kinematic analysis of Cenozoic rift basins in South China Sea: A synthesis: Earth-Science Reviews, v. 216, https://doi.org/10.1016/j.earscirev.2021.103522.

Wang, P.L., Li, Y.J., Duan, F.H., Zhuang, Y.J., Zhi, Q., Gu, P.Y., Gao, J.P., and Yang, G.X., 2023, Petrogenesis and geodynamic setting of the Xiaosaishiteng Mountain biotite monzonitic granite and quartz diorite in the western part of the northern margin of the Qaidam Basin: Constraints from zircon U-Pb geochronology, geochemistry and Hf isotope: Acta Geologica Sinica, v. 97, no. 10, p. 3292–3313 [in Chinese with English abstract].

Wang, Q.Y., Chen, N.S., Li, X.Y., Hao, S., and Chen, H.H., 2008, LA-ICPMS zircon U-Pb geochronological constraints on the tectonothermal evolution of the early Paleoproterozoic Dakendaban Group in the Quanji block, NW China: Chinese Science Bulletin, v. 53, no. 18, p. 2849–2858, https://doi.org/10.1007/s11434-008-0265-x.

Wang, Q.Y., Pan, Y.M., Chen, N.S., Li, X.Y., and Chen, H.H., 2009, Proterozoic polymetamorphism in the Quanji block, northwestern China: Evidence from microtextures, garnet compositions and monazite CHIME ages: Journal of Asian Earth Sciences, v. 34, no. 5, p. 686–698, https://doi.org/10.1016/j.jseaes.2008.10.008.

Wang, S.L., and Zhou, L.F., 2016, LA-ICP-MS zircon U-Pb dating, geochemistry and tectonic implication of the bojite in the Zongwulong Mountain: Journal of Northwest University: Natural Science Edition, v. 46, no. 5, p. 716–724 [in Chinese with English abstract].

Wang, W.T., Zhang, P.Z., Garzione, C.N., Liu, C.C., Zhang, Z.Q., Pang, J.Z., Wang, Y.Z., Zheng, D.W., Zheng, W.J., and Zhang, H.P., 2022, Pulsed rise and growth of the Tibetan Plateau to its northern margin since ca. 30 Ma: Proceedings of the National Academy of Sciences of the United States of America, v. 119, no. 8, https://doi.org/10.1073/pnas.2120364119.

Wang, Y.Z., Bai, Y.S., and Lu, H.L., 2001, Geological characteristics of Tianjunnanshan ophiolite in Qinghai and its forming environment: Geology of Qinghai, no. 1, p. 29–35 [in Chinese with English abstract].

Wang, Z.X., Chen, R.X., Zheng, Y.F., Xia, Q.X., Wang, Z.M., Yin, Z.Z., and Hu, Z., 2021b, Contrasting zircon and garnet behaviors during metamorphic transformation from eclogite to granulite facies: Constraints from orogenic metabasites from North Qaidam in northern Tibet: Journal of Asian Earth Sciences, v. 220, https://doi.org/10.1016/j.jseaes.2021.104924.

Wiedenbeck, M., Allé, P., Corfu, F., Griffin, W.L., Meier, M., Oberli, F., Von Quadt, A., Roddick, J.C., and Spiegel, W., 1995, Three natural zircon standards for U-Th-Pb, Lu-Hf, trace element and REE analyses: Geostandards Newsletter, v. 19, no. 1, p. 1–23, https://doi.org/10.1111/j.1751-908X.1995.tb00147.x.

Wu, C., Yin, A., Zuza, A.V., Zhang, J.Y., Liu, W.C., and Ding, L., 2016, Pre-Cenozoic geologic history of the central and northern Tibetan Plateau and the role of Wilson cycles in constructing the Tethyan orogenic system: Lithosphere, v. 8, no. 3, p. 254–292, https://doi.org/10.1130/L494.1.

Wu, C., Zuza, A.V., Chen, X.H., Ding, L., Levy, D.A., Liu, C.F., Liu, W.C., Jiang, T., and Stockli, D.F., 2019a, Tectonics of the Eastern Kunlun Range: Cenozoic reactivation of a Paleozoic–early Mesozoic orogen: Tectonics, v. 38, no. 5, p. 1609–1650, https://doi.org/10.1029/2018TC005370.

Wu, C., Li, J., and Ding, L., 2021a, Low-temperature thermochronology constraints on the evolution of the Eastern Kunlun Range, northern Tibetan Plateau: Geosphere, v. 17, p. 1193–1213, https://doi.org/10.1130/GES02358.1.

Wu, C., Li, J., Zuza, A.V., Haproff, P.J., Chen, X.H., and Ding, L., 2022, Proterozoic–Phanerozoic tectonic evolution of the Qilian Shan and Eastern Kunlun Range, northern Tibet: Geological Society of America Bulletin, v. 134, p. 2179–2205, https://doi.org/10.1130/B36306.1.

Wu, C., Ding, L., and Chen, X.H., 2023a, Tectonic evolution and Cenozoic deformation history of the Qilian orogen: Earth Science Frontiers, v. 30, no. 3, p. 262–281 [in Chinese with English abstract].

Wu, C., Zuza, A.V., Levy, D.A., Li, J., and Ding, L., 2023b, Discovery of Permian–Triassic eclogite in northern Tibet establishes coeval subduction erosion along an ~3000-km-long arc: Geology, v. 51, p. 833–838, https://doi.org/10.1130/G51223.1.

Wu, C.L., Wu, D., Mattinson, C., Lei, M., and Chen, H.J., 2019b, Petrogenesis of granitoids in the Wulan area: Magmatic activity and tectonic evolution in the North Qaidam, NW China: Gondwana Research, v. 67, p. 147–171, https://doi.org/10.1016/j.gr.2018.09.010.

Wu, D.Q., Sun, F.Y., Pan, Z.C., Yu, L., Li, L., Gao, H.C., Tian, N., and Xu, C.H., 2021b, Neoproterozoic magmatic and metamorphic imprints in the East Kunlun orogenic belt, north Tibetan Plateau, NW China: Implications for the assembly and initial breakup of the Rodinia supercontinent: Precambrian Research, v. 354, https://doi.org/10.1016/j.precamres.2020.106076.

Wu, S.K., Zhang, Y., Yang, Q.A., Wu, J.H., He, L., Ma, G.H., Li, C.B., and Duo, G.D., 2021c, The forming age and geological characteristics of the metamorphic intrusion of Hualong rock group in the eastern tectonic belt of Nanshan, Qinghai: Northwest Geology, v. 54, no. 2, p. 19–29 [in Chinese with English abstract].

Wu, Y.W., Zhang, J.X., Zhang, B., Mao, X.H., Lu, Z.L., Zhou, G.S., Teng, X., and Guo, Q., 2023c, Early Paleozoic oblique convergence from subduction to collision: Insights from timing and structural style of the transpressional dextral shear zone in the Qilian orogen, northern Tibet of China: Geological Society of America Bulletin, v. 136, p. 1889–1915, https://doi.org/10.1130/B36947.1.

Xia, Y.Q., 1996, Contact relation between the Tanjianshan Group and Dakendaban Group on northern margin of Qaidam: Journal of Stratigraphy (Dicengxue Zazhi), v. 20, no. 2, p. 123–133 [in Chinese with English abstract].

Xie, L.W., Zhang, Y.B., Zhang, H.H., Sun, J.F., and Wu, F.Y., 2008, In situ simultaneous determination of trace

elements, U-Pb and Lu-Hf isotopes in zircon and baddeleyite: Chinese Science Bulletin, v. 53, p. 1565–1573, https://doi.org/10.1007/s11434-008-0086-y.

Xie, Q.F., Zhou, L.F., and Liu, Y., 2014, LA-ICP-MS zircon U-Pb ages of Gangchadasi granite in Qinghai Province and their geological significance: Geological Bulletin of China (Dizhi Tongbao), v. 33, no. 9, p. 1379–1390 [in Chinese with English abstract].

Xie, R.X., Chen, L., Yin, A., Xiong, X., Chen, Y.J., Guo, Z., and Wang, K., 2023, Two phases of crustal shortening in northeastern Tibet as a result of a stronger Qaidam lithosphere during the Cenozoic India-Asia collision: Tectonics, v. 42, no. 1, https://doi.org/10.1029/2022TC007261.

Xin, H.T., Hao, G.J., Wang, H.C., Chen, N.S., Han, Y.S., and Qi, S.S., 2002, New idea on Precambrian strata in the northern margin of Qaidam massif: Progress in Precambrian Research, v. 25, no. 2, p. 113–119 [in Chinese with English abstract].

Xu, H.Q., Yan, Y.F., Qu, G.J., Yuan, J.P., and Wang, Q.Y., 2019, Material composition and evolutionary characteristics of the western section of Zongwulong tectonic belt: Journal of Qinghai University, v. 37, no. 3, p. 87–93 [in Chinese with English abstract].

Xu, Z.Q., Yang, J.S., Li, W.C., Li, H.Q., Cai, Z.H., Yan, Z., and Ma, C.Q., 2013, Paleo-Tethys system and accretionary orogen in the Tibet Plateau: Acta Petrologica Sinica (Yanshi Xuebao), v. 29, no. 6, p. 1847–1860 [in Chinese with English abstract].

Xu, Z.Q., Wang, Q., Li, Z.H., Li, H.Q., Cai, Z.H., Liang, F.H., Dong, H.W., Cao, H., Chen, X.J., Huang, X.M., Wu, C., and Xu, C.P., 2016, Indo-Asian collision: Tectonic transition from compression to strike slip: Acta Geologica Sinica, v. 90, no. 1, p. 1–23 [in Chinese with English abstract].

Xu, Z.Q., Zheng, B.H., and Wang, Q., 2021, From accretion to collision: Situation and outlook: Acta Geologica Sinica, v. 95, no. 1, p. 75–97 [in Chinese with English abstract].

Yan, Y.F., Xu, H.Q., Yang, B., Li, H.X., and Li, W.F., 2017, LA-ICP-MS zircon U-Pb dating of metamorphic and intrusive rock (system) of Zongwulongshan intruded into Dakendaban and its geological significance: Journal of Qinghai University, v. 35, no. 6, p. 102–108 [in Chinese with English abstract].

Yan, Z., Aitchison, J., Fu, C.L., Guo, X.Q., Niu, M.L., Xia, W.J., and Li, J.L., 2015, Hualong Complex, South Qilian terrane: U-Pb and Lu-Hf constraints on Neoproterozoic micro-continental fragments accreted to the northern Proto-Tethyan margin: Precambrian Research, v. 266, p. 65–85, https://doi.org/10.1016/j.precamres.2015.05.001.

Yan, Z., Fu, C.L., Aitchison, J.C., Buckman, S., Niu, M.L., Cao, B., Sun, Y., Guo, X.Q., Wang, Z.Q., and Zhou, R.J., 2019, Retro-foreland basin development in response to Proto-Tethyan Ocean closure, NE Tibet Plateau: Tectonics, v. 38, no. 12, p. 4229–4248, https://doi.org/10.1029/2019TC005560.

Yan, Z., Fu, C.L., Aitchison, J.C., Zhou, R.J., Buckman, S., and Chen, L., 2020, Silurian sedimentation in the South Qilian belt: Arc-continent collision-related deposition in the NE Tibet Plateau?: Acta Geologica Sinica (English Edition), v. 94, no. 4, p. 901–913, https://doi.org/10.1111/1755-6724.14551.

Yan, Z., Fu, C.L., Aitchison, J.C., Niu, M.L., Buckman, S., Xiao, W.J., Zhou, R.J., Chen, L., and Li, J.H., 2022, Arc-continent collision during culmination of Proto-Tethyan Ocean closure in the Central Qilian belt, NE Tibetan Plateau: Geological Society of America Bulletin, v. 134, p. 3079–3098, https://doi.org/10.1130/B36328.1.

Yang, Y.W., Lu, X.X., Wang, L.W., Yang, Y., Yang, C.K., and Huang, F., 2022, Dangjiasi granite complex and Late Triassic dykes in Qinghai Nanshan tectonic zone, and its constraints on the early Mesozoic tectonic environment: Modern Geology (Xiandai Dizhi), v. 36, no. 3, p. 796–811 [in Chinese with English abstract].

Yang, Z.Z., Sun, J., Zhao, X.K., Tian, Z., Zhao, Z.Y., Sun, D.L., Li, D.L., Yang, B.Z., and Yang, Q.S., 2017, LA-ICP-MS U-Pb age of the zircons from the volcanic rocks in Maoniushan Formation in Shidiquan area, Delingha, Qinghai, and its geological significance: Geological Review (Dizhi Lunping), v. 63, no. 6, p. 1613–1623 [in Chinese with English abstract].

Yin, A., 2010, Cenozoic tectonic evolution of Asia: A preliminary synthesis: Tectonophysics, v. 488, no. 1–4, p. 293–325, https://doi.org/10.1016/j.tecto.2009.06.002.

Yin, A., and Harrison, T.M., 2000, Geologic evolution of the Himalayan-Tibetan orogen: Annual Review of Earth and Planetary Sciences, v. 28, p. 211–280, https://doi.org/10.1146/annurev.earth.28.1.211.

Yin, A., and Nie, S.Y., 1996, A Phanerozoic palinspastic reconstruction of China and its neighboring regions, *in* Yin, A., and Harrison, T.M., eds., The Tectonic Evolution of Asia: New York, Cambridge University Press, p. 442–485.

Yin, A., and Taylor, M.H., 2011, Mechanics of V-shaped conjugate strike-slip faults and the corresponding continuum mode of continental deformation: Geological Society of America Bulletin, v. 123, p. 1798–1821, https://doi.org/10.1130/B30159.1.

Yin, A., Manning, C.E., Lovera, O., Menold, C.A., Chen, X.H., and Gehrels, G.E., 2007, Early Paleozoic tectonic and thermomechanical evolution of ultrahigh-pressure (UHP) metamorphic rocks in the northern Tibetan Plateau, Northwest China: International Geology Review, v. 49, no. 8, p. 681–716, https://doi.org/10.2747/0020-6814.49.8.681.

Yin, A., Dang, Y.Q., Wang, L.C., Jiang, W.M., Zhou, S.P., Chen, X.H., Gehrels, G.E., and Mcrivette, M.W., 2008, Cenozoic tectonic evolution of Qaidam Basin and its surrounding regions (Part 1): The southern Qilian Shan–Nan Shan thrust belt and northern Qaidam Basin: Geological Society of America Bulletin, v. 120, p. 813–846, https://doi.org/10.1130/B26180.1.

Yu, M., Dick, J.M., Feng, C.Y., Li, B., and Wang, H., 2020, The tectonic evolution of the East Kunlun orogen, northern Tibetan Plateau: A critical review with an integrated geodynamic model: Journal of Asian Earth Sciences, v. 191, https://doi.org/10.1016/j.jseaes.2019.104168.

Yu, S.Y., Zhang, J.X., Li, S.Z., Sun, D.Y., Li, Y.S., Liu, X., Guo, L.L., Suo, Y.H., Peng, Y.B., and Zhao, X.L., 2017a, Paleoproterozoic granulite-facies metamorphism and anatexis in the Oulongbuluke block, NW China: Respond to assembly of the Columbia supercontinent: Precambrian Research, v. 291, p. 42–62, https://doi.org/10.1016/j.precamres.2017.01.016.

Yu, S.Y., Zhang, J.X., Li, S.Z., Santosh, M., Li, Y.S., Liu, Y.J., Li, X.Y., Peng, Y.B., Sun, D.Y., Wang, Z.Y., and Lv, P., 2019a, TTG-adakitic-like (tonalitic-trondhjemitic) magmas resulting from partial melting of metagabbro under high-pressure condition during continental collision in the North Qaidam UHP terrane, western China: Tectonics, v. 38, p. 791–822, https://doi.org/10.1029/2018TC005259.

Yu, S.Y., Peng, Y.B., Zhang, J.X., Li, S.Z., Santosh, M., Li, Y.S., Liu, Y.J., Gao, X.Y., Ji, W.T., Lv, P., Li, C.Z., Jiang, X.Z., Qi, L.L., Xie, W.M., and Xu, L.J., 2021, Tectono-thermal evolution of the Qilian orogenic system: Tracing the subduction, accretion and closure of the Proto-Tethys Ocean: Earth-Science Reviews, v. 215, https://doi.org/10.1016/j.earscirev.2021.103547.

Yu, X.J., Fu, S.T., Wang, Z.D., Li, Q., and Guo, Z.J., 2017b, The discovery of early Paleoproterozoic high-Na trondhjemite in the northeastern Qaidam Basin: Evidence from the drilling core samples: Precambrian Research, v. 298, p. 615–628, https://doi.org/10.1016/j.precamres.2017.04.002.

Yu, X.J., Guo, Z.J., Guan, S.W., Du, W., Wang, Z.D., Bian, Q., and Li, L.L., 2019b, Landscape and tectonic evolution of Bayin River watershed, northeastern Qaidam Basin, northern Tibetan Plateau: Implications for the role of river morphology in source analysis and low-temperature thermochronology: Journal of Geophysical Research: Earth Surface, v. 124, no. 7, p. 1701–1719, https://doi.org/10.1029/2018JF004989.

Zappettini, E.O., Rubinstein, N., Crosta, S., and Segal, S.J., 2017, Intracontinental rift-related deposits: A review of key models: Ore Geology Reviews, v. 89, p. 594–608, https://doi.org/10.1016/j.oregeorev.2017.06.019.

Zhang, C., Yu, X.Y., Yang, F., Santosh, M., and Huo, D., 2021, Petrology and geochronology of the Yushigou nephrite jade from the North Qilian orogen, NW China: Implications for subduction-related processes: Lithos, v. 380–381, https://doi.org/10.1016/j.lithos.2020.105894.

Zhang, G.D., Xu, Z.Q., Gong, J., Feng, J., Han, Y.B., Zhang, J.W., Zhou, Y., Huang, Z.S., Zeng, X.F., Zhang, K.J., Wang, J.K., and Cheng, J., 2016, Geochronology and significance of intermediate-acid intrusive rocks in Quanji area, Gangcha, Qinghai: Geological Journal of China Universities (Gaoxiao Dizhi Xuebao), v. 22, no. 1, p. 113–126 [in Chinese with English abstract].

Zhang, L., Liao, F.X., Ba, J., Xu, L.P., Wang, Q.Y., and Chen, N.S., 2011, Mineral evolution and zircon geochronology of mafic enclave in granitic gneiss of the Quanji block and implications for Paleoproterozoic regional metamorphism: Earth Science Frontiers, v. 18, no. 2, p. 79–84 [in Chinese with English abstract].

Zhang, L., Wang, Q.Y., Chen, N.S., Sun, M., Santosh, M., and Ba, J., 2014, Geochemistry and detrital zircon U-Pb and Hf isotopes of the paragneiss suite from the Quanji massif, SE Tarim craton: Implications for Paleoproterozoic tectonics in NW China: Journal of Asian Earth Sciences, v. 95, p. 33–50, https://doi.org/10.1016/j.jseaes.2014.05.014.

Zhang, S.C., Yao, X.D., and Li, Y.P., 2019a, Zircon U-Pb age evidence and geochemical features of Late Ordovician granitic complex in Nanshan area, Qinghai Province: China's Manganese Industry, v. 37, no. 1, p. 45–50 [in Chinese with English abstract].

Zhang, X.P., Wang, Q.F., Hui, J., Chang, X., and Tong, H.K., 2015, Chemical characteristics of volcanic rocks from the Tanjianshan Group on the northern margin of the Qaidam Basin and its tectonic environment: Journal of Mineral Petrology, v. 35, no. 1, p. 18–26 [in Chinese with English abstract].

Zhang, Y.M., 2017, Indosinian Tectonic-Magmatism and Regional Tectonic Evolution in the Qinghainanshan tectonic Belt [Ph.D. thesis]: Xi'an, China, Chang'an University, 169 p.

Zhang, Y.M., Pei, X.Z., Li, Z.C., Li, R.B., Liu, C.J., Pei, L., Chen, Y.X., Chen, G.C., and Wang, M., 2017a, LA-ICP-MS zircon U-Pb dating, geochemistry and geological significance of the Heimahe granitic pluton in the western segment of the Qinghainanshan tectonic belt: Geological Review (Dizhi Lunping), v. 63, no. 4, p. 1079–1101 [in Chinese with English abstract].

Zhang, Y.M., Pei, X.Z., Li, Z.C., Li, R.B., Liu, C.J., Pei, L., Chen, Y.X., Chen, G.C., Wang, M., and Lin, G.C., 2017b, LA-ICP-MS zircon U-Pb dating and geochemistry of the Dangjiasi granitic complex in the Qinghai Nanshan tectonic zone, and its geological implications: Acta Geologica Sinica, v. 91, no. 3, p. 523–541 [in Chinese with English abstract].

Zhang, Y.M., Pei, X.Z., Li, Z.C., Li, R.B., Liu, C.J., Pei, L., Chen, Y.X., Wang, M., and Chen, G.C., 2017c, LA-ICP-MS zircon U-Pb dating, petrogenesis of the Gouhou complex in the Qinghai Nanshan tectonic zone, and its geological implications: Geotectonica et Metallogenia (Dadi Gouzao Yu Chengkuangxue), v. 41, no. 5, p. 908–932 [in Chinese with English abstract].

Zhang, Y.M., Pei, X.Z., Li, Z.C., Li, R.B., Liu, C.J., Pei, L., Chen, Y.X., and Wang, M., 2019b, Zircon U-Pb geochronology, geochemistry and its geological implication of the early Indosinian basic complex in the Qinghai Nanshan tectonic belt: Earth Science, v. 44, no. 7, p. 2461–2477 [in Chinese with English abstract].

Zhang, Y.M., Pei, X.Z., Li, Z.C., Li, R.B., Liu, C.J., Pei, L., Chen, Y.X., and Wang, M., 2019c, Zircon U-Pb age, geochemical characteristics and geological significance of the Caledonian strongly peraluminous granites in the Nanshan area, Qinghai Province: Geological Bulletin of China (Dizhi Tongbao), v. 38, no. 5, p. 742–756 [in Chinese with English abstract].

Zhao, W.T., 2023, Pre-Triassic Tectonic Evolution of the Zongwulong Tectonic Belt on the Northeastern Qinghai-Tibet Plateau: Constraints from Sedimentology, Detrital Zircon U-Pb Chronology and Lithogeochemistry [Ph.D. thesis]: Beijing, China, China University of Geosciences (Beijing), 153 p.

Zhao, W.T., Liu, S.F., and Chen, M., 2020, Detrital zircon geochronology and its geological significance from Turgendaban formation in Shengge area of Zongwulong

structural belt: China Mining Magazine, v. 29, no. S2, p. 234–240 [in Chinese with English abstract].

Zhao, W.T., Liu, S.F., Chen, M., and Xue, C.J., 2022, Detrital zircon characteristics of the Triassic Longwuhe Formation in the western segment of the Zongwulong tectonic belt and its tectonic significance: Acta Petrologica et Mineralogica, v. 41, no. 3, p. 569–591 [in Chinese with English abstract].

Zhu, X.H., Chen, D.L., Feng, Y.M., Ren, Y.F., and Zhang, X., 2022, Granitic magmatism and tectonic evolution in the Qilian Mountain Range in NW China: A review: Earth Science Frontiers, v. 29, no. 2, p. 241–260 [in Chinese with English abstract].

Zhuang, Y.J., Gu, P.Y., Gao, Y.W., Peng, X., He, S.P., and Li, P.T., 2020, Petrogenesis of middle Permian gabbro in Saishiteng Mountain of the northern Qaidam Basin and its constraint to the time of Zongwulong Ocean subduction: Acta Petrologica et Mineralogica, v. 39, no. 6, p. 718–734 [in Chinese with English abstract].

Zou, F.H., Wu, C.L., Deng, L.H., Gao, D., and Gao, Y.H., 2022, Petrological and geochemical constraints on the petrogenesis of granitoids in the Gonghe geothermal basin, western Qinling (China): Applied Geochemistry, v. 136, https://doi.org/10.1016/j.apgeochem.2021.105176.

Zuza, A.V., and Yin, A., 2016, Continental deformation accommodated by non-rigid passive bookshelf faulting: An example from the Cenozoic tectonic development of northern Tibet: Tectonophysics, v. 677–678, p. 227–240, https://doi.org/10.1016/j.tecto.2016.04.007.

Zuza, A.V., and Yin, A., 2017, Balkatach hypothesis: A new model for the evolution of the Pacific, Tethyan, and Paleo-Asian oceanic domains: Geosphere, v. 13, p. 1664–1712, https://doi.org/10.1130/GES01463.1.

Zuza, A.V., Cheng, X.G., and Yin, A., 2016, Testing models of Tibetan Plateau formation with Cenozoic shortening estimates across the Qilian Shan–Nan Shan thrust belt: Geosphere, v. 12, p. 501–532, https://doi.org/10.1130/GES01254.1.

Zuza, A.V., Wu, C., Reith, R.C., Yin, A., Li, J.H., Zhang, J.Y., Zhang, Y.X., Wu, L., and Liu, W.C., 2018, Tectonic evolution of the Qilian Shan: An early Paleozoic orogen reactivated in the Cenozoic: Geological Society of America Bulletin, v. 130, p. 881–925, https://doi.org/10.1130/B31721.1.

Zuza, A.V., Gavillot, Y., Haproff, P.J., and Wu, C., 2020, Kinematic evolution of a continental collision: Constraining the Himalayan-Tibetan orogen via bulk strain rates: Tectonophysics, v. 797, https://doi.org/10.1016/j.tecto.2020.228642.

Science Editor: Mihai Ducea
Associate Editor: Junpeng Wang

Manuscript Received 9 February 2024
Revised Manuscript Received 30 April 2024
Manuscript Accepted 10 May 2024